DOE/BC/14600-14
Distribution Category UC-122

SUPRI HEAVY OIL RESEARCH PROGRAM
Fourteenth Annual Report
October 1, 1989-September 30, 1990

DOE/BC/14600--14

DE92 001011

By
Khalid Aziz
Henry J. Ramey Jr.
Louis M. Castanier

December 1991

Work Performed Under Contract No. FG22-90BC14600

Prepared for
U.S. Department of Energy
Assistant Secretary for Fossil Energy

Thomas B. Reid, Project Manager
Bartlesville Project Office
P. O. Box 1398
Bartlesville, OK 74005

Prepared by
Stanford University
Petroleum Research Institute
Stanford, CA 94305

TABLE OF CONTENTS

LIST OF TABLES

LIST OF FIGURES

Page

SUMMARY

This page summarizes the progress made during the 1989-1990 fiscal year. The organization of this report in sections refers to the following projects:

Project 1: Flow Properties

A study of end effects in oil/water displacements is in progress. The experimental apparatus has been built and calibrated. One run has been made and it showed that inlet end effects may be important during imbibition. The work on the CT Scanner has focused on software implementation and development of new experiments on fractured media, drying and wetting fluids distribution and validation of other nondestructive measurements.

Project 2: In-Situ Combustion

Results of a study of metallic additives for in-situ combustion are presented. Tube runs and kinetics experiments have been performed on Huntington Beach and Hamaca crudes. The equipment was updated by replumbing all the lines, installing pressure relief valves and acid scrubbers ahead of the gas analyzers and improving gas and liquid analysis by addition of two chromatographs. Oil samples have been requested from several companies. A study of residual oil saturation after steam injection and how it relates to the fuel consumption has been initiated. Correlations of residual oil saturation with gravity will be attempted and verified experimentally. As a first step distillation data have been obtained and are now being analyzed.

Project 3: Steam with Additives

A model for transient foam flow is being developed. The results of the model will be compared with experimental data. Screening of surfactants in the presence of residual oil has continued. It appears that the injection procedure greatly affects the performance of the process. A new micromodel for foam observations is being built using computer technology. This micromodel will be used to study the effect of oil on the flow behavior of foams at the pore level. A three dimensional steam injection model allowing measurement of saturations by CT scan has been built. Preliminary runs with steam displacing water showed that the model can be operated as planned and that saturations in gas-liquid systems can be accurately measured. Foam runs are now in progress.

Project 4: Formation Evaluation

A study of the evaluation of saturations following waterflooding has been completed. Work on the numerical simulation of well-to-well tracer tests has continued. The main problem in this project remains numerical dispersion for large cell Peclet numbers. More research is needed to solve this problem.

Project 5: Field Support

Although no specific section on this project appears in this report, SUPRI has continued communicating with industry via our Industrial Advisory Committee and to advise the Department of Energy on a variety of field projects. SUPRI personnel also attended SPE meetings and various other technical conferences.

1.1 A STUDY OF END EFFECTS IN DISPLACEMENT EXPERIMENTS

(S. Qadeer)

The capillary discontinuities at the inlet and outlet ends of cores in displacement experiments results in the development of sharp saturation gradients. These saturation gradients are generally called capillary end effects. The outlet end effect has received a lot of attention from researchers, but the inlet effect is little understood. The purpose of this study is to fully understand these effects. To achieve this goal, flow experiments will be performed using consolidated sandstone cores. The saturations will be measured using a CT scanner.

Preliminary runs indicate a strong gravity segregation of oil and water near the inlet end during imbibition runs. This causes the oil to be trapped near the inlet face. As a result water can enter only through half of the core face. More runs are planned to study the effect of different parameters on saturation distribution near the inlet and outlet ends.

1.1.1 EXPERIMENTAL SETUP

The experiments are being performed using a core holder built from PVC. The details of this setup are given in the previous report (Brigham, et al. 1990).

One of the parameters being studied is the geometry of the flow ports in inlet and outlet end plugs. Presently we are using only one 1/8th in. hole in the middle of the plugs (there are no distribution grooves). These runs will provide data for the base case. Distribution grooves will be added and their effectiveness studied. Additional ports in both end plugs have been added so that pressures can be measured right at the face of the core. Figure 1.1.1 gives the details of the modified end plugs.

1.1.2 EXPERIMENTAL PROCEDURE

The cores used in this study are Berea sandstone. The cores are two inches in diameter and about ten inches long. After cutting the cores to desired dimensions, they are baked in an oven at 600°C for six hours and then left inside the oven overnight for slow cooling. The core is then transferred to the core holder. The air is displaced with carbon dioxide. The core is then evacuated. The sequence of injecting carbon dioxide and evacuation is repeated twice to ensure that no air is left trapped inside the core. At this point, the core is scanned at twelve locations. The scan locations are shown in Fig. 1.1.2.

Sodium iodide brine (2%) is then allowed to flow into the core under vacuum. The core is left overnight in contact with brine. After that, brine is flowed through the core at low flow rate for a day, under a back pressure of 45 psi. This is done to avoid any entrapment of gas phase in the core. The flow is then stopped and the core is again scanned to get the CT numbers for 100% brine saturated core.

At this point the oil phase is injected into the core for primary drainage. The cores are scanned at the preselected locations right at the start of the primary drainage and then after each fifteen minutes, until breakthrough. The scanning interval is then changed as required. This allows us to generate the saturation history of the process. After the primary drainage run is over, sodium iodide brine is injected into the core to get imbibition data. The scans are repeated at the same locations. We hope to get good saturation history data by this technique.

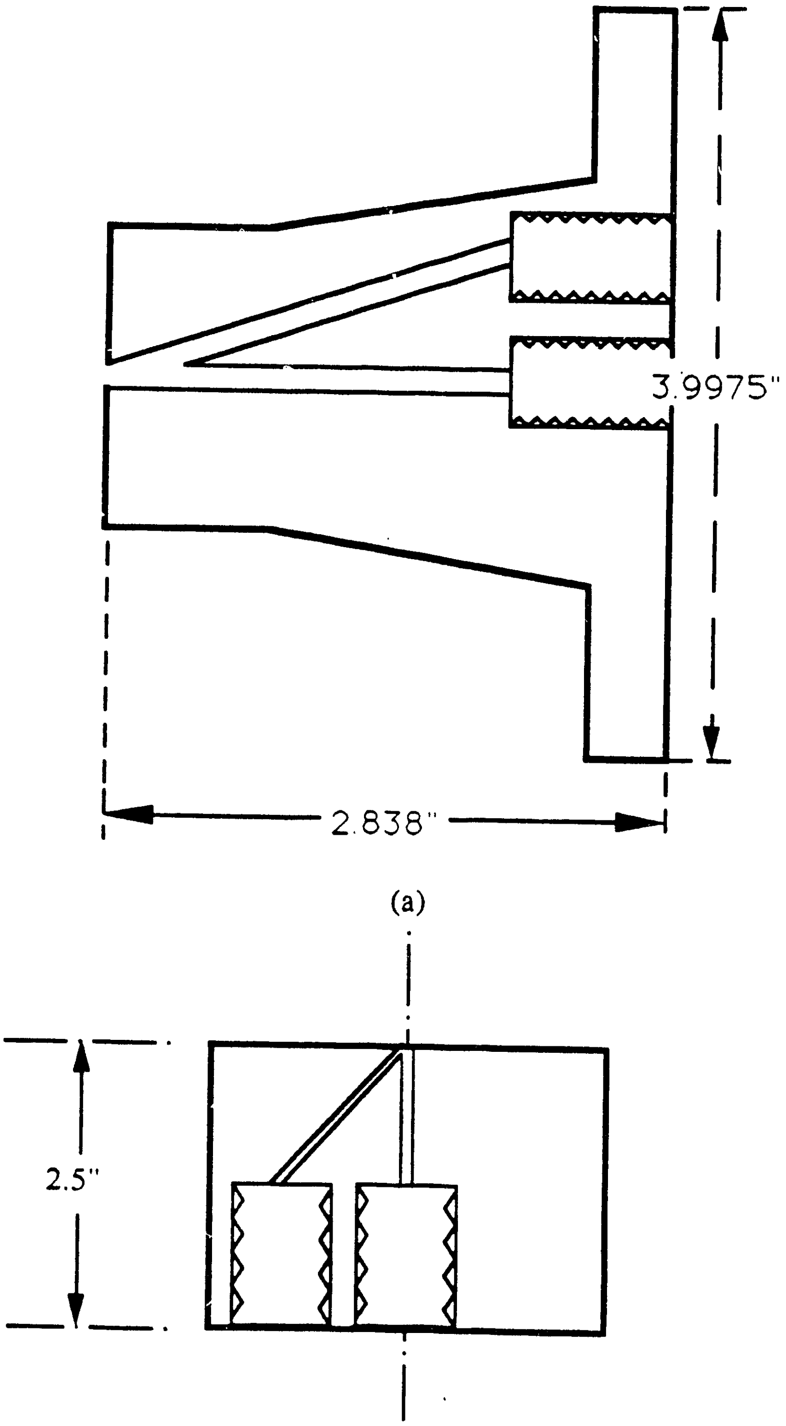

(a)

(b)

Figure 1.1.1 Modified End Plugs: (a) Inlet End Plug. (b). Outlet End Plug.

1.1.3 PROBLEMS DURING PRELIMINARY RUNS

The preliminary runs were made using cyclo-hexane as the oil phase. It was observed that the rubber sleeve in the core holder and the stoppers used in the separator absorbs cyclo-hexane, and thus they expand. The increase in the volume of core sleeve in the core holder causes the overburden pressure to increase continuously. The swelling of the stoppers in the separator causes errors in data. This absorption also introduces a large material balance error, thus the recovery data are unreliable.

The rest of the system operated as designed. No problems were found in re-circulating the injected fluids. The separation system was effective in separating the oil and brine.

1.1.4 RESULTS

The objectives of the preliminary runs were two-fold: one was to check the operation of the experimental setup, and the other was to confirm that the scanner can be used to determine saturations with required accuracy.

The experimental setup worked adequately except for the sleeve and some other rubber components. The data acquisition system also worked.

The results from the scanner computer are shown in Figs. 1.1.3 through 1.1.7 and 1.1.9. These images were obtained by digitizing the image generated by the scanner computer using our Macintosh computer and enhancing the contrast and brightness by the image processing software. All the images were processed at the same settings to avoid any artifacts or false contrasts in different scans. Table 1.1.1 shows some typical CT numbers obtained from these scans.

Figure 1.1.3 shows the scans from the dry, evacuated core. The CT numbers are about 350 units. All of the CT pictures show that there is considerable beam hardening. This causes some concentric artifacts to appear in the scans. By looking at all the scans we can see that the core used is quite uniform.

Scans from the fully saturated core with 2% sodium iodide brine are shown in Fig. 1.1.4. The averaged CT numbers in each scan are about 100 units greater than those of the dry core. These scans show beam hardening. It can be noted that the beam hardening has different characteristics at different scan locations.

After measuring the absolute permeability, cyclo-hexane was injected into the core at a rate of 1.0 cc/min. The scans were taken at intervals of 15 minutes up to the breakthrough time. The scanning interval was increased to half an hour after breakthrough. The scans at the end of primary drainage are shown in Fig. 1.1.5. The CT numbers dropped by about 50 units from those of 100% brine saturated core. This gives us enough resolution to calculate saturation of brine in subsequent runs.

The measurements of CT numbers follow statistical distribution. We are in the process of analyzing the data to determine the accuracy with which we measure the saturations.

At the end of drainage, brine was injected into the core at a rate of 1 cc/min. The scans after injecting about 0.5 PV are shown in Fig. 1.1.6. The CT numbers again increased. The most interesting feature of the imbibition was observed near the inlet end. It appeared that the injected brine was strongly underriding the in-place oil at the inlet. The scans of the inlet at different times of injection are shown in Fig. 1.1.7. As can be seen, the brine enters the core through the lower half of the inlet face. Some oil is trapped in the upper half near the inlet end.

At the end of the imbibition, the inlet end of the core was scanned at the locations shown in Fig. 1.1.8. The purpose of these scans was to determine the extent of gravity underride. The results are shown in Fig. 1.1.9. As is obvious, the brine imbibes upwards in a very short

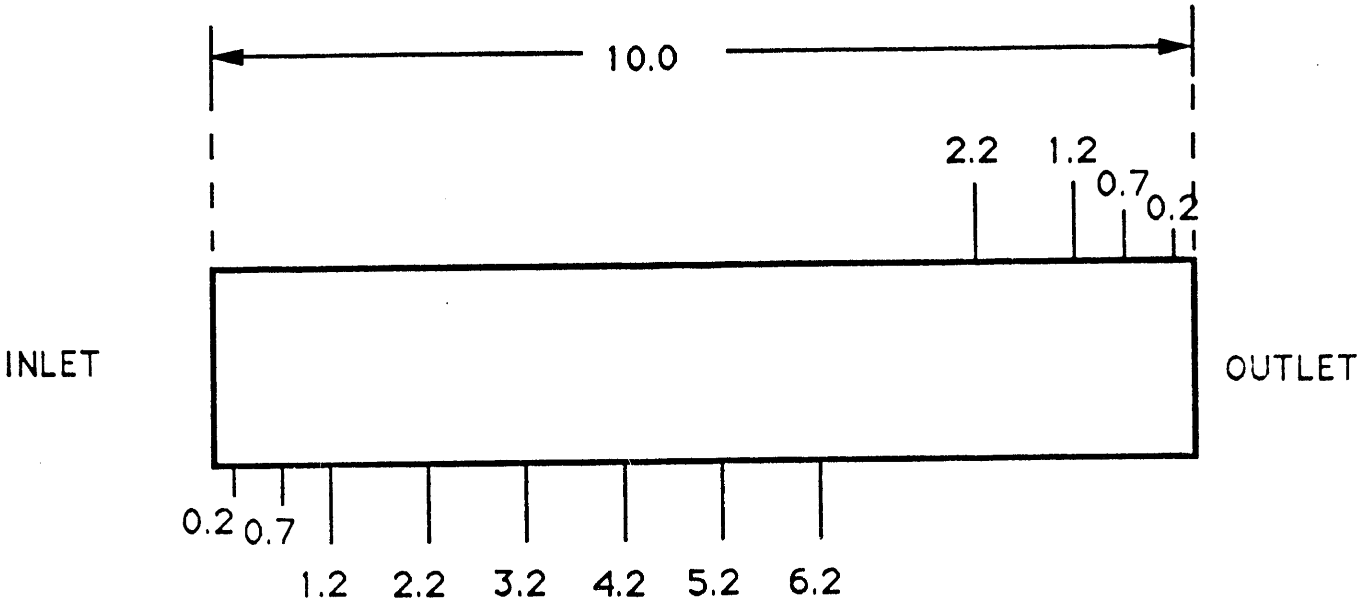

Figure 1.1.2 CT Scan Locations.

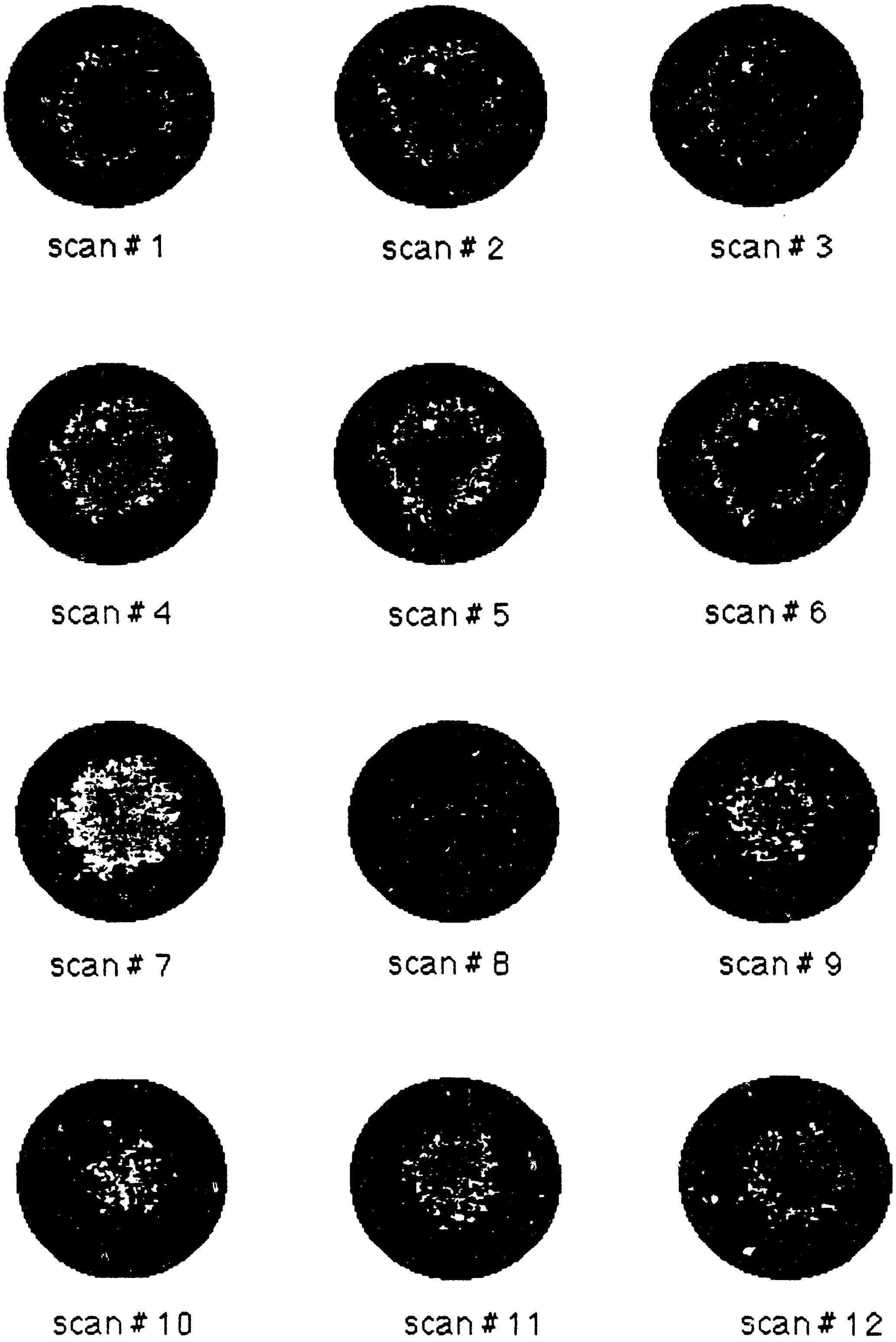

scan # 1

scan # 2

scan # 3

scan # 4

scan # 5

scan # 6

scan # 7

scan # 8

scan # 9

scan # 10

scan # 11

scan # 12

Figure 1.1.3 CT Images of Dry Core.

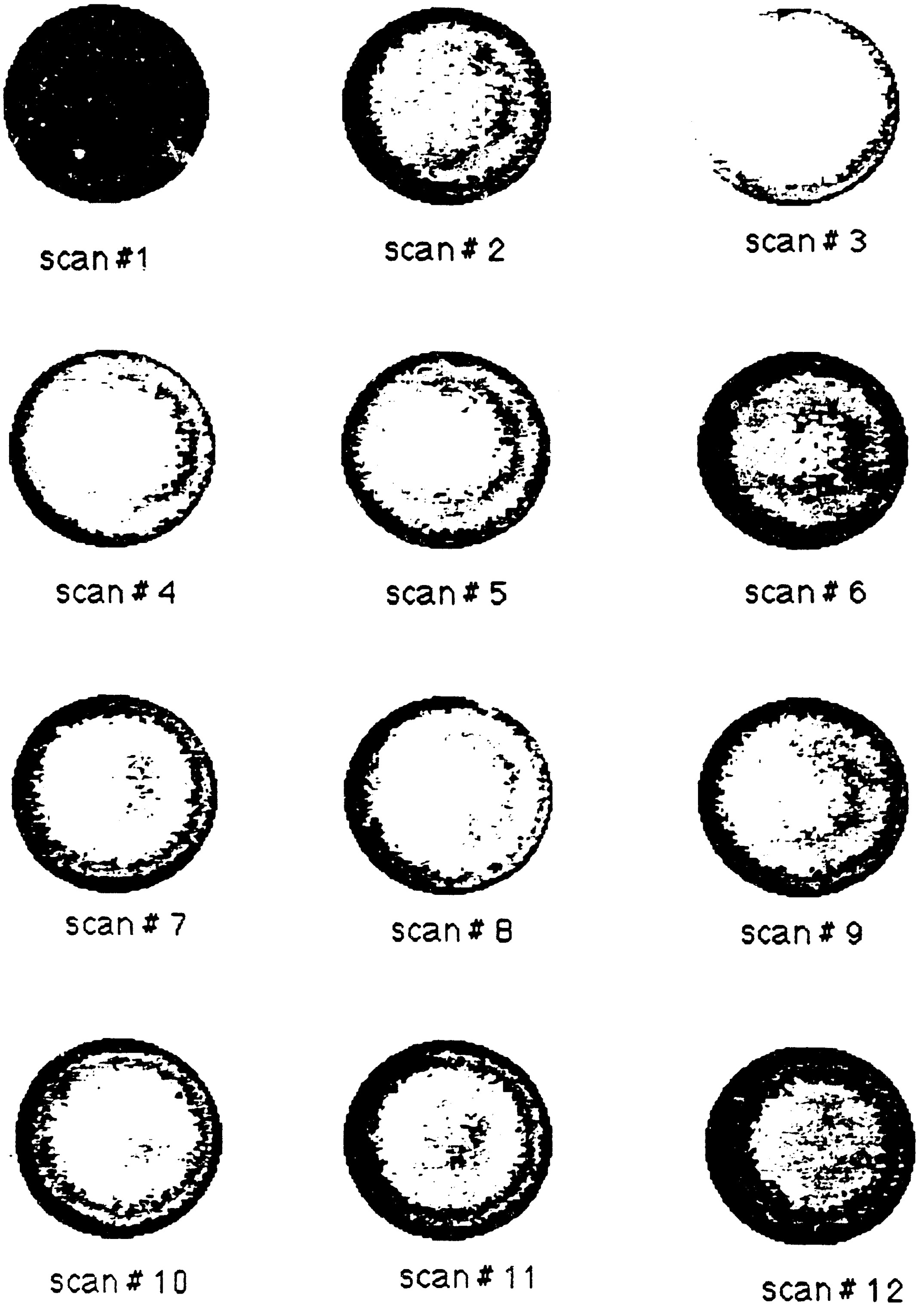

scan #1 scan # 2 scan # 3

scan # 4 scan # 5 scan # 6

scan # 7 scan # 8 scan # 9

scan # 10 scan # 11 scan # 12

Figure 1.1.4 CT Images From 100% Brine Saturated Core.

Table 1.1.1 Typical CT Numbers

SCAN LOCATION	CT #'s			
1	363	414	311	↗ 324 ↘ 412
6	342	471	429	460
12	356	456	448	466
	DRY	100%	D	I

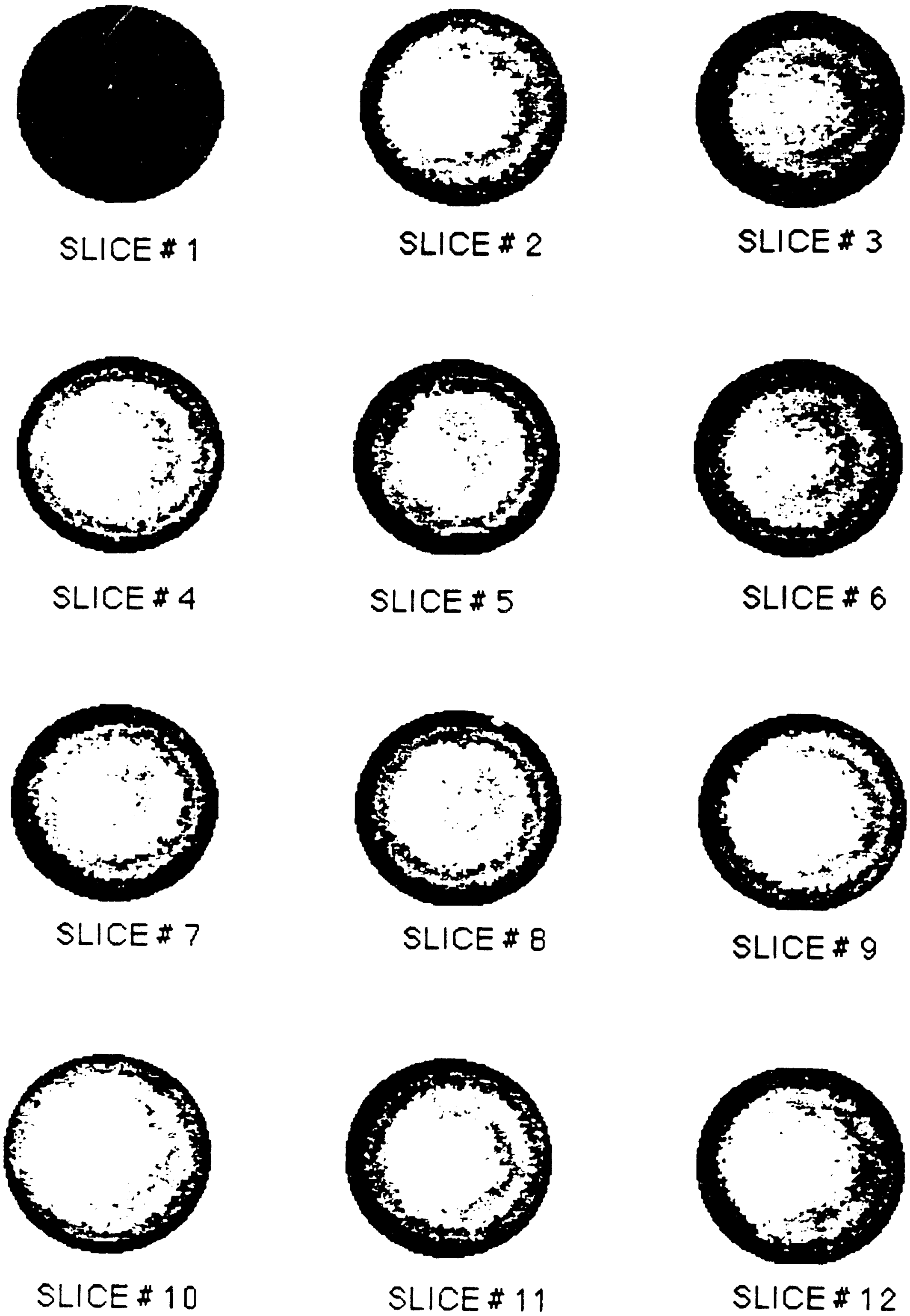

SLICE # 1

SLICE # 2

SLICE # 3

SLICE # 4

SLICE # 5

SLICE # 6

SLICE # 7

SLICE # 8

SLICE # 9

SLICE # 10

SLICE # 11

SLICE # 12

Figure 1.1.5 CT Images at the End of the Drainage Run.

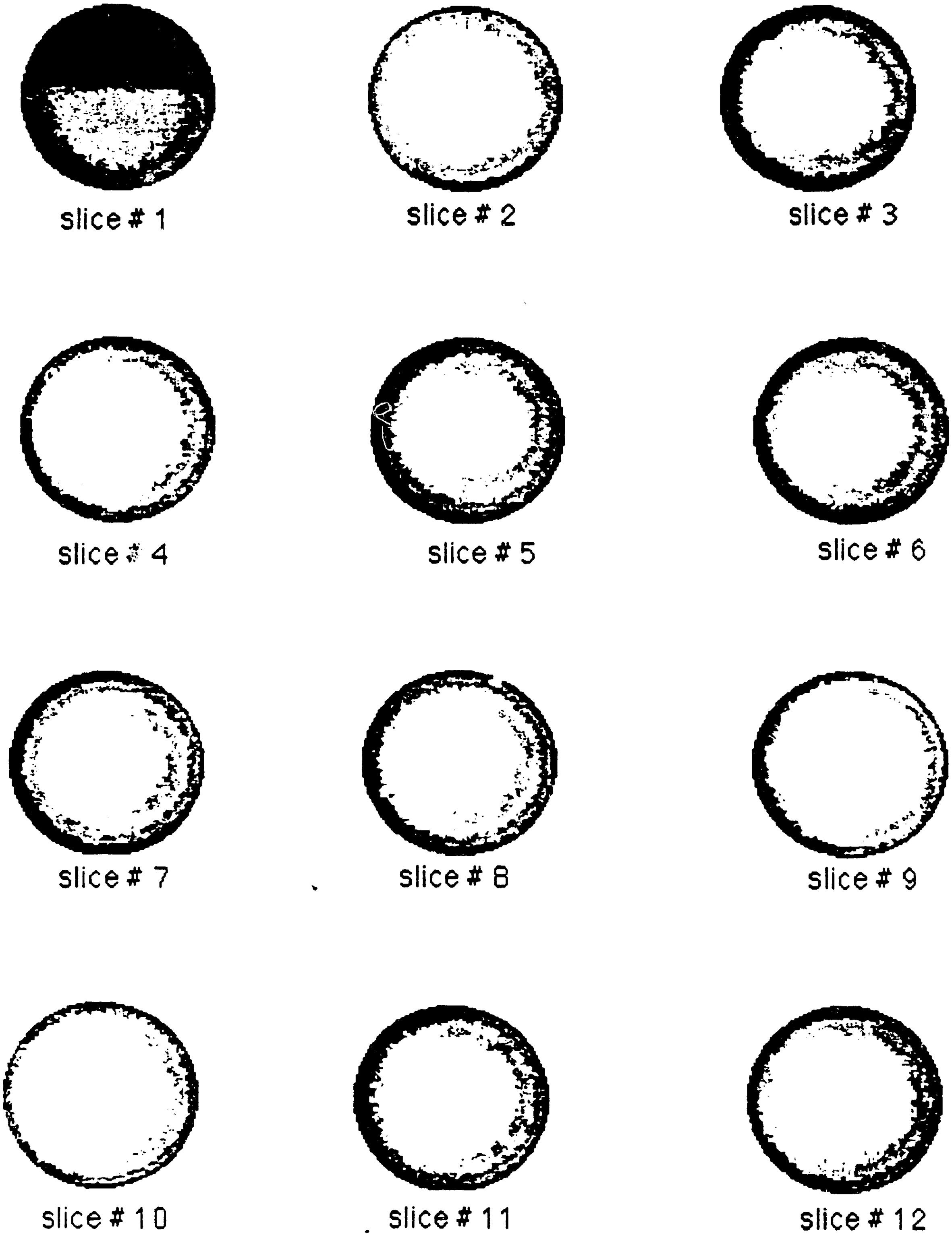

slice # 1 slice # 2 slice # 3

slice # 4 slice # 5 slice # 6

slice # 7 slice # 8 slice # 9

slice # 10 slice # 11 slice # 12

Figure 1.1.6 CT Scans After Imbibition Run.

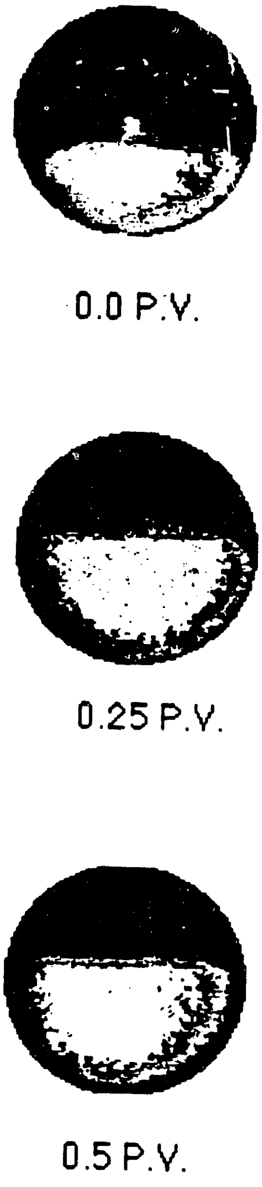

0.0 P.V.

0.25 P.V.

0.5 P.V.

Figure 1.1.7 Inlet End at Different Times.

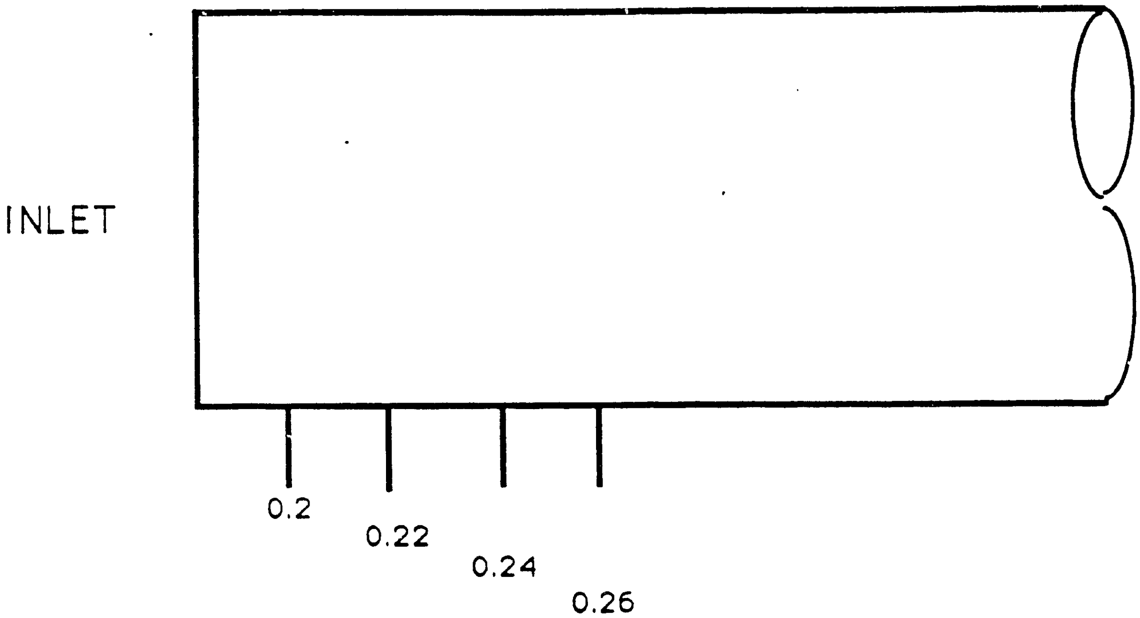

Figure 1.1.8 Scan Location for Figure 1.1.9.

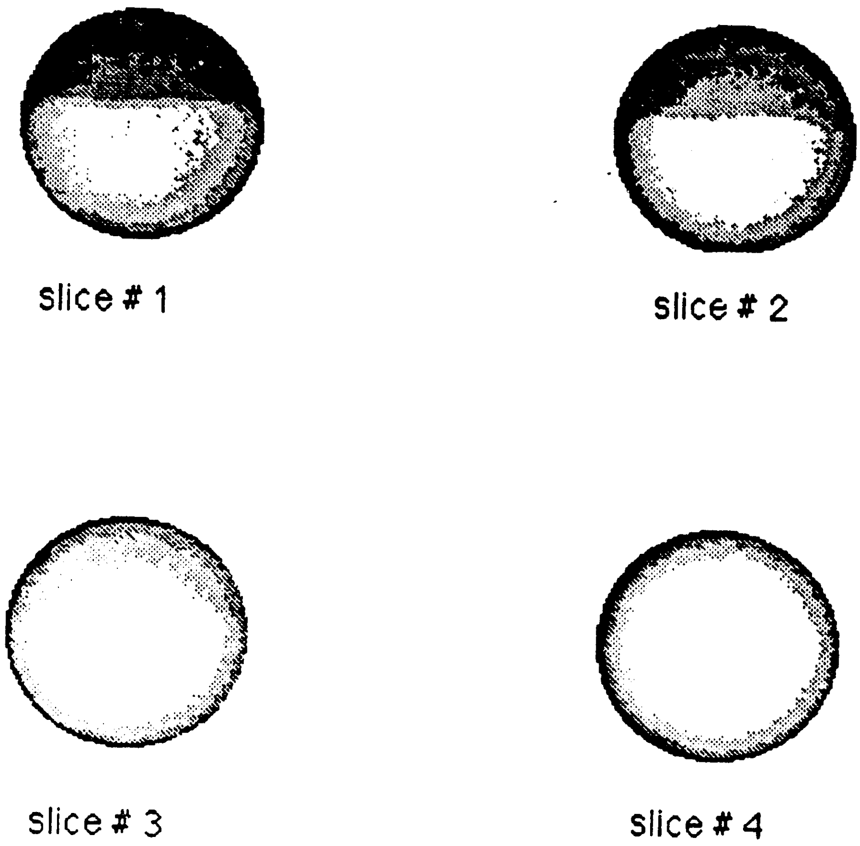

slice # 1

slice # 2

slice # 3

slice # 4

Figure 1.1.9 Scans to Determine the Extent of the Inlet Effect.

length. This is expected because of the strong capillary forces in the core.

Although some qualitative results were obtained in these experiments, the detailed analysis of the CT data has not been completed. This will require processing of the CT numbers and calculating the saturations at each cross-section. The results obtained so far are preliminary.

1.1.5 FUTURE PLAN

It is clear from the results obtained during preliminary runs that special software is required to process CT data in order to obtain saturations. We are in the process of acquiring a SUN work station which will allow us to use the SHELL CATPIX software for saturation determination. Additional software is required to transfer CT data from the CT computer to the SUN work station. This work is already in progress.

After acquiring the capability to calculate saturations from the CT data more runs will be made to fully understand the end effects.

To cover a broad range of operating conditions the effects of changing the viscosity ratio, the absolute permeability of the core, different end plug configurations (different geometry of the distribution grooves) will be studied. An appropriate numerical model for the inlet and outlet effects will be developed.

1.2 CAT SCAN STATUS REPORT
(L. Castanier)

Efforts during this year have focused on two main areas: software implementation and new experiments.

1.2.1 SOFTWARE IMPLEMENTATION

A SUN SPARC workstation was purchased in order to increase our image processing capability. Transfer of the CATPIX software to the SPARC system was made without problems. Shell's CATPIX software is now installed and working on our computers. Image formating, however, remains difficult because of the nonstandard nature of our scanner. A program to transfer directly the data as CT numbers on a pixel by pixel basis from the EMI CAT scanner computer to the SPARC via RS232 interface is being written. This should allow full use of the CATPIX software specially for three-phase saturation calculations from scanner measurements. A new version of IMAGE (version 28) was obtained for use on the Macintosh. This version allows direct capture of the pictures from the video signal originating at the diagnostic console. We now have the possibility of quickly displaying and analyzing results.

1.2.2 NEW EXPERIMENTS

In addition to the transient foam flow, end effect and three-dimensional steam model experiments described elsewhere in this report, several new projects have been initiated. Although most of these are not part of the thermal recovery research program we will give a brief description of the planned research.

Fractured Media

A new epoxy core holder has been designed and built in order to study multiphase flow in fractured porous media. Two Berea sandstone cores coming from the same block will be used for oil/water flow experiments. One of the cores is compact, the other has been cut in half to simulate a fracture. The two cores will be drained and imbibed at the same rates under the scanner. Pressure gradients and saturations will be measured. Numerical simulation will be used to deduce relative permeabilities.

Drying and Wetting Fluid Distribution

In a drying or wetting porous medium fluid distribution is important. Even in the simple case of water/air systems the wetting and drying behavior of various rock samples of permeability and porosity spanning a broad range needs to be investigated. Preliminary experiments have been performed on Fontainebleau and Berea cores in order to design a proper experimental procedure.

Validation of Other Nondestructive Measurements

For the calibration of measurement methods such as resistivity or acoustic propagation it is necessary to have the saturation distribution in the sample. Measurements of saturations by CAT scan will be compared with results obtained by resistivity and sonic velocity measurements on the same cores. Design and construction of a special coreholder is in progress. This work will be performed in cooperation with the Stanford Geophysics Department.

2.1 MODIFYING IN-SITU COMBUSTION WITH METALLIC ADDITIVES

(L. Castanier)

2.1.1 ABSTRACT

In-situ combustion is the most energy efficient of thermal enhanced oil recovery methods. In light oil reservoirs, too little fuel may be deposited and in very heavy oil reservoirs too much fuel may be deposited. A research program has been initiated to try to solve these problems. We decided to test water soluble additives to attempt to modify the fuel deposition reactions. In the first stage, kinetics experiments were run on Huntington Beach (18.5° API) and Hamaca, Venezuela (10.5° API) oils in the presence of aqueous solutions of metallic salts. The results were compared with control runs with no metal present. While the presence of copper, nickel and cadmium had little or no effect; iron, tin, zinc and aluminum increased fuel laydown for Huntington Beach oil. The results were similar for the heavier Hamaca oil as no reduction in fuel was noticed with any of the metallic additives. Ketals were mixed with Hamaca oil as a way to reduce fuel. No effect was observed when the ketals were used. Eight combustion tube runs were made in the second stage of the study. Metallic additives iron, tin and zinc improved the combustion efficiency in all cases. As a result, the front velocities were increased by the metallic additives. Changes were also observed in H/C ratio of the fuel, heat of combustion, air requirements and density of the crude produced. The amount of fuel deposited varied between the two oils. For Huntington Beach oil, the amount of fuel increased in the order: zinc, control, tin and iron while for the Hamaca crude the order was: control, iron and tin. To date we have not been able to find a suitable additive to reduce fuel deposition. Iron and tin salts seem suitable agents to increase fuel when that is needed.

2.1.2 INTRODUCTION

One of the methods used to recover heavy or medium gravity crude oils is in-situ combustion. During an in-situ combustion field project, air or oxygen is injected into the reservoir to burn part of the oil in place which generates a heat front propagating through the reservoir (Fig. 2.1.1). Heat is conducted forward by conduction, convection of the combustion gasses and condensation. The oil ahead of the combustion front is displaced by gas drive from the combustion gasses, by hot water and steam drive as well as miscible drive provided by the condensed light ends. The process is controlled by the kinetics of the combustion reactions as well as the deposition of the heavy portions of the crude on the rock matrix. The "fuel" burnt is the unrecoverable carbon rich residue deposited as a result of distillation, thermal cracking and some catalytic cracking. An important parameter for the economics of the process is the amount of air needed to recover a given volume of oil (air/oil ratio). This in turn depends on the nature and amount of fuel deposited. Two limits in the amount of fuel can exist:

- For very heavy crudes, too much fuel may exist, causing excessive air requirement.
- For light crudes, not enough fuel may be deposited to sustain the combustion.

The objectives of this work are to investigate means to modify the nature and the amount of fuel burned by adding water soluble additives to the system. General screening was performed by kinetics experiments and some of the most promising products were tested in our combustion tube.

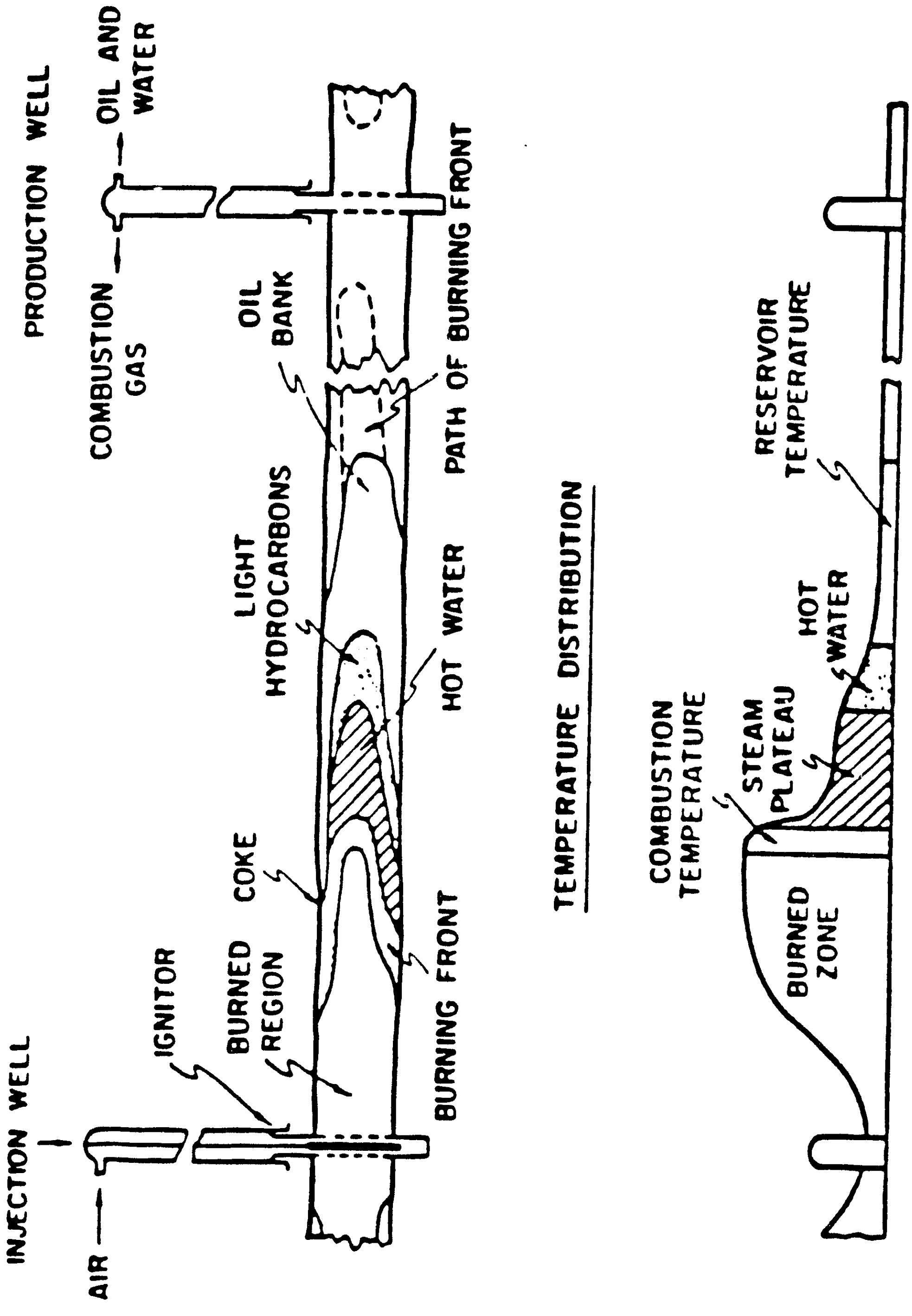

Figure 2.1.1 Cross Section of a Reservoir Subjected to In-situ Combustion.

2.1.3 KINETICS EXPERIMENTS

The oxidation of oil during in-situ combustion involves numerous competing reactions occurring over different temperature ranges. A common procedure involves subjecting a mixture of oil, water and reservoir rock to a linear heating schedule. The effluent gasses produced when passing air through the mixture are analyzed for oxygen and carbon oxides. Numerous studies (Bousaid and Ramey, 1968, Burger and Sahuquet, 1972, Fassihi et al., 1984) established that the reactions may be grouped in three classes of competing reactions occurring over different temperature ranges. The three classes are:

- Low temperature oxidation (heterogeneous gas-liquid reactions) produced no carbon oxides.
- Medium temperature fuel formation reactions (homogeneous in the gas phase).
- Heterogeneous high temperature fuel combustion reactions.

The rates of the three classes of oxidation are considered to be functions of the oxygen partial pressure and of the fuel concentration. Metals have long been recognized for their catalytic potential in both hydrocarbon cracking and oxidation reactions. In addition, two methods to reduce fuel laydown have been suggested in the literature. The first one involves injection of a ketone acetal (ketal). The second uses surfactant to increase the oil displacement by the water bank ahead of the front. We tested only the first case because of lack of information on thermal stability of surfactants at combustion temperatures.

Experimental Apparatus and Procedure

A cell is charged with a mixture of sand, oil and water, or an aqueous solution of the additive to be tested. The cell is heated at a constant rate of temperature increase while air is passed through the sample at controlled rate and pressure. The effluent gasses are analyzed for oxygen, carbon monoxide and carbon dioxide. The experimental apparatus and procedure are similar to the ones used by Fassihi et al. (1984). They are also discussed in detail by Shallcross et al. (1989). The main components of the equipment are shown on Fig. 2.1.2. The analysis of the data was performed using the method developed by Fassihi et al. (1984) and modified by Shallcross et al. (1989). The results are expressed in terms of classic kinetics parameters in terms of Arrhenius' constants and order of reaction for the partial pressure of oxygen. Table 2.1.1 gives some properties of the crudes and describes the additives used in the experimental program.

Results and Discussion

This section is only a short summary because of space limitations. More details can be found in De los Rios (1988) and Shallcross et al. (1989). Table 2.1.2 shows the kinetic parameters obtained for Huntington Beach oil for the low temperature, medium temperature and high temperature reactions. Figures 2.1.3 - 2.1.5 show the experimental data for selected additives. The presence of stannous chloride or ferrous chloride (Fig. 2.1.3 for example) increased the level of oxygen consumed in all three reactions with these additives. The reactions occurred at lower temperatures than for the control runs. Oxygen consumption and carbon oxides production started at lower temperatures and increased in magnitude. Table 2.1.2 shows that significant changes in reaction order, activation energy and pre-Arrhenius constant were also observed for these two additives. Cupprous sulfate nickel and cadmium did not affect the results.

Table 2.1.1 Crude Oil Properties and Kinetics Program

Crude Properties

Source	Huntington Beach	Venezuela
Gravity (°API)	18.5	10.5
%C	84.50	82.61
%H	11.53	10.47
Atomic H/C Ratio	1.64	1.52

Kinetics Program

Additive	Molar Concentration of Additive (mole %)	Pressure (psig)
None	--	80
None	--	43
$FeCl_2 \cdot 4H_2O$	1.99	79
$FeCl_2 \cdot 4H_2O$	1.99	43
$SnCl_2 \cdot 2H_2O$	2.02	82
$SnCl_2 \cdot 2H_2O$	2.02	39
$CuSO_4 \cdot 5H_2O$	1.01	81
$CuSO_4 \cdot 5H_2O$	1.01	40
$ZnCl_2$	1.90	83
$MgCl_2 \cdot 6H_2$	1.98	83
$K_2Cr_2O_7$	2.02	80
$Al_2Cl_3 \cdot 6H_2O$	2.00	82
$MnCl_2 \cdot 4H_2O$	2.00	80
$Ni(NO_3)_2 \cdot 6H_2O$	2.00	40
$3CdSO_4 \cdot 8H_2O$	2.00	40

Table 2.1.2 Kinetic Parameters for Temperature Oxidation

Additive	Pressure (psig)	n_H	E_H/R ($°K \times 10^{-3}$)	β_H
High				
None	80	0.8	12.4	3.8×10^5
None	43	0.7	12.7	6.1×10^5
$FeCl_2$	79	1.2	18.4	2.5×10^8
$FeCl_2$	43	0.9	15.5	2.1×10^7
$SnCl_2$	82	1.0	14.0	1.3×10^6
$SnCl_2$	39	0.8	15.5	2.6×10^7
$CuSO_4$	81	0.7	11.9	4.9×10^5
$CuSO_4$	40	0.8	14.3	6.4×10^6
$ZnCl_2$	83	0.8	11.0	3.2×10^4
$MgCl_2$	83	0.9	12.4	2.1×10^5
$K_2Cr_2O_7$	80	0.9	11.5	6.7×10^4
Al_2Cl_3	82	0.8	12.5	3.2×10^5
$MnCl_2$	80	0.8	12.6	3.2×10^5
$Ni(NO_3)_2$	40	0.8	14.5	7.3×10^6
$CdSO_4$	40	0.8	15.4	2.1×10^7
Medium				
None	80	0.9	8.67	6.3×10^3
None	43	0.9	8.65	4.4×10^3
$FeCl_2$	79	1.0	7.62	2.0×10^2
$FeCl_2$	43	0.9	8.37	4.5×10^3
$SnCl_2$	82	1.1	9.03	3.9×10^3
$SnCl_2$	39	1.3	10.1	3.1×10^3
$CuSO_4$	81	0.8	8.22	4.5×10^3
$CuSO_4$	40	1.0	8.17	8.3×10^2
$ZnCl_2$	83	1.1	10.3	4.0×10^4
$MgCl_2$	83	1.2	10.7	2.7×10^4
$K_2Cr_2O_7$	80	1.2	10.5	2.8×10^4
Al_2Cl_3	82	1.0	8.52	2.9×10^3
$MnCl_2$	80	1.0	9.11	1.0×10^4
$Ni(NO_3)_2$	40	1.2	10.5	1.6×10^4
$CdSO_4$	40	1.3	10.3	5.9×10^3
Low				
None	80	0.9	8.15	9.6×10^3
None	43	0.9	8.17	5.6×10^3
$FeCl_2$	79	0.8	6.24	5.8×10^2
$FeCl_2$	43	0.8	5.90	2.4×10^2
$SnCl_2$	82	0.8	7.33	3.5×10^3
$SnCl_2$	39	0.7	6.11	3.8×10^2
$CuSO_4$	81	0.8	8.41	3.2×10^4
$CuSO_4$	40	0.7	8.47	2.7×10^4
$ZnCl_2$	83	0.8	7.51	5.5×10^3
$MgCl_2$	83	0.8	6.70	8.8×10^2
$K_2Cr_2O_7$	80	0.7	5.87	4.0×10^2
Al_2Cl_3	82	0.8	6.64	1.0×10^3
$MnCl_2$	80	0.7	6.48	1.1×10^3
$Ni(NO_3)_2$	40	0.7	6.98	2.1×10^3
$CdSO_4$	40	0.7	6.22	5.3×10^2

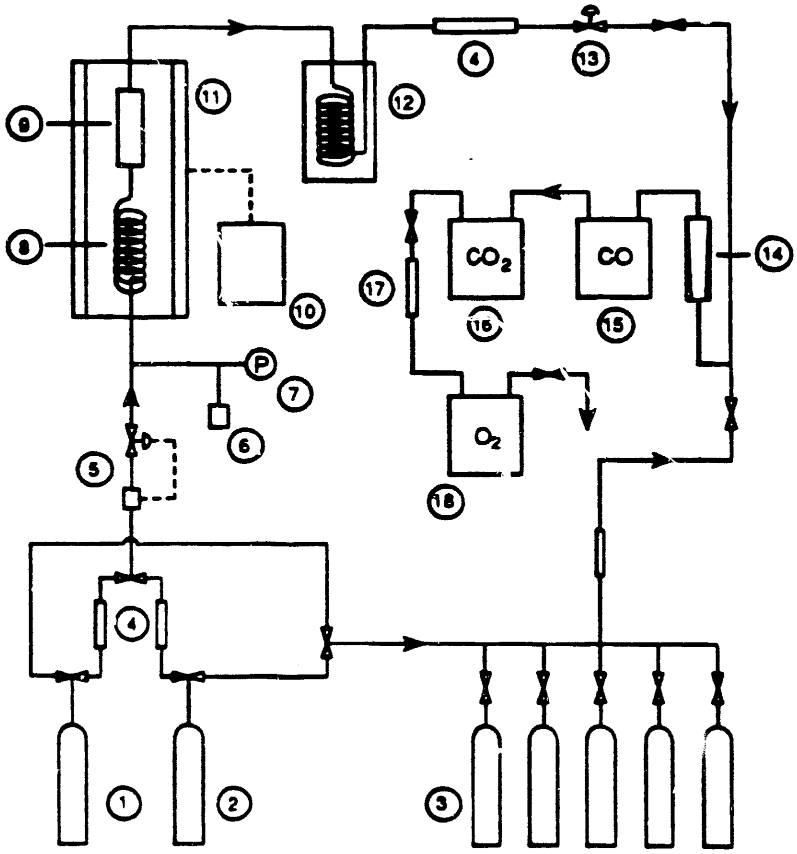

1 Air supply
2 Nitrogen supply
3 Analyzer calibration gases
4 Dryer
5 Mass flowrate controller
6 Pressure transducer
7 Pressure gauge
8 Preheating coil
9 Combustion cell
10 Oven temperature controller
11 Oven
12 Production gas condenser
13 Backpressure regulator
14 Rotameter
15 Carbon monoxide analyzer
16 Carbon dioxide analyzer
17 Acid gas scrubber
18 Oxygen analyzer

Figure 2.1.2 Schematic Representation of the Kinetics Studies Apparatus.

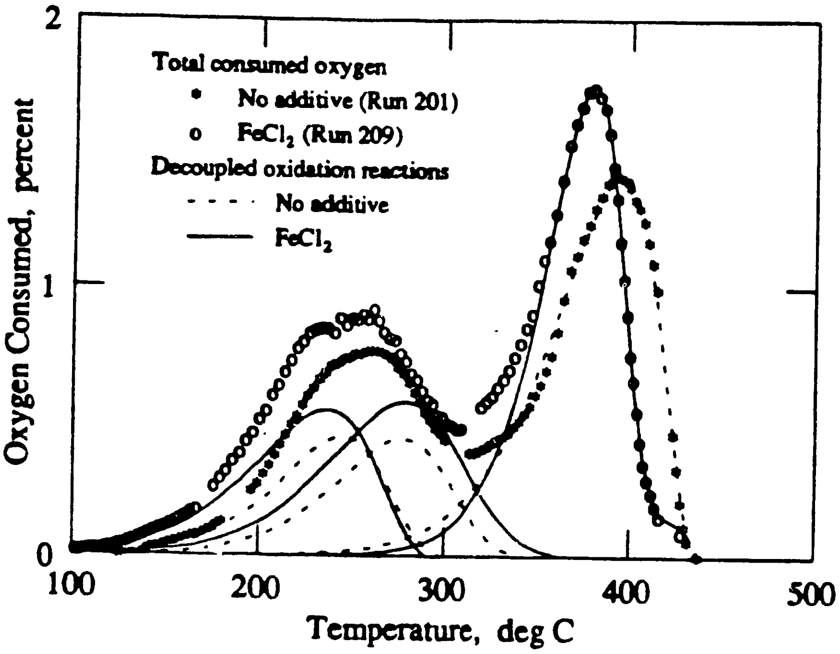

Figure 2.1.3 Effect of $FeCl_2$ Additive.

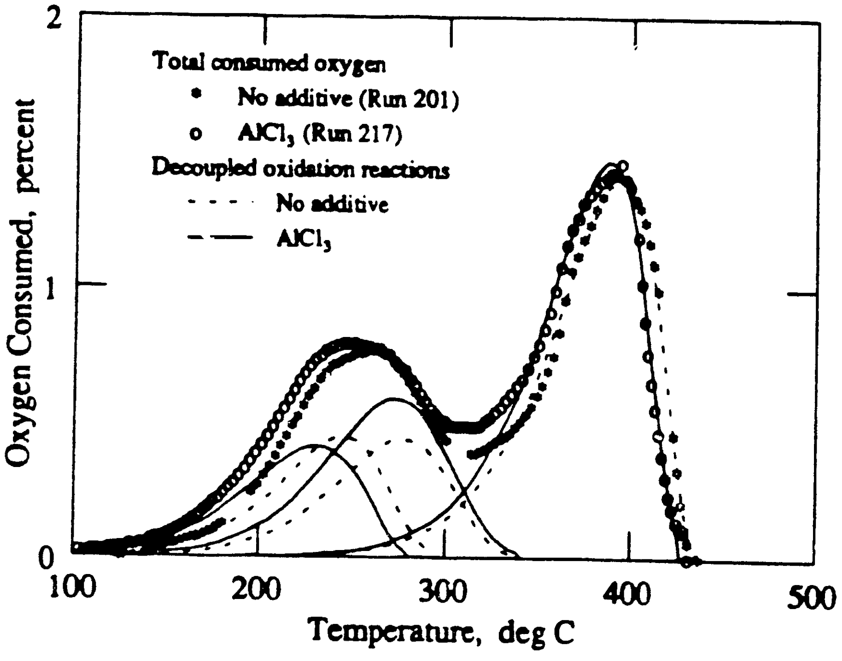

Figure 2.1.4 Effect of $AlCl_3$ Additive.

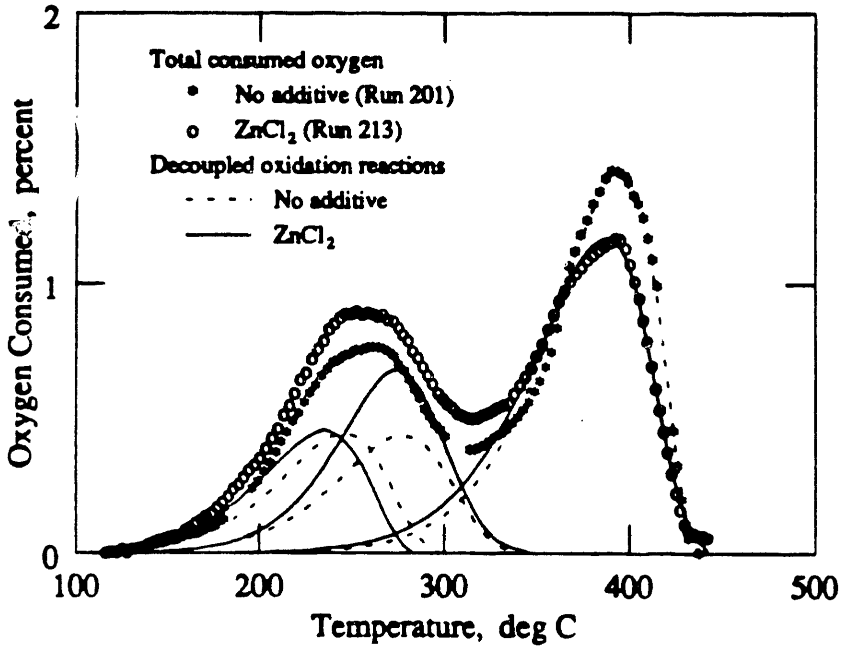

Figure 2.1.5 Effect of $ZnCl_2$ Additive.

Aluminum chloride merely shifted the temperature peak to a lower temperature (Fig. 2.1.4). Manganese has a similar effect. Zinc, chromium and magnesium increased oxygen consumption at lower temperature but decreased it over the higher temperatures (Fig. 2.1.5). The order of the low temperature reactions is relatively insensitive to the additives while a slight increase was observed in the order of the middle temperature reactions with additives. Iron and tin significantly increased the order of the high temperature reactions. For the heavier Venezuelan oil (Fig. 2.1.6), the high temperature combustion peak is more pronounced; this observation supports the conclusion that more fuel is laid down by the Hamaca oil than by the Huntington Beach oil. A ketal was added to the mixture for one run performed with Hamaca oil. If anything the fuel deposition increased slightly.

2.1.4 COMBUSTION TUBE RUNS

The kinetics experiments showed changes in the reactions of combustion caused by the presence of metallic additives. In order to obtain quantitative information on the amount and nature of the fuel formed and the air required to propagate a combustion front, it is necessary to experimentally simulate an in-situ combustion project via tube runs. Only a few combustion tube experiments have been performed to study the effect of metallic additives as catalytic agents for in-situ combustion (Racz, 1985). Based on the results of the kinetics studies a combustion tube runs program was implemented.

Experimental Apparatus and Procedure

The equipment is similar to the one used by a number of researchers at Stanford University (Satman, 1982, Fassihi et al., 1984). A schematic diagram of the system is shown on Fig. 2.1.7. The tube itself is a thin walled stainless steel cylinder of 7.6 cm diameter and 1 m length. The tube is packed with a mixture of sand, clay, oil and water or water containing the additive. Ignition is started by an electric heater at the top of the tube and combustion propagates vertically from top to bottom. Temperatures are monitored via a central thermal well. Pressures and exit gas compositions as well as flow rates are continuously measured. Fluid samples are collected and analyzed. All runs were carried on at the same flow rates, pressures and initial temperature levels. Table 2.1.3 summarizes the experimental program for Huntington Beach Oil. Hamaca oil was also tested with iron and tin additives at the same experimental conditions.

Results and Discussion

The data obtained in the tube runs were analyzed using the classic procedure of Dew and Martin (1964,1965). Some observations can be made at this stage.

Front temperatures: The temperature profiles taken during the runs exhibit distinct regions (Fig. 2.1.1). Ahead of the combustion front, there is a region at reservoir temperature. This is followed by a region where the temperature increases due to heat transfer ahead of the steam plateau. Next is the steam plateau where the temperature is constant. All of our runs having been performed at the same pressure, the steam plateau temperature ranged from 129°C to 132°C. Next the temperature rapidly increases until peak temperature is reached at the combustion front. The region behind the front shows decreasing temperatures caused by heat losses and heating of the injected air. The front temperatures for the control runs for Huntington Beach oil averaged 500°C. For stannous chloride they were around 535°C while for iron and zinc they were slightly lower than for the control runs. Temperature behavior was similar for the Hamaca oil. One must notice that the combustion front velocities increased with the presence of metallic additives.

Table 2.1.3 Summary of Combustion Tube Runs

Operating Pressure: 100-105 psig
Operating Temperature: 50-75 °C
Air Flow Rate: 3.0 standard litres per minute.

Run Designation	Control Run	Ferrous Chloride $FeCl_2.4H_2O$	Stannic Chloride $SnCl_4.5H_2O$	Zinc Chloride $ZnCl_2$
Length of Pack, cm	90.77	83.06	91.15	89.90
Porosity	35.73	35.00	39.10	39.27
Oil Saturation, %	37.47	38.67	32.43	32.21
Water Saturation, %	27.05	27.92	23.41	23.25
Concentration of Metal Salt in Water, wt. %	0.00	1.0	1.0	1.0
Vol. Oil/Vol. Rock	20.828	20.824	20.821	20.828
Vol. Water/Vol. Rock	15.035	15.031	15.030	15.034

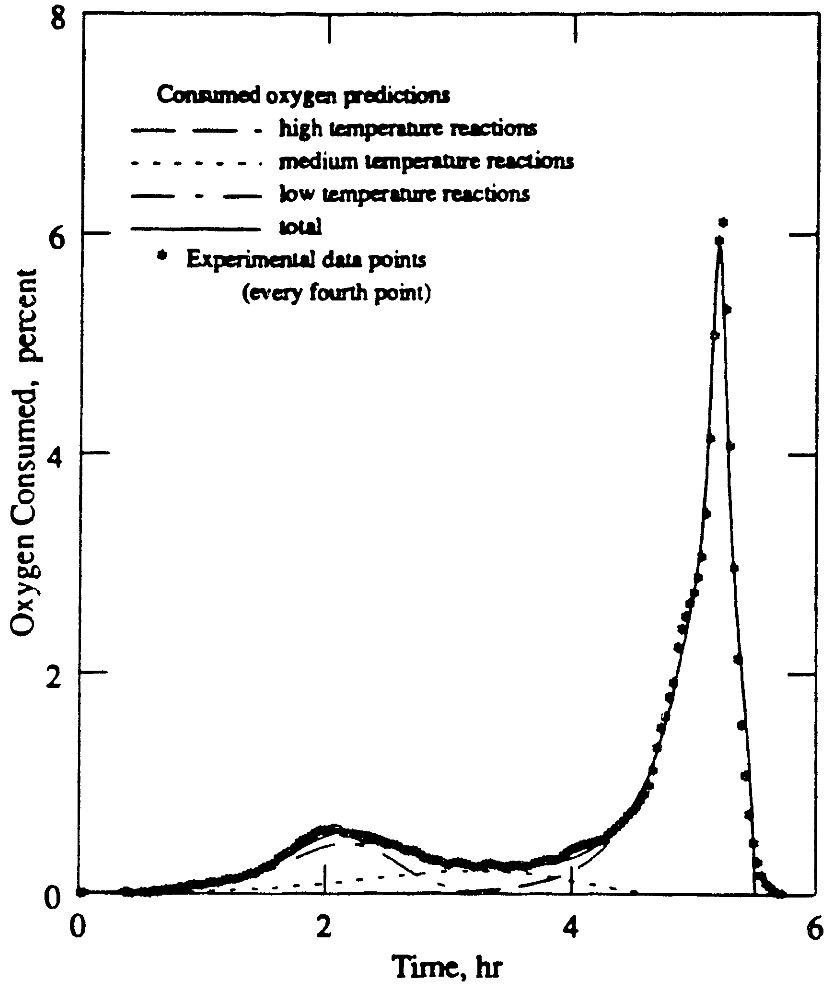

Figure 2.1.6 Oxygen Consumption for Venezuelan Oil Without Additive.

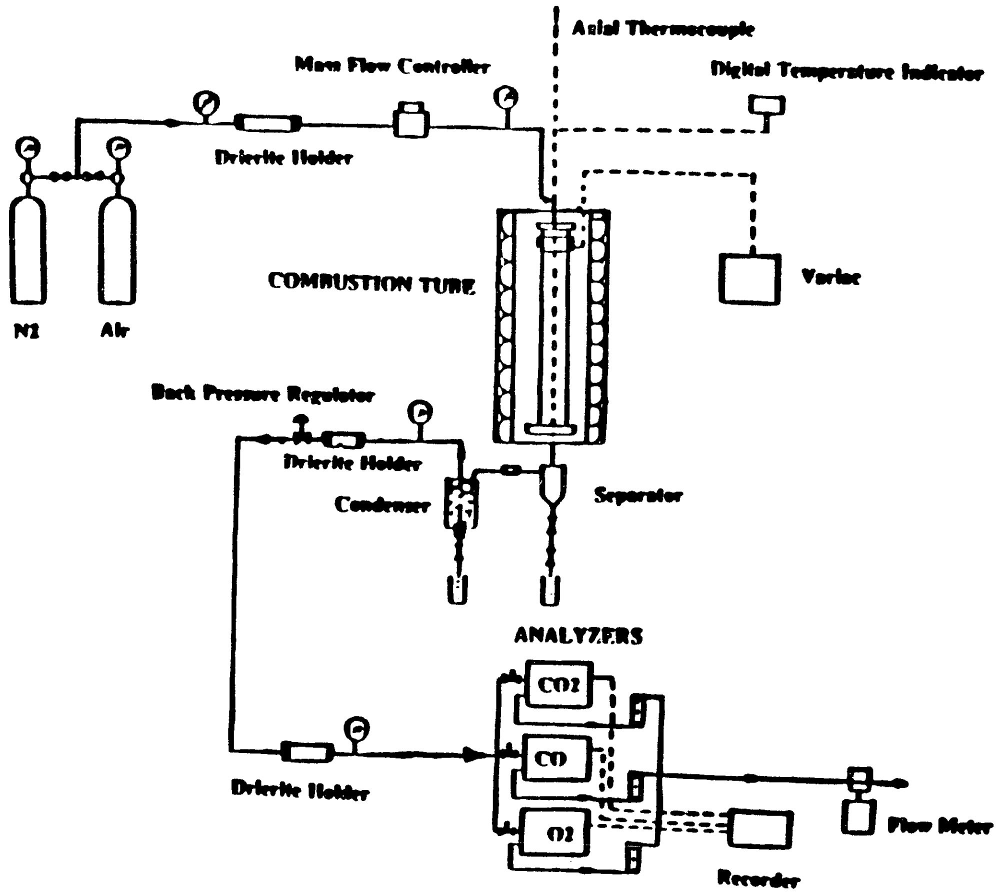

Figure 2.1.7 Schematic Diagram of the Tube Runs System.

Oxygen utilization and produced gasses: In the control runs, an average of 4 to 5 % oxygen was produced unreacted at the end of the tube. This amount was reduced to 1.3% by addition of iron in the Huntington Beach oil case and decreased to almost nothing when using tin for both oils as well as when using iron for Hamaca oil. Conversely the CO_2 produced increased in the order: control tin and iron; while the CO produced increased in the order: iron, control and tin. The CO_2/CO ratio m increased for both oils in the order: control tin and iron, ranging from 2.2 to 3.7. The H/C ratio of the fuel burnt n can be calculated from the produced gasses (Alexander et al., 1962). The two oils tested exhibited different behaviors. While for the 18.5 API Huntington Beach oil n increased in the order control, iron and tin ranging from slightly over 0 to 0.9, n for the 10.5API Hamaca oil increased in the order tin, iron and control and ranged from 1.2 to 1.8. We cannot explain this result at this stage.

Economic parameters: The economic parameters were calculated based on the gas produced with the exception of the amount of fuel burnt per unit volume of reservoir which has to be estimated from the front velocities and a material balance on the oxygen consumed. Although a detailed analysis of the results is outside the scope of this report and can be found in Baena (1990) and Tavares (1990) some comments can be made at this stage. The heat of combustion of the fuel which depends on its nature increased with the metallic additives for the lighter oil but slightly decreased for the heavy oil. The air required by unit mass of fuel burnt followed the same trends. The amount of fuel burnt per unit volume of reservoir was not changed for the lighter oil but increased in the order control, iron and tin for the heavier oil. Air/oil ratios decreased in the order control, tin and iron ranging from 14.3 to 11.5.

2.1.5 CONCLUSIONS

The metallic additives cause changes in the nature and the amount of fuel formed during an in-situ combustion process. These changes appear to depend on the type of oil used. Crude oil may be affected differently by different additives. The rock matrix in these experiments was sand and clay. It would be useful to repeat these tests with reservoir cores. The efficiency of various metals as additives does not follow the usually admitted order for cracking reactions that form coke. In general metallic additives increase the amount of fuel deposited and seem to be applicable to light oil projects where the fuel deposited without additives is not enough to sustain combustion. In heavy oil reservoirs, the presence of metals may render the process uneconomic because of increased air requirements. To date no additive has been found to decrease the fuel burnt.

2.2 KINETICS OF COMBUSTION
(D. Mamora)

Based on the frontal advance (FA) model (Tadema, 1959), the steam zone ahead of the combustion front drives a condensed hot water zone which in turn drives a cold water front and the original oil. In the steam zone, distillation of the oil would occur, leaving behind the heavier oil components as residual oil. This residual oil provides the fuel available for combustion. Logically, the denser the oil, the greater the amount of residual oil, and hence, fuel availability. This conclusion appears to be corroborated by the experimental work of Showalter (1953), which indicates an increase in the amount of fuel burned with decreasing API oil gravity. Research in SUPRI-A on the effect of steam distillation on residual oil is given in Section 2.3.

The fuel concentration at the combustion front, an important parameter for project evaluation and design, is probably the least understood parameter in in-situ combustion. This research is being carried out to obtain a better understanding of the kinetics of combustion, and is aimed at answering two basic questions:

(a) What constitutes fuel?

(b) What are the parameters that determine fuel deposition?

Two other factors affect the fuel concentration at the combustion front. Firstly, at the combustion front, the temperatures are significantly higher than the temperature in the steam zone. For high temperature oxidation (HTO) — at temperatures in excess of some 650°F — cracking occurs, resulting in the formation of lighter oil components, part or all of which can be displaced ahead of the combustion front. This would then result in a decrease in the fuel concentration. Secondly, low temperature oxidation (LTO) — ahead of the combustion front and at temperatures less than some 650°F — has been indicated to result in an increase in the fuel concentration (Alexander, et al. 1962).

From the foregoing, it is clear that the kinetics of the combustion reactions are rather complex. The main objectives of this research will be to investigate the following.

(i) The nature and amount of fuel and produced fluids.

(ii) The effect of varying oxygen concentration and pressure on the kinetics of combustion.

Kinetic cell and combustion tube experiments are planned, varying the type of crude and sand, oil saturation, air flux and, for kinetics experiments, the oxygen concentration and pressure. The oil will be analyzed for both composition and type (paraffin, aromatic and asphaltene ratios).

2.2.1 PROGRESS TO DATE

Research work commenced six months ago. Most of the time was spent in setting up the kinetics/combustion laboratory, as summarized below.

1. All previous equipment was dismantled and mounted on panels for safe and easy operation. Gas and liquid flow lines were replumbed, 1/8 inch steel tubings being used wherever possible to minimize fluid travel time from the combustion source to the measuring instruments. Electric cable routing was modified for safe operation. A 10 psi pressure relief valve and an acid scrubber were installed in the sample gas stream prior to the

Beckman CO and CO_2 analyzers to avoid accidental damage to these instruments. A new water cooled condenser was constructed to serve both the kinetic cell and the combustion tube. Instead of having a manifold at the calibration gas cylinders, a single gas line was installed between the measuring instruments and the calibration gas cylinder to be sampled to avoid contamination.

2. A gas chromatograph (HP 5710A) was installed, incorporating two 8' × 1/8 in. Carbosphere packed columns (for measuring Nitrogen) and a Vici 8 port automatic gas sampler.
3. A high performance liquid chromatograph (Waters Model 440) was repaired and installed. The packed columns for oil composition analysis are yet to be selected and purchased.
4. An IBM-AT computer was installed and a program was written which enables the computer to both store data and control the measuring instruments via the HP 3497A data logger. In addition, CO_2, CO, O_2, N_2, thermocouple temperature and gas chromatograph readings can be continuously plotted on the computer screen. Further, the program also integrates the gas chromatograph readings and computes the Nitrogen percentage in the sample gas stream.
5. Fabrication of a new kinetic cell and of a combustion tube was completed.
6. Four crude oil samples were received. Three were from Thums Oil's Wilmington field and one from Esso Canada's Cold Lake field.

A schematic of the experimental set-up is shown in Fig. 2.2.1, while a schematic of the data acquisition and control system is given in Fig. 2.2.2.

The main problem to date has been the malfunction of the Beckman CO and CO_2 analyzers. After a lengthy investigation, it was determined that the detector cell windows in both analyzers were leaking. This caused concern since the detectors were replaced only about two years ago. Communication with the manufacturer indicated that the cause of these leaks was most likely the presence of HCl gas in the sample gas stream, which attacked the epoxy used to seal the detector windows. HCl gas was certainly produced in the sample gas during previous combustion experiments using metal additives, eg. $FeCl_2$, $SnCl_2$. Both detectors were then replaced, and an isolation cap was installed (Fig. 2.2.3) between the detector and sample gas cell to avoid direct contact between the sample gas and the detector window.

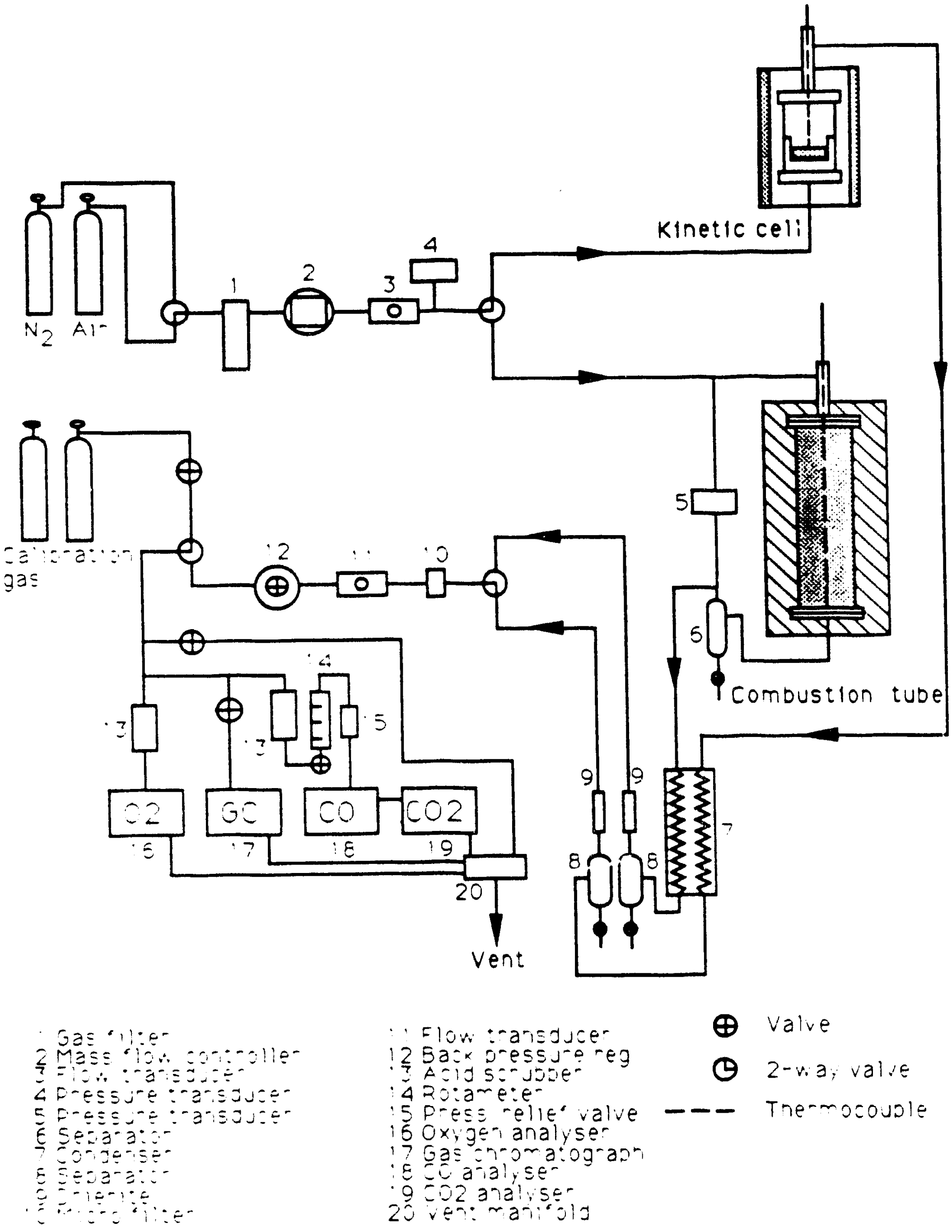

Figure 2.2.1 Schematic of Experimental Set-up.

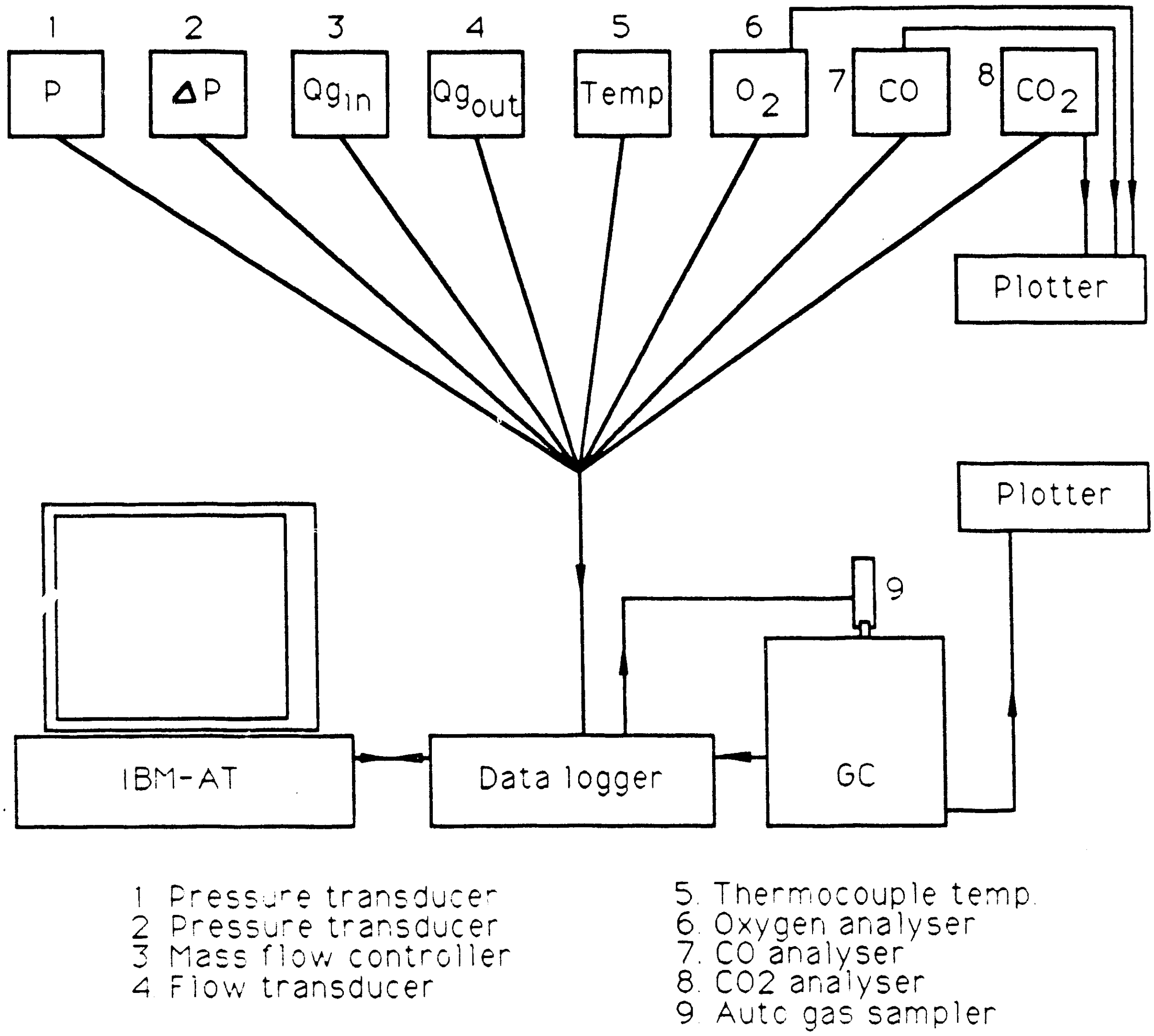

Figure 2.2.2 Data Acquisition/Control Schematic.

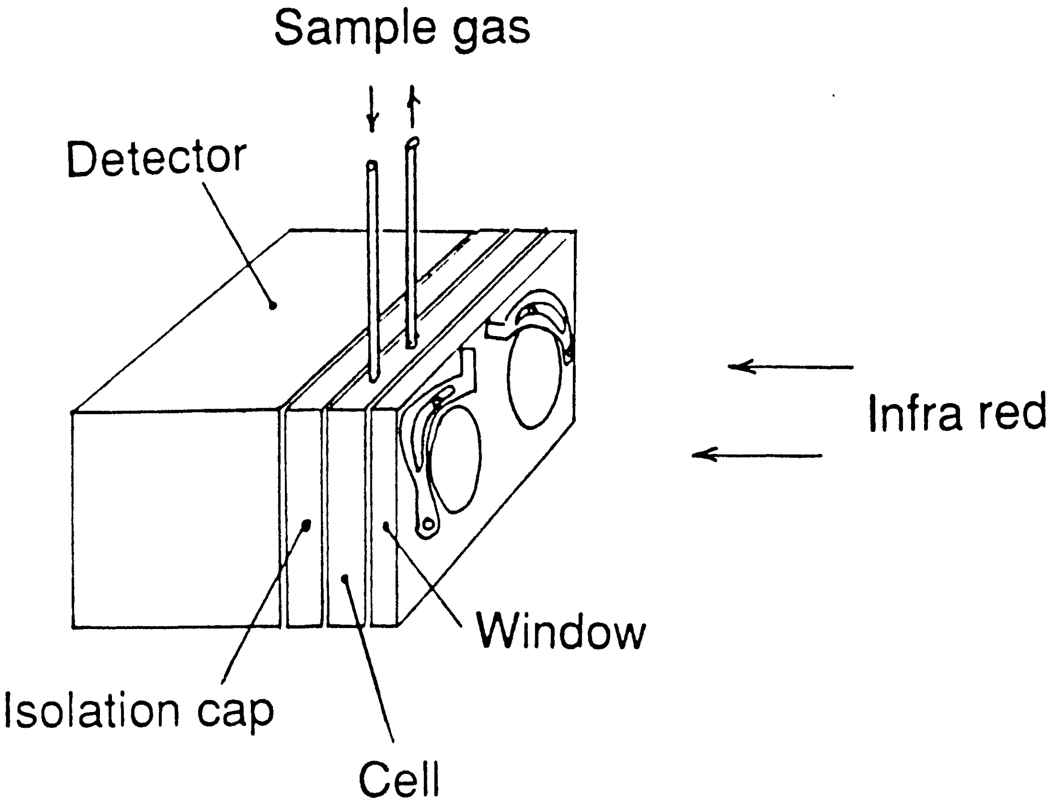

Figure 2.2.3 Schematic of Beckman Analyzer Detector.

2.3 STUDY OF RESIDUAL OIL SATURATION FOR STEAM INJECTION AND FUEL CONCENTRATION FOR IN-SITU COMBUSTION

(K. T. Lim)

2.3.1 ABSTRACT

Steam distillation is the main mechanism which reduces residual oil during steam injection. It is the main recovery mechanism in steamflooding of light oil reservoirs. It distills lighter components from the initial oil. The residuum becomes heavier. Mixing of the distilled components with initial oil ahead of steam front results in lighter produced oil. A generalized approach to quantify these quality changes has been developed for California crude. Application of the results to the determination of fuel concentration and hydrogen-to-carbon ratio for in-situ combustion will be investigated.

2.3.2 INTRODUCTION

In a steamflood four characteristic zones advance radially outwards. The steam zone drives a condensed hot water and hydrocarbon zone, which in turn drives a cold water front and reservoir oil. In essence a cold waterflood and then hot waterflood preceeds the steam zone. When there is steam override and gravity segregation, mixing of these zones may occur.

Willman et. al. (1961) studied the contributions of various recovery mechanisms associated with steam injection. They concluded that the principal mechanisms responsible for additional oil are thermal expansion of oil, viscosity reduction and steam distillation. Studies by Duerksen and Hsueh[2] concluded that steam distillation yields can be significant, even for heavy crudes.

Steam distillation is the main mechanism which reduces the residual oil behind the hot water front during a steamflood. Willman et. al. (1961) also concluded that the steam zone residual oil saturation is independent of initial oil saturation. At a given steam injection condition, the residual oil saturation is essentially composition dependent.

In reservoirs containing light oil, steam distillation is the major mechanism contributing towards improved recovery. The emergence of steam distillation drive as an important enhanced recovery method has been discussed by Belvins et. al. (1984).

Distillation of the in-situ crude oil causes the produced oil to be lighter than the initial oil. An increase of 2° to 4° API has been observed both during laboratory experiments (Willman et. al. 1961, Wu and Fulton, 1971) and field tests (Konopnicki et. al. 1979, Valleroy et. al. 1967, Volek and Pryor, 1972). Consequently, the residual oil in the steam zone has an increasing content of heavier components. Similar observations have been made during in-situ combustion field tests (Gates and Ramey, 1958). A major objective of this study will be to determine from the information available changes in quality of produced oil (compared to the initial oil). Existing laboratory and field data will be interpreted in the light of the findings.

Information regarding the quality change in residual and produced oil is not widely available in the literature. Konopnicki (1979) estimated that the residual oil API gravity decreased from 35.2 to 25.6 for the initial oil in the case of Shiells Canyon Field. Although other authors mentioned that residual oils were analyzed, no quantitative data appears to be available.

Information on the crude quality change during steamflooding can be useful. The amount and API gravity of the residual oil can be calculated from material balance. Information on residual oil can be related to the fuel concentration for in-situ combustion. During an in-situ combustion process, the mechanism ahead of the combustion region closely resembles a steamflooding process.

2.3.3 OBJECTIVES

This project has the following main objectives:

1. To develop a general procedure to quantify residual oil saturation and crude oil quality changes as a result of steam injection,

2. To correlate steamflood residual oil saturation and gravity with fuel concentration and hydrogen-to-carbon ratio for in-situ combustion, and

3. To verify the correlations experimentally.

2.3.4 STEAM DISTILLATION YIELDS

Steam distillation has been studied by many authors. The general observation is that steam distillation can be significant, even for heavy crudes. Attempts to correlate steam distillation yields with API gravity, viscosity, simulated distillation yields and other factors have been made. Wu and Brown, (1975) Wu and Elder (1983) observed a linear relationship between steam distillation yield and API gravity. Duerksen and Hsueh (1983) pointed out the effect of wax content on steam distillation yield and stated that the steam distillation yield for California crudes with low wax content is approximately

$$\% \text{ Yield} = 2 \times (^\circ\text{API})$$

Some steam distillation data found in the literature are plotted in Fig. 2.3.1. Each set of data displays some form of linear relationship. However, they are unique to the conditions at which the experiments were carried out.

It was also observed that the studies cited either the experimental temperature or pressure, and not both. It may be assumed that the experiments were carried out at saturated steam conditions. This is generally true. At a given temperature, the partial pressure of hydrocarbon at cut-off steam-oil ratios may become very small. The total pressure in the system will, therefore, be very close to the saturated steam pressure. As will be discussed later, it is important to measure both the temperature and pressures at which an experiment is conducted.

The correlations cited in the literature may be unique to the respective experimental conditions. Without a common basis, they may not be compared directly. A common basis of comparing these data is proposed below.

2.3.5 BUREAU OF MINES (BuMines) DISTILLATION DATA

The BuMines Routine Method Distillation database contains crude assay of all major reservoirs in the United States. Atmospheric distillation yields up to 527°F, and yields at 40mmHg and temperature up to 527°F are reported. Useful information can be retrieved from this database without having to resort to more complicated laboratory experiments.

Equivalent atmospheric distillation temperatures for sub-atmospheric pressure distillation conditions were determined using vapor pressure calculations. Vapor pressure charts of (Lee and Kesler, 1980) were used. With known vapor pressure and temperature, the equivalent normal boiling point, NBP, of the hydrocarbon can be determined. This NBP represents the equivalent atmospheric distillation temperature. Assumption was made here that at the 'cut' conditions vapor pressure is contributed solely by the heaviest distilled hydrocarbon component.

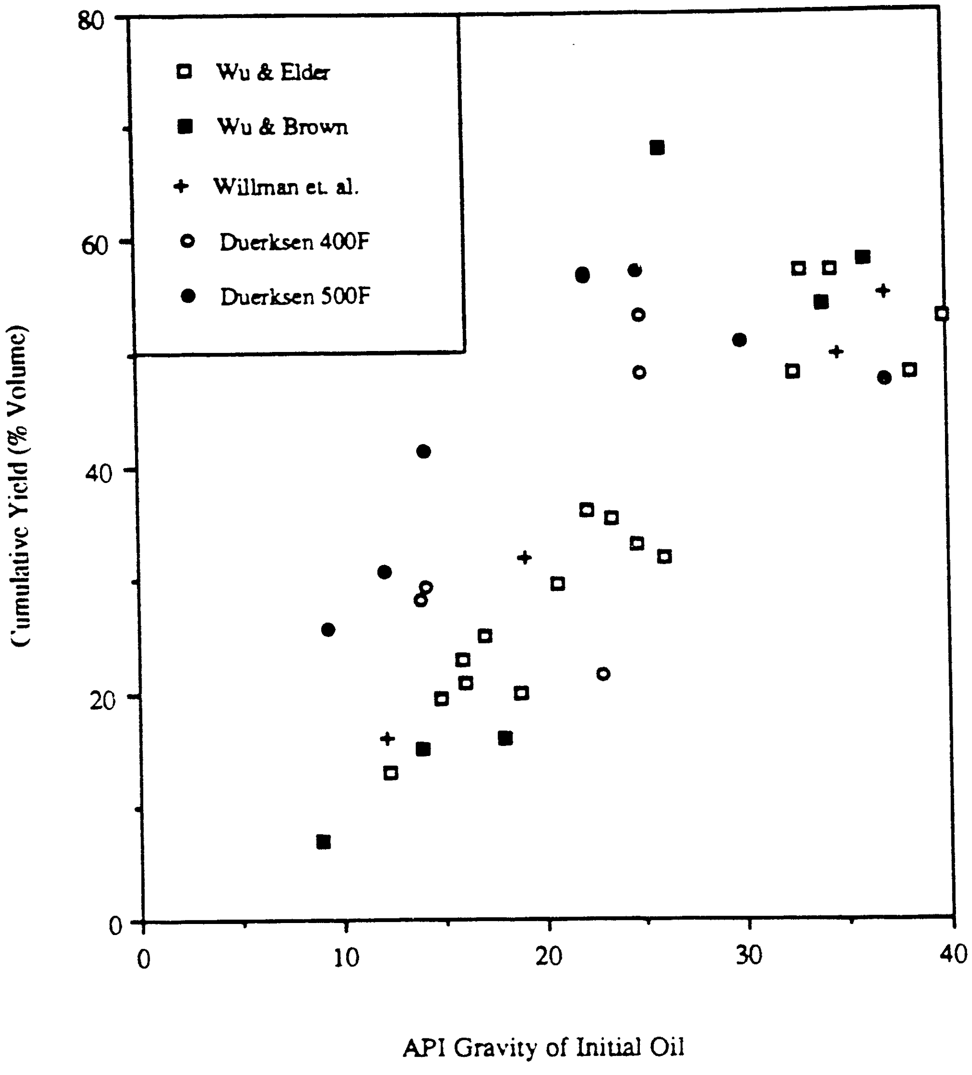

Figure 2.3.1 Steam Distillation Data From Literature.

In this study data from 71 California crude samples were analyzed. These data are extracted from a DOE report by Coleman et. al. (1978). Figure 2.3.2 shows the cumulative distillation yield as a function of API gravity for cut number 12. This is the equivalent gas-oil cut at 437°F and 40 mmHg. The equivalent normal boiling point is 634°F. A linear relation in the form

$$\% \text{ Yield} = 1.75 * {}^{\circ}\text{API of initial oil}$$

gives a satisfactory correlation. Cumulative yields for other distillation cuts are shown in Fig. 2.3.3. Where applicable, the equivalent normal boiling points are listed.

It is apparent from Fig. 2.3.3 that the cumulative yield is temperature dependent. Higher temperatures results in progressively higher yields.

2.3.6 COMPARING STEAM DISTILLATION DATA AND BuMines DATA

The equivalent atmospheric distillation temperature, or its equivalent NBP, of various steam distillation conditions can be calculated. This would enable comparison of steam distillation yields and BuMines data on a common basis.

Both the steam distillation temperature and pressure are required. Partial pressures of steam and hydrocarbon make up the total pressure. At a given temperature,

$$\begin{aligned}\text{Total vapor pressure} &= \text{vapor pressure of steam}\\ &\quad + \text{vapor of hydrocarbon}\end{aligned}$$

Vapor pressure of saturated steam at a given temperature can be easily determined, either from well known equations or physical data handbooks. Vapor pressure of the hydrocarbon being distilled should be the difference between the total pressure and vapor pressure of saturated steam.

Knowing the vapor pressure and temperature, the equivalent NBP of the hydrocarbon can be determined. A vapor pressure equation, or chart (Lee and Kesler, 1980) can be used. The NBP is the same as the equivalent atmospheric distillation temperature. In this way distillation yields at similar at NBP, or equivalent atmospheric distillation temperatures, can be compared directly.

As noted above, steam distillation data available in the literature quoted either the experimental temperature or pressure, not both. Comparisons are not possible at this moment.

A problem of similar nature arises in field applications. Measurements of both pressure and temperature in the reservoir may be scarce, or not available. Further studies into this aspect of the problem will be necessary.

2.3.7 CHANGES IN CRUDE OIL QUALITY

Steam distillation extracts lighter components of the initial oil. The residuum, therefore, must become heavier. Blending of the distilled portion with the initial oil ahead of the steam front results in lighter produced oil. This phenomena has been observed in steam injection projects. API Gravity of produced oil is some 2 to 4 degrees higher than the initial oil. Similar observation has also been made in in-situ combustion projects.

The change in API gravities can be calculated by material balance. Consider the oil as a two component system. One component is distillable and the other not distillable at a given condition. If API gravities of both the distilled component and residuum can be predicted, then the material balance can be accomplished.

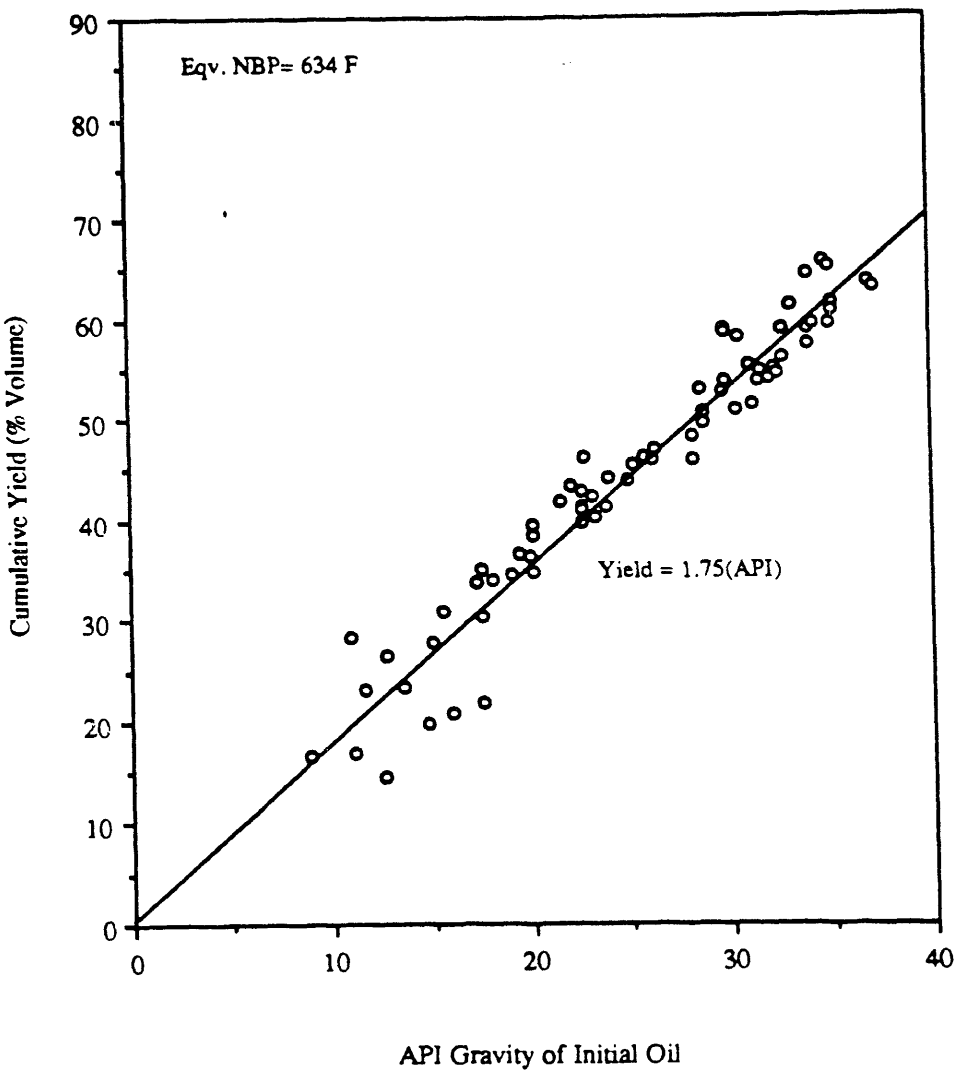

Figure 2.3.2 California Crude Distillation, BuMines Routine Method: Cumulative Yield to Cut #12 (437F, 40mmHg).

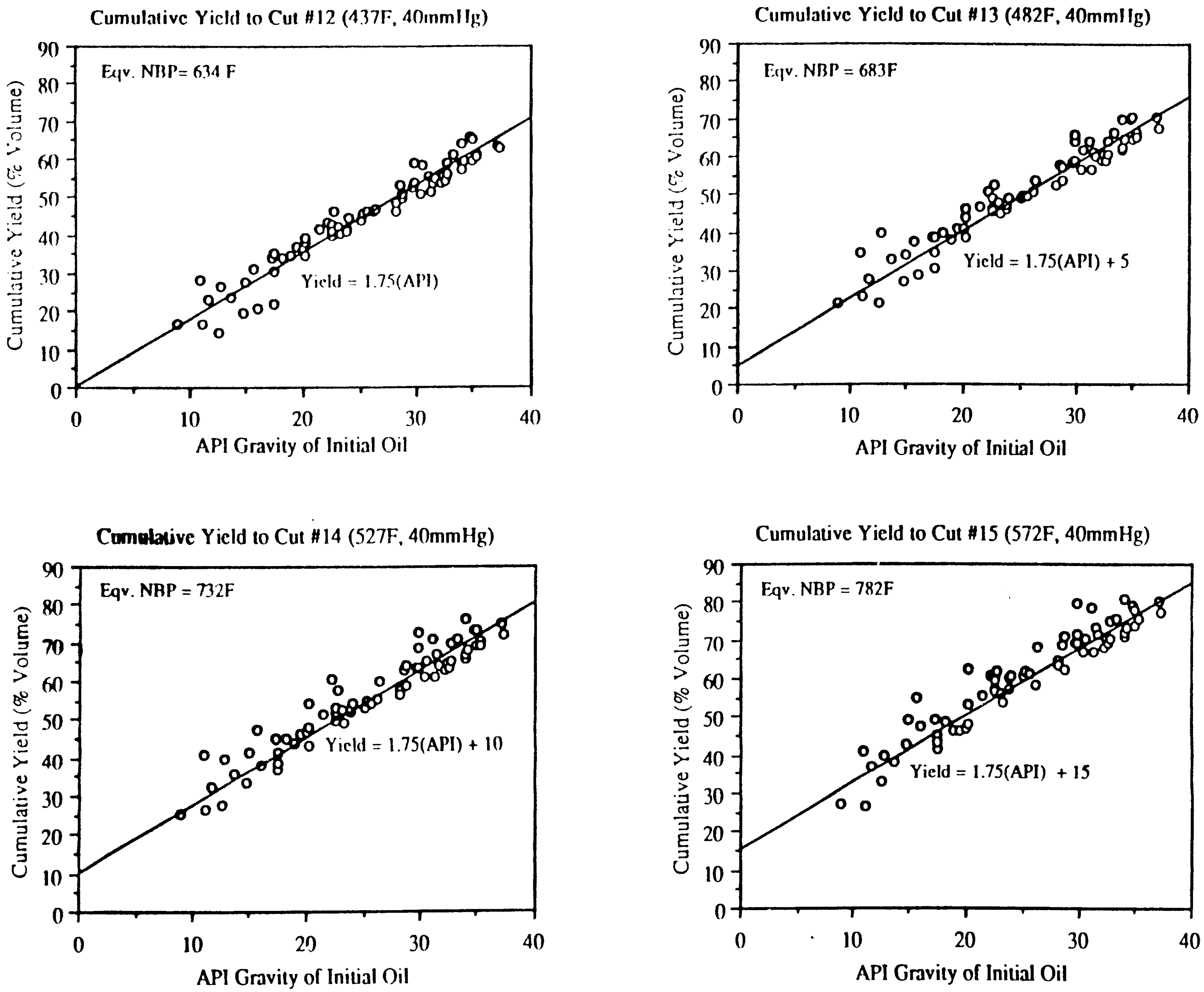

Figure 2.3.3 California Crude Distillation by BuMines Routine Method: Cumulative Yield at Various Cuts.

Figure 2.3.4 shows the distilled and residuum API gravities for California crude at a given distillation cut. The distilled portion is substantially lighter than the initial oil. For example light components distilled from a 15° API oil is about 36° API. This is more than twice the initial API. On the other hand, the reduction in API gravity of the residuum is less drastic. An oil initially of 15° API will have residuum of 11° API.

When the distilled component is mixed with the initial oil, change in the produced oil is evident. Figure 2.3.5 shows the effect of mixing one volume of distilled component with an equal volume of initial oil. The same set of data from Fig. 2.3.4 was used. A 2 to 4° API increase in the API gravity can be expected from oil initially at 10 to 20° API. This is consistent with laboratory and field observations.

The ratio of 1:1 mix is approximately what can be expected in the reservoir with steam override and gravity segregation. Plots similar to Fig. 2.3.5 for various distillation cuts, or equivalent normal boiling points do not display substantially different results.

It is apparent that a general approach to calculate the API gravity change of produced oil has been developed. The application of these correlations can be viewed in a different light. If the amounts and qualities of both the initial oil and produced oil are known, the amount and gravity of residual oil can be calculated. This information can be extended to the estimation of fuel concentration and hydrogen-to-carbon, H/C, ratio for in-situ combustion. Similar approach can also be used to predict the change in produced oil quality for in-situ combustion projects.

2.3.8 FUEL CONCENTRATION FOR IN-SITU COMBUSTION

Fuel concentration for in-situ combustion can be derived from residual oil saturation and gravity. Other factors such as rock type and surface area are also of importance and are being studied.

Another parameter of interest is the hydrogen-to-carbon ratio, H/C. It is proposed that the universal-oil-product constant, UOP K-factor, be used as a correlating parameter (Hougen et. al. 1954). Figures 2.3.6 and 2.3.7 are charts from which API gravity and H/C can be related. The UOP K-factor and boiling point can be determined from known API gravity and viscosity at 122°F (or 50°C) using Fig. 2.3.6. Figure 2.3.7 relates the UOP K-factor and boiling point to the per-cent hydrogen by weight. It can be translated to H/C ratio with ease. The possibility of integrating Figs. 2.3.6 and 2.3.7 into one relating API gravity and H/C ratio, with UOP K-factor as the variable will be investigated.

2.3.9 EXPERIMENTAL SETUP

An experiment is currently being set up. The main purpose is to verify the general correlation described above. A schematic of the experiment is shown in Fig. 2.3.8.

Sand pack in 2 inch ID, 20 inch long aluminum tubing will be steamflooded at constant temperature. Quality changes will be monitored. The construction of aluminum tubing allows for computer-aided-tomography, CAT, scanning. This will enable in-situ measurement of saturation profiles, before and after steam injection.

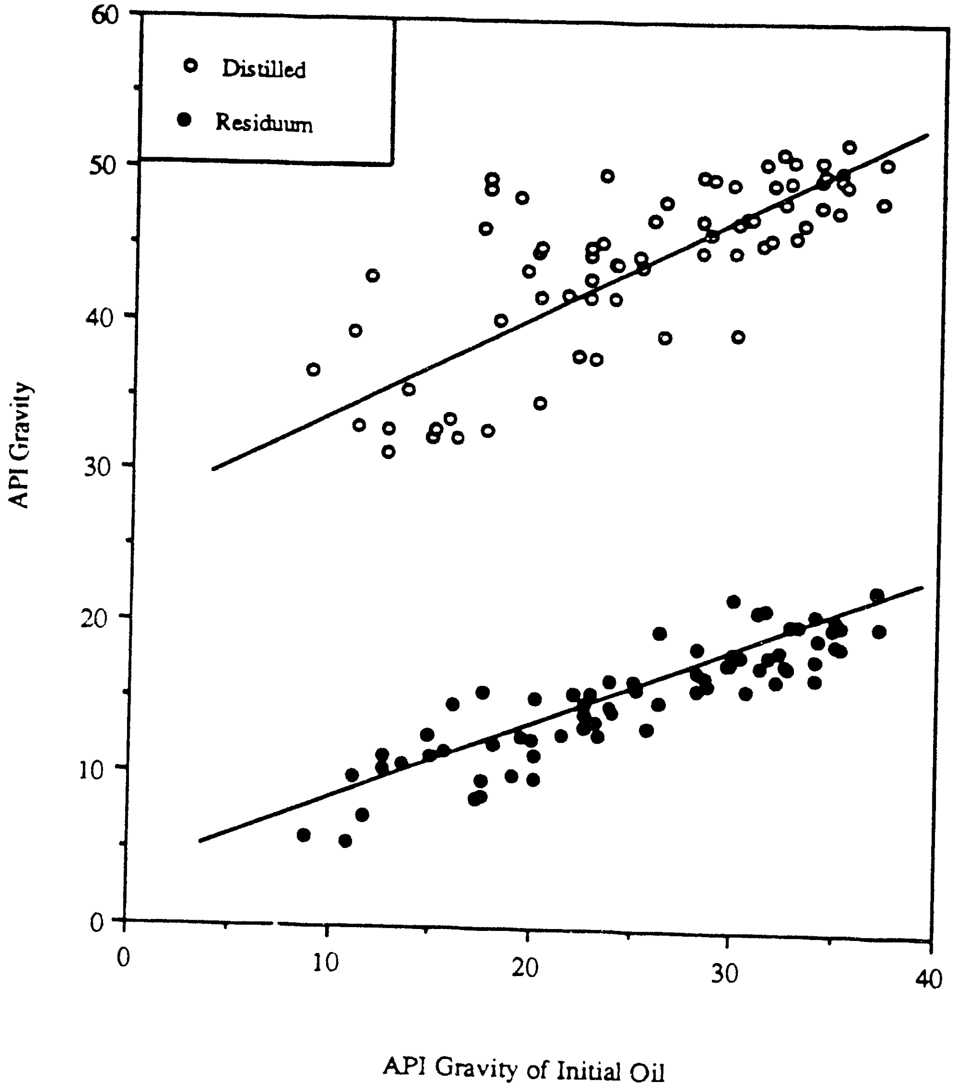

Figure 2.3.4 California Crude Distillation by BuMines Routine Method: Distilled & Residuum API, Cut = 527°F, 760 mmHg.

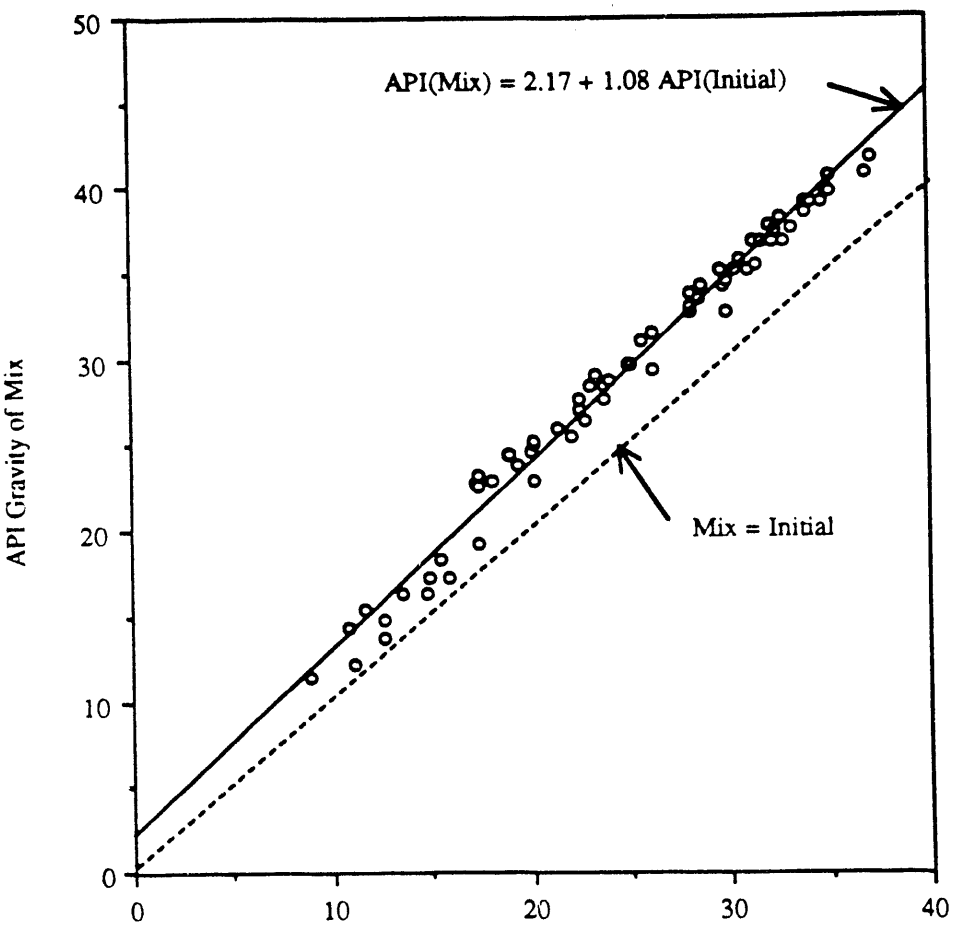

Figure 2.3.5 Gravity of Mix (Distilled + Initial Oil) (Ratio 1:1).

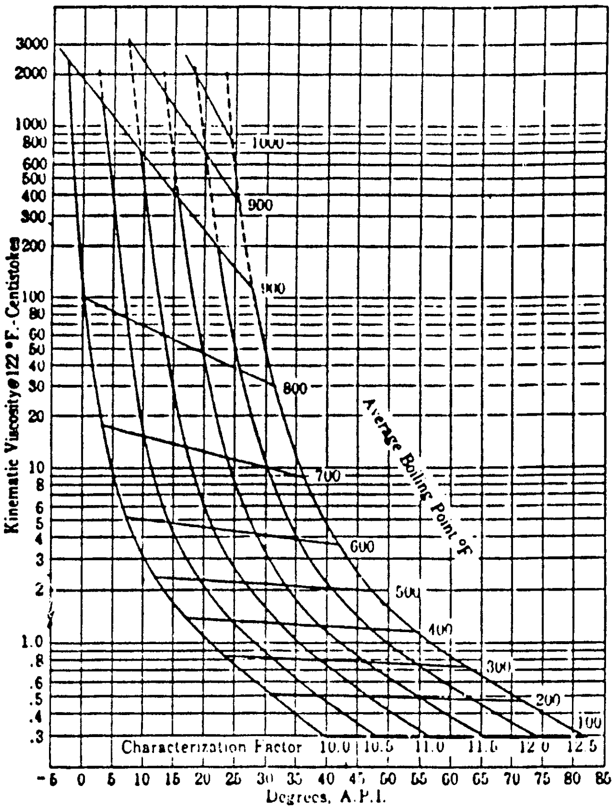

Figure 2.3.6 UOP Characterization Factor Correlation Chart.

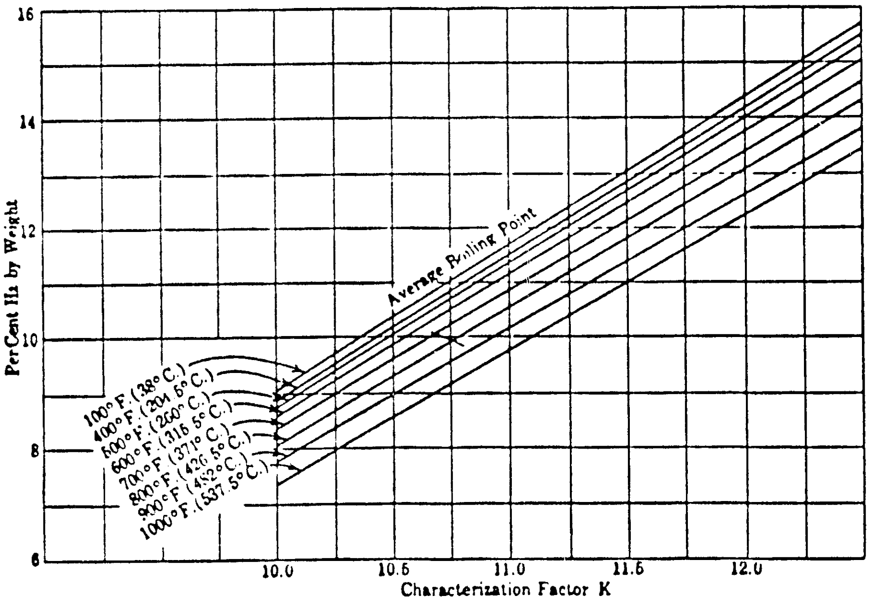

Figure 2.3.7 Characterization Factor vs. Weight % H_2.

(Source: Hougen et al., "Chemical Process Principles -- Part 1")

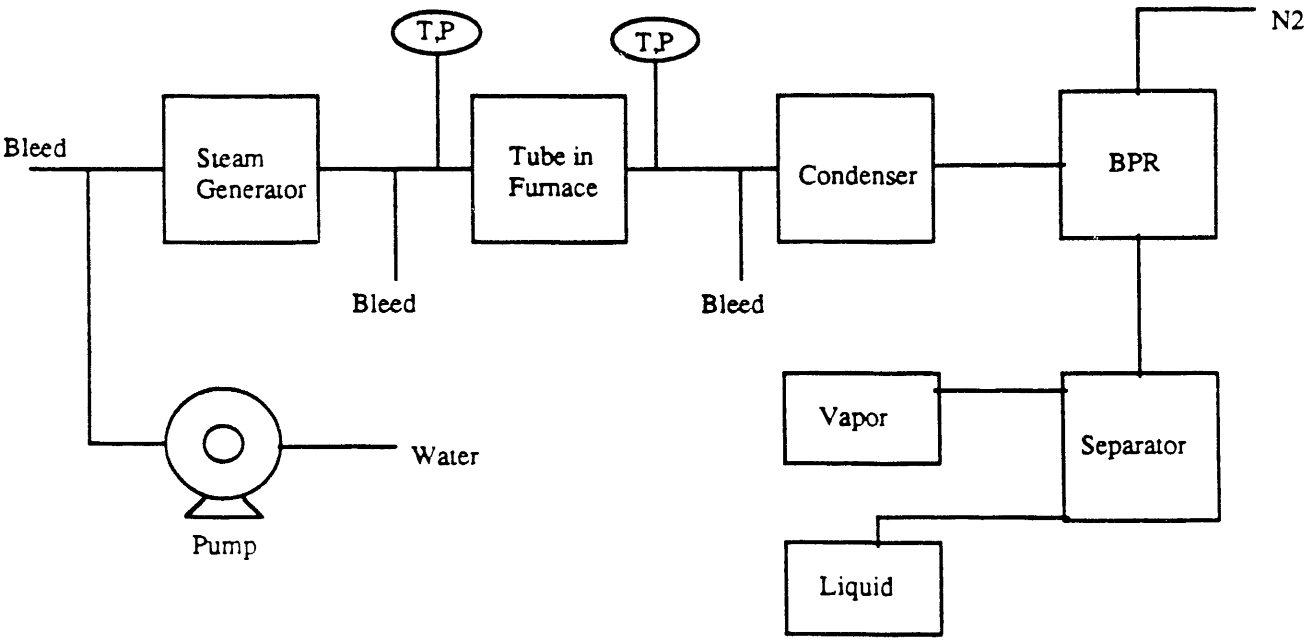

Figure 2.3.8 Schematic of Experiment Setup.

2.3.10 FUTURE WORK

Future works on this subject will comprise the following.

1. Material balance studies, using experimental and field data.
2. Steamflooding experiments.
3. Verification and further development of correlations and concepts.
4. Application of results of this study to field projects.

3.1 ANALYSIS OF TRANSIENT FOAM FLOW IN 1-D POROUS MEDIA WITH COMPUTED TOMOGRAPHY

(D. Liu)

3.1.1 ABSTRACT

Transient behavior is likely to dominate over most of the duration of a foam injection field project. Due to the lack of experimental data, little is presently known about transient foam flow. Foam flow does not follow established models such as the Buckley Leverett theory and no general predictive model has been derived. Therefore, experimental data are badly needed. Transient foam flow is being studied in a simple linear porous medium.

Foam is injected at a constant volumetric rate into a one-dimensional sandpack of 1-inch diameter and 24-inch length, initially saturated with distilled water. The system is placed in a CAT-Scanner. Data are accumulated at low temperature and pressure including the pressure field and saturations obtained by scanning. The liquid saturation can be obtained at each point of a cross section of the pack with less than 1% error over the range of interest. Calculations from the numbers obtained from the scanner show that the best spacial resolution available is a volume element (voxel) of 0.5×.5×5 mm. Hence a relationship can be found between saturation and pore volume injected for each location in the sandpack. Pressure profiles show that the pressure drop along the sandpack is not evenly distributed and varies with time. The pressure gradient is much greater between the injection end and the foam front than it is ahead of that front. Moreover, the pressure gradient keeps changing as the foam advances in the sandpack. It is this behavior that differs from the standard Buckley-Leverett theory. The CT-scan results demonstrate that foam displacement is not piston-like. Gas channeling appears near the front, and eventually the foam blocks all channels. The foam flows through the sandpack by continuously breaking and reforming. It takes several pore volumes of foam injection to reach residual liquid saturation.

The saturation versus pore volumes injected relationships for a given section of the sandpack have been matched with power law formulas. In general, the matches are satisfactory, however the exponents and constants in the formulas vary as a function of the position of the section considered. Graphing the data as saturation versus equivalent pore volumes injected reduces the range of these variations but does not eliminate them. We are unable to model this behavior to date.

Techniques of measurement of saturations by X-ray cat-scanning as well as interpretation of CT data were also presented this past year. This year we have focused on an attempt to model the process.

3.1.2 THEORETICAL AND COMPUTER MODELING

Basically, the idea is to treat foam as an infinite number of gas slugs with various viscosities displacing the in-situ fluid (water). The theory behind this is the fractional flow curve construction method (Lake, 1989). A computer program for this theory was written to facilitate the understanding and to incorporate the experimental data in to the model in the future.

To obtain the fractional flow curves, the relative permeabilities have to be determined first. In this case, the semi-empirical model is used as in the following equations:

$$k_{rw} = k_{rw}^{o} \left[\frac{S_w - S_{wc}}{1 - S_{wc} - S_{gr}} \right]^{n_w}$$

$$k_{rg} = k_{rg}^{o} \left[\frac{S_g - S_{gr}}{1 - S_{wc} - S_{gr}} \right]^{n_g}$$

where

k_{rw} --- water relative permeability
k_{rg} --- gas relative permeability
k_{rg}^{o} --- endpoint relative permeability for water at residual gas saturation
k_{rw}^{o} --- endpoint relative permeability for gas at irreducible water saturation
S_w --- water saturation
S_g --- gas saturation
S_{gr} --- residual gas saturation
S_{wc} --- irreducible water saturation
n_w --- relative permeability index for water
n_g --- relative permeability index for gas

Then the fractional flow of gas is calculated as:

$$f_g = \frac{M^o \, S^{n_g}}{M^o \, S^{n_g} + (1 - S)^{n_w}}$$

$$S = \frac{S_g - S_{gr}}{1 - S_{wc} - S_{gr}}$$

$$M^o = \frac{K_{rg}^{o} \, \mu_w}{K_{rw}^{o} \, \mu_g}$$

where

f_g --- fractional flow for gas
S --- reduced gas saturation
M^o --- gas-water endpoint mobility ratio
μ_w --- water viscosity
μ_g --- gas viscosity

As an example, the fractional flow curves are shown in Fig. 3.1.1 for a series of gas slugs displacing water with gas viscosities ranging from 0.02 cp to 20 cp. In between, the viscosities are calculated so that the later saturation profile is smooth. Here for numerical limits, only 20 different viscosities are considered.

Since the surfactant adsorption is significant at the foam (gas) front, it can not be neglected. The frontal advance loss can take a variety of forms. At this stage, Langmuir-type isotherm (Langmuis, 1915) is chosen as the basis, it will be modified if experimental data require it. Combining the fractional flow curve construction method and the frontal advance

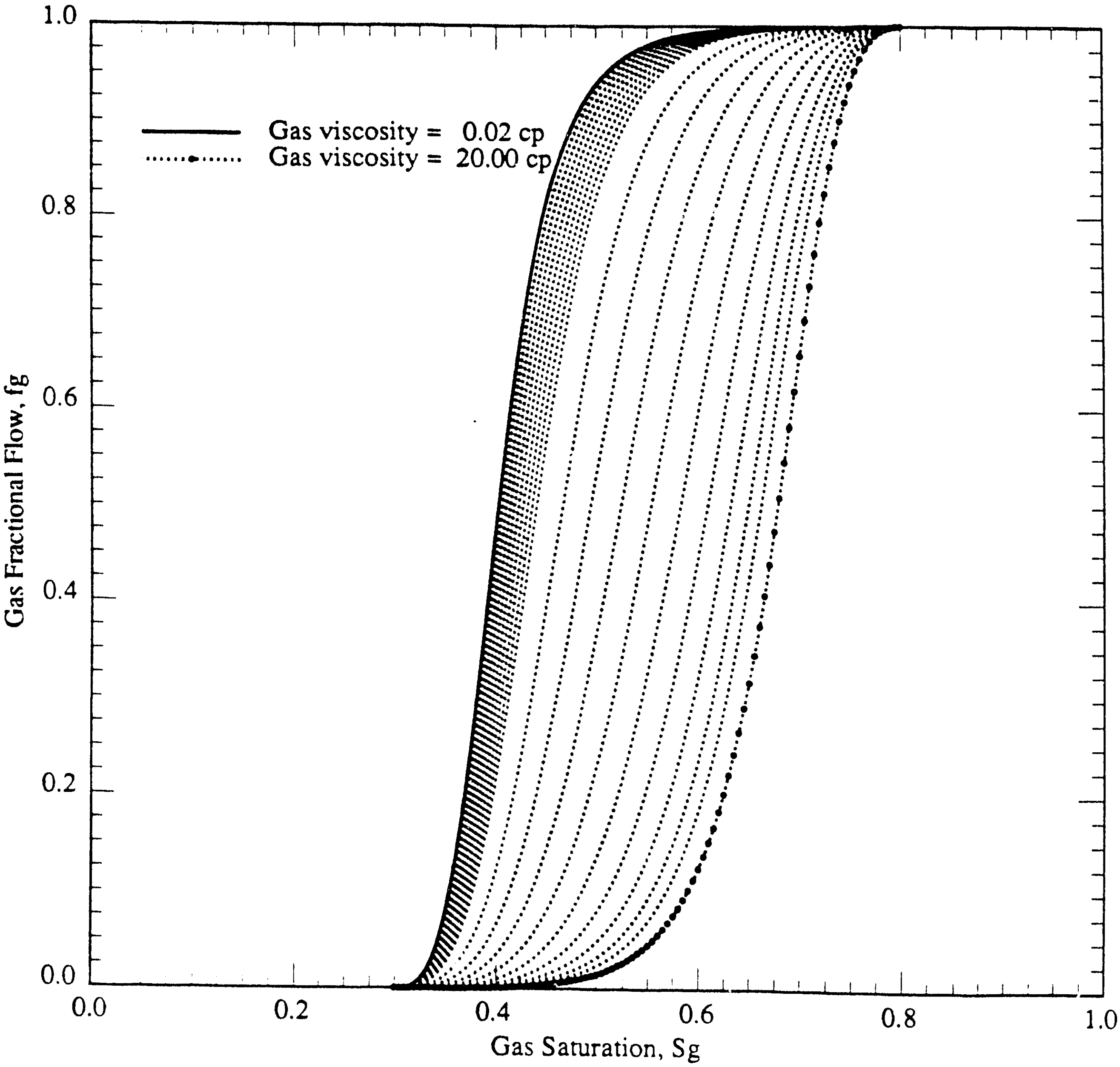

Figure 3.1.1 Fractional Flow Curves.

loss, the first gas shock velocity is calculated as:

$$\upsilon_1 = \frac{f_{g_1} - f_{g_o}}{S_{g_1} + D_1} = f_{g_1}'$$

$$D_1 = \frac{a}{1 + bC_1}$$

where

υ_1 --- first gas shock viscosity
f_{g_1} --- gas fractional flow at first shock
f_{g_o} --- gas fractional flow at initial condition
f_{g_1}' --- tangent of first fractional flow curve
S_{g_1} --- gas saturation at first shock
D_1 --- frontal advance loss of surfactants
a,b --- Langmuir constants
C_1 --- Surfactant concentration at first shock

The second and subsequent shocks are:

$$\upsilon_2 = \frac{f_{g_2} - f_{g_1}}{(S_{g_2} + D_2) - (S_{g_1} + D_1)} = f_{g_2}'$$

$$D_2 = \frac{a}{1 + bC_2}$$

where

υ_2 --- second gas shock velocity
f_{g_2} --- gas fractional flow at second shock
f_{g_2}' --- tangent of second fractional flow curve
6S_{g_2} --- gas saturate at second shock
D_2 --- frontal advance loss at second shock
C_2 --- surfactant concentration at second shock

According to the above two equations for shock velocities, the first shock velocity is equal to the slope of the tangent to the first fractional flow curve (the lowest gas velocity) starting from $f_g = 0$ and $S_g = -D_1$. As shown in Fig. 3.1.1, the tangential point on the curve gives rise to the gas flow fraction and the gas saturation for the first shock. The second shock velocity is the slope of the tangent to the second fractional flow curve (the next higher gas viscosity) starting from f_g (first shock) and S_g (first shock)-$(D_2 - D_1)$. The rest of the shocks are treated the same way. Then the material balance is taken into account to modify the shock velocities. Figure 3.1.2 shows the velocities for each shock represented by the dimensionless quantities: dimensionless distance X_D and dimensionless time t_D.

For a given time, the saturation profile can readily be obtained from the velocities of each shock, as shown in Fig. 3.1.3 at the time of 0.5. For comparison, the saturation profiles are also calculated for the cases of pure gas displacements at viscosities 0.02 cp and 20 cp, respectively.

Figure 3.1.3 is redrawn in Fig. 3.1.4 to enlarge the middle part by using reduced gas saturation vs. dimensionless distance.

The saturation profile can also be shown as the saturation vs. equivalent pore volume at a given location. Figure 3.1.5 is shown in the liquid saturation-EPV relationship at the outlet ($X_D = 1$).

The above theory is capable of explaining the gas channeling and adsorption observed in the experiments (discussed in the 1989 annual report). However, this is still in the category of Buckley-Leverett theory whereas foam flow is not. So it does not explain why experimental saturation profiles stretch differently at different locations.

3.1.3 FUTURE WORK

1. More experiments will be conducted.
2. Mixing theory will be added to the above-mentioned model to take care of the saturation profile stretching observed in the experiments.
3. Experimental data will be incorporated into the model.
4. Hopefully, a semi-analytical model can be derived from the computer modeling investigation combined with experimental data.

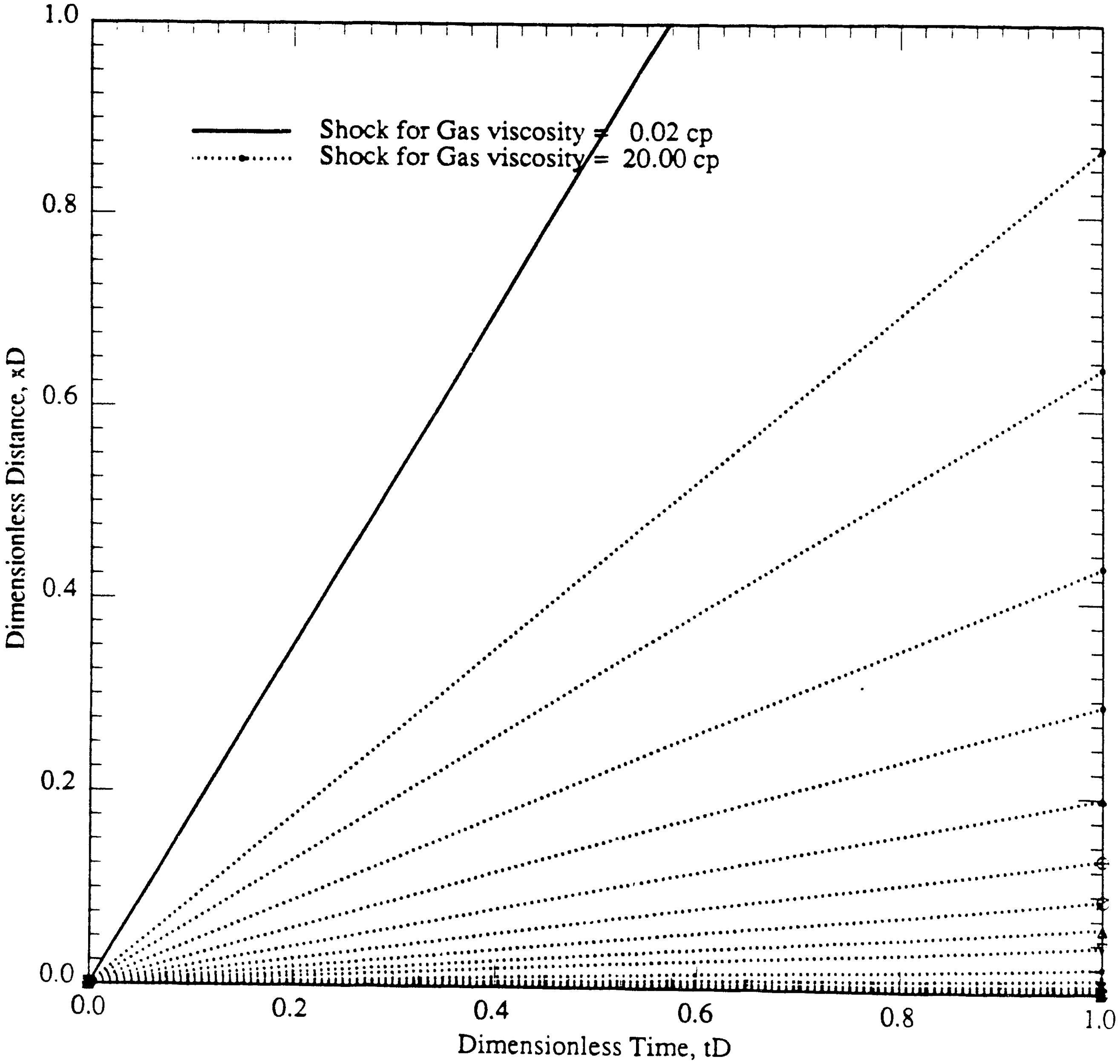

Figure 3.1.2 Shock Velocities.

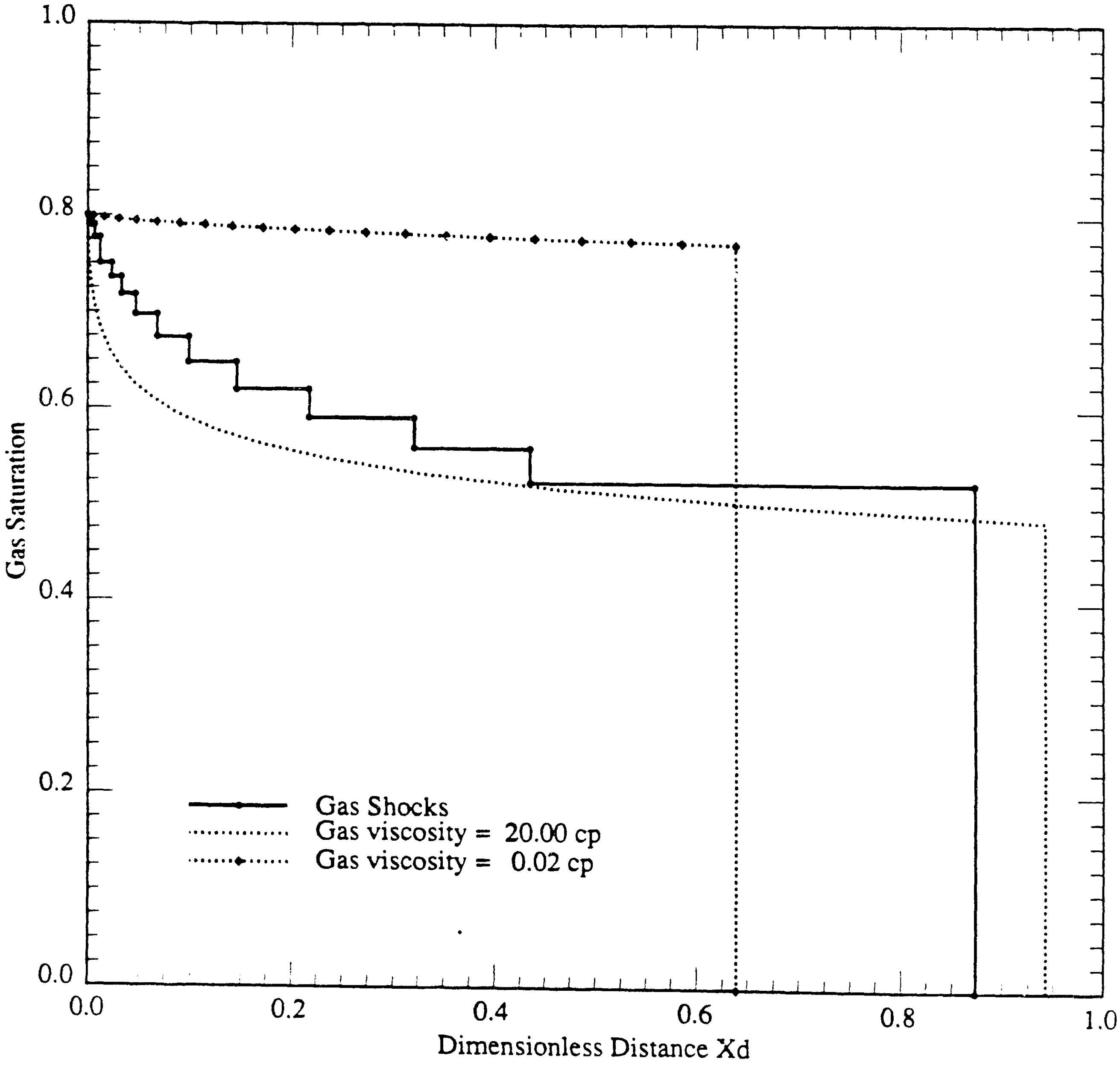

Figure 3.1.3 Saturation Profiles at $t_D = 0.5$.

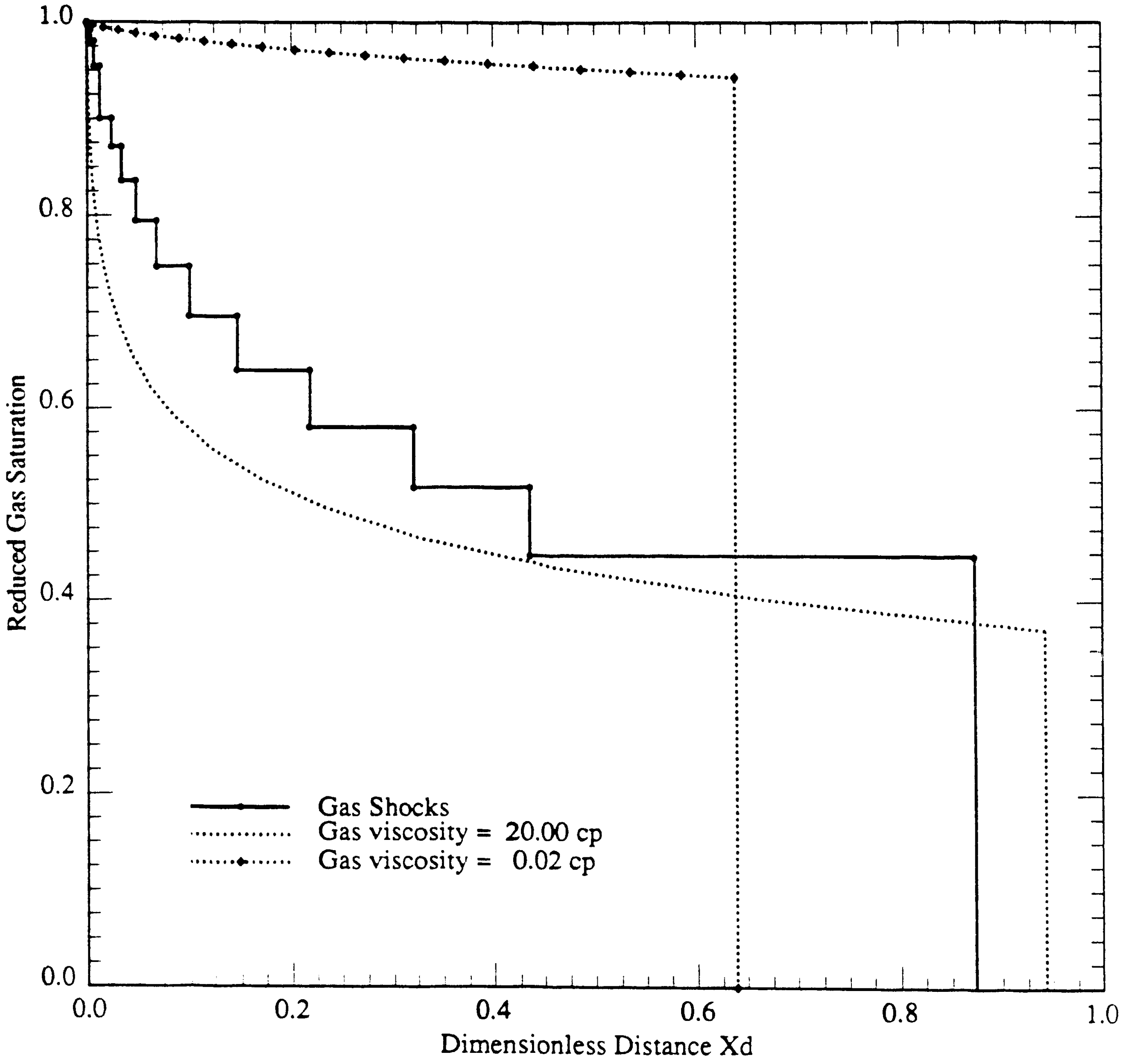

Figure 3.1.4 Saturation Profiles at t_D = 0.5 (Reduced Gas Saturation).

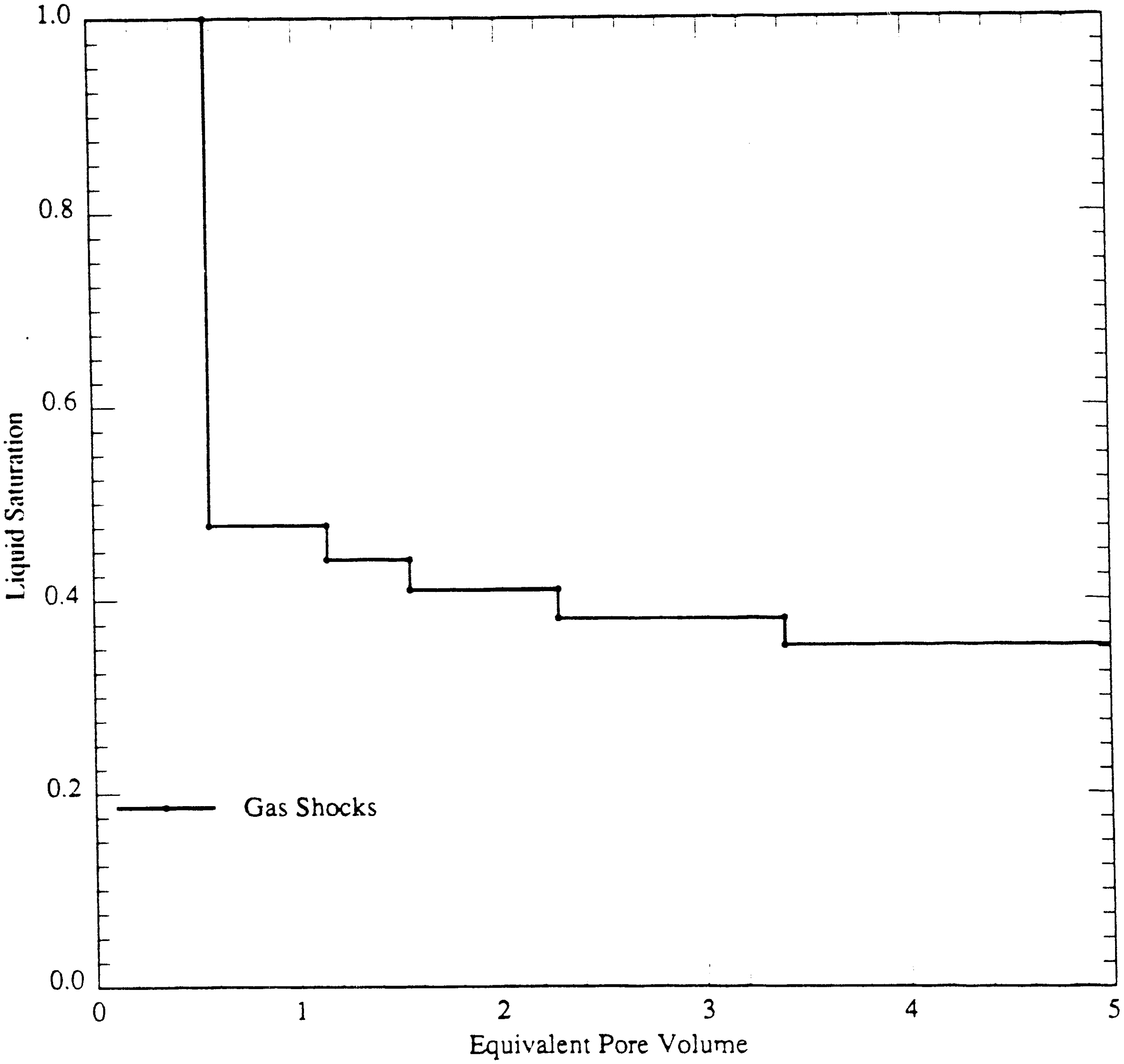

Figure 3.1.5 Saturation Profile at Outlet.

3.2 STEAM-FOAM STUDIES IN THE PRESENCE OF RESIDUAL OIL

(D. A. Hutchinson)

3.2.1 ABSTRACT

The efficiency of a steamflood can be increased by the addition of surfactants which produce foam. The generation of a steam-foam reduces the steam mobility and forces the steam to seek a path to the producer not previously taken and, therefore, to displace unswept oil.

Since the principal purpose of a steam-foam is to divert steam to previously unswept areas, it is important to understand the behavior of surfactant in the presence of oil. However, since surfactant use is generally applied only after stream breakthrough, the focus of this research is to understand foam behavior in the presence of residual oil.

The results show that foam can be generated in the presence of residual oil when an alternating injection technique — surfactant slug followed by steam and nitrogen — is used. Additionally, the results indicate that the slug size may be reduced without any apparent reduction in the pressure response, hinting that an optimum may be determined.

3.2.2 EXPERIMENTAL SET-UP

LINEAR MODEL: A schematic of the linear model being used is shown in Figure 3.2.1. The model is a cylindrical stainless steel [ss#321] tube having a 6 ft. length, a 2.16 in. inside diameter, and a 2.25 in. outside diameter. The 21 thermocouples used to monitor temperature are separated between 2 in. (near the inlet) to 5 in. (near the outlet). Their location within the sandpack alternates between being at the center of the pack or being 0.5 in. from the top of the pack. The 5 pressure taps located at 16, 32, 52, and 72 in. from the inlet allow for monitoring of pressure changes within four separate sections of the model. The 5 heat flux sensors are used to measure the heat losses, obtain the overall heat transfer coefficient and, eventually, the steam quality along the sandpack. One of the heat flux sensors is located at the top of the tube, 38 inches from the inlet. The other 4 are located at the top, bottom, and sides of the tube at a distance of 25.5 inches from the inlet. The clean sand used to pack the model resulted in a system having 35% porosity and 85 Darcy permeability.

SUPPORTING EQUIPMENT: A simplified schematic of the experimental set-up is shown in Figure 3.2.2. Two Constametric Model III pumps are for fluid injection, with one being used exclusively for supplying distilled water to the steam generator, while the other is used for both surfactant injection and cleaning fluid injection. In addition, a Marshall Model #1056 tubular furnace is used to generate steam, a Matheson Model 8141 mass flowmeter is used to control the nitrogen injection rate, and an IBM-XT computer via an HP Model 3497A data-acquisition system is used to record temperature and pressure data from the 21 thermocouples and 5 pressure transducers.

3.2.3 PRIOR WORK

FRED WANG (1986): The linear model herein described was built and first used by Fred Wang. He examined one surfactant, SUNTECH IV, and found that a reduction in steam mobility could be obtained with as little as 0.1 wt% of surfactant in a 10% pore volume (PV) slug. The linear model in all cases was water saturated. A significant result from his work is that simultaneous injection of steam and nitrogen lessened the amount of surfactant needed to obtain a given pressure increase when compared with injection of steam alone.

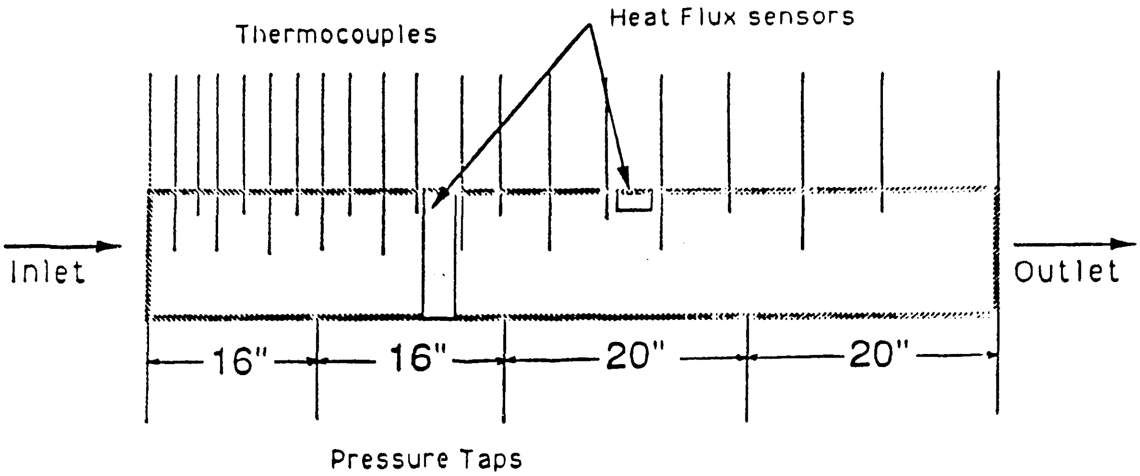

Figure 3.2.1 Linear Sandpack Model.

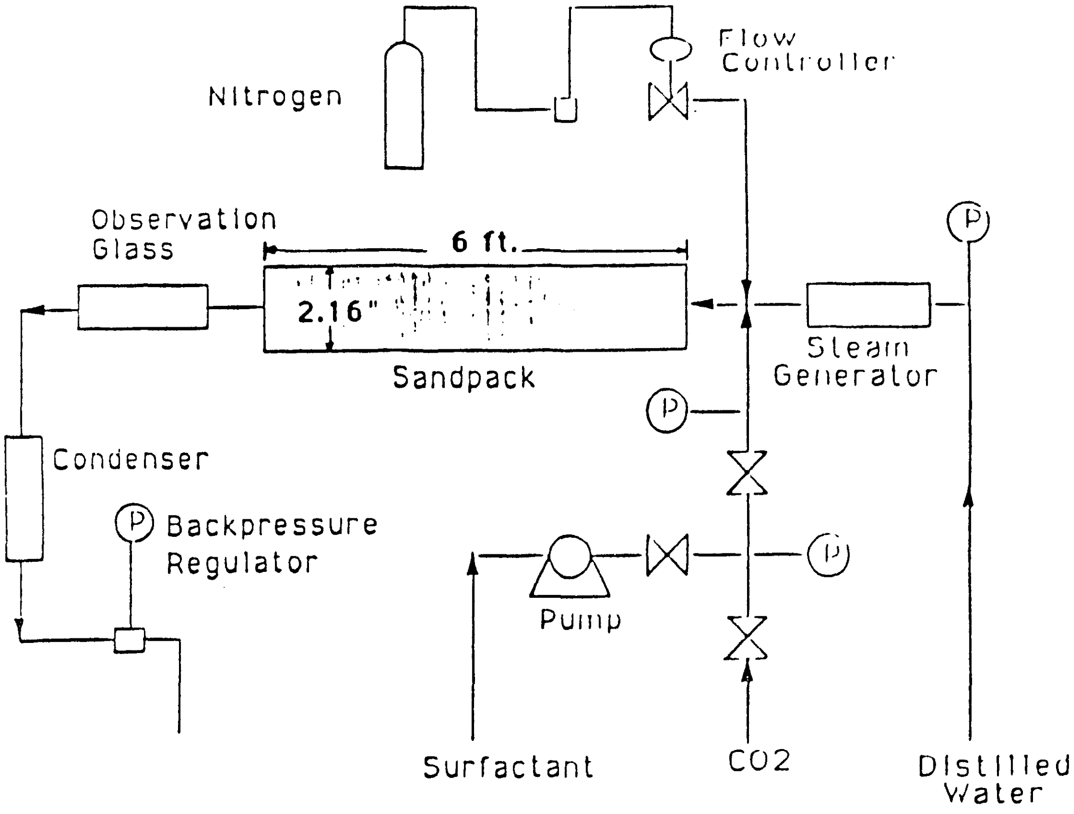

Figure 3.2.2 Experimental Set up.

DAVID SHALLCROSS (1988): Extensive work was done by David Shallcross who tested seventeen surfactants, at various injection concentrations, rating their relative strengths based upon the size of the pressure increase resulting from their injection into the linear model. A summary of his results is given in Table 3.2.1. Inspection of the table shows that, for a given chemical group, there is a trend favoring larger molecular weight surfactants. As with the work of Fred Wang, the work of David Shallcross was for a 100% water saturated system.

FARID HAMIDA (1990): Farid Hamida, duplicating some of the Shallcross work, tested the top seven surfactants listed in Table 3.2.1. An additional surfactant, AOS2024DE, having an increased disulfonate content as compared with AOS2024, was also tested in the water saturated linear model. A comparison between these two surfactants indicates that increasing disulfonate content will reduce foam strength. The results regarding alkyl chain length were the same as those obtained by Shallcross, that is, the foam strength exhibited by surfactants in a given chemical group increased with increasing molecular weight. Further surfactant tests were made with residual oil in the model, however, the surfactants in all such tests were unable to cause a pressure increase.

3.2.4 RECENT WORK

A troubling result from the Hamida report was the complete surfactant failure in the presence of residual oil even though some of the surfactants used had been successfully field tested (Patzek and Koinis, 1988) and lab tested (Demiral and Okandan, 1987) in the presence of oil. No obvious explanation was forthcoming, however, Demiral did observe that most of the successful oil runs were those where steam and nitrogen were injected only after the surfactant-slug injection was completed. Such an alternating injection scheme (AIS) can be contrasted with the simultaneous injection scheme (SIS) used by Hamida, where the surfactant slug, steam, and nitrogen were all injected together. Recently the AIS method was applied to a residual-oil system and gave positive results, with pressure increases across the sandpack of about 20 psi (Figure 3.2.3). Although the observed pressure response is relatively small in comparison with the 100% water saturated runs, such an attenuated response is in accordance with results obtained by other investigators (Bernard et al. (1964), Duerken (1986), Robin (1987), Olsen (1989), Lau and Borchard (1989), and somewhat to be expected since oil partitioning of the surfactant will occur.

The reasons for the success of the AIS method over the SIS method is not understood, but a possible explanation is that different surfactant concentrations are seen by the steam depending upon the method used. In the AIS method, the slug has displaced oily water with distilled water that is surfactant full. Thus, when steam first enters the model, it encounters a surfactant concentration identical to what was injected in the original slug. Any injected steam must make a path through a surfactant rich volume of liquid. However, for the SIS method the entering steam initially encounters a surfactant-free solution. Should the steam take a specific path not followed by the fluid, it is possible that the steam never sees a sufficiently high surfactant concentration to produce foam. This presupposes that a higher surfactant concentration is needed to initiate foam production for residual oil systems vs 100% water saturated systems, but such an assumption is not unreasonable since oil can destabilize foam bubbles.

An additional observation from the residual-oil runs suggests that work is needed to optimize the slug size and injection frequency. Preliminary results show that a larger pressure response is obtained with less overall surfactant when the slug size is decreased but the slug injection-frequency increased (Figure 3.2.3). This result would be in agreement with the above mentioned hypothesis since, almost regardless of the slug size, if the AIS method is used the entering steam and nitrogen see a high surfactant concentration immediately, thus a large slug size is not needed. This could have important economic implications concerning proper field application.

Table 3.2.1 Results for Seventeen Surfactants (Shallcross 1988)

Surfactant	Manufacturer	Minimum Foaming Concentration (wt %)	Maximum Pressure Drop (psi)	Duration of Pressure Response (min)
Enordet AOS 2024	Shell	0.10	234	85
Enordet AOS 1618	Shell	0.10	132	68
Enordet LTS 18	Shell	0.10	58	> 120
Chaser SD 1000	Chevron	0.10	6	29
Enordet IOS 1720	Shell	0.25	217	79
Enordet IOS 2024	Shell	0.25	209	83
Hostapur OS II	Hoechst	0.25	65	45
Hostapur SAS 60	Hoechst	0.50	> 215	76
Enordet IOS 1517	Shell	0.50	161	100
C 1416 AOS	Shell	0.50	71	> 118
Enordet LTS 1618D	Shell	0.50	42	> 206
Enordet LXS 18	Shell	1.00	246	> 85
Enordet LXS 16	Shell	1.00	230	87
Enordet LXS 1314	Shell	1.00	201	> 126
Enordet LXS 1112	Shell	Foaming did not occur at 1.00 wt %		
Enordet LXS 814	Shell	Foaming did not occur at 1.00 wt %		
Chaser SD 1020	Chevron	Foaming did not occur at 1.00 wt %		

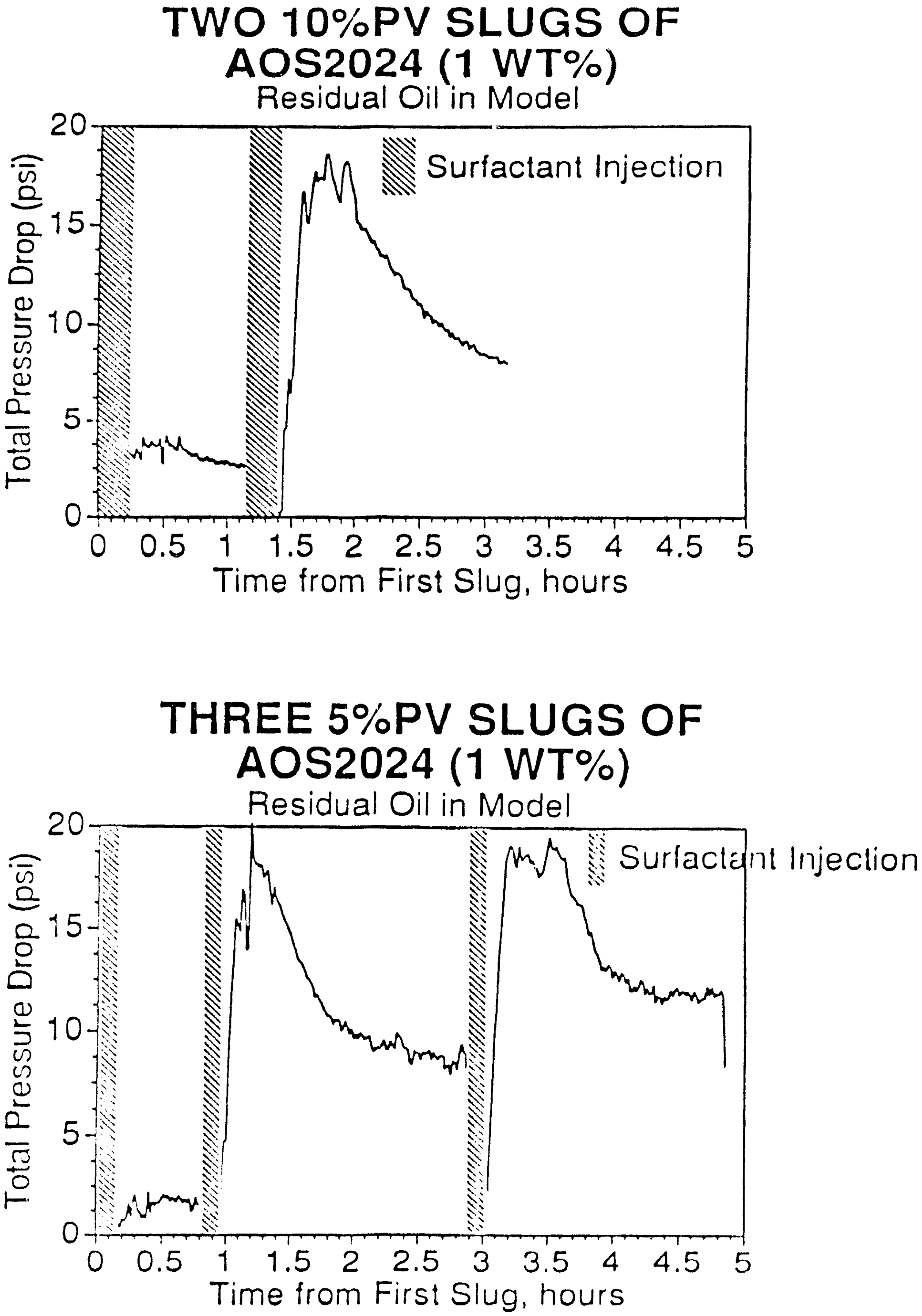

Figure 3.2.3 Pressure Response to Various Slug Sizes.

3.2.5 FUTURE WORK

The direction of future work is aimed at better understanding steam-foam flow in the presence of residual oil. Initially, this will involve comparing the AIS and SIS injection schemes under various inlet steam qualities. Later, an attempt will be made to optimize the injection procedure in general.

The sequence of the planned work is the following:

1) With residual oil in the model and using the AIS method, make two separate runs for each of the following surfactants:

   AOS202 4LTS18 IOS1720

   The two runs will a include a low and a high steam quality. These three are the strongest foamers within their respective groups as determined by Shallcross.

2) Pick the strongest of the three surfactants and, using a low steam quality, make a run using the SIS method. If a pressure response is obtained then several runs will be made at various steam qualities.

3) Repeat step (2) but with the AIS method. Depending upon the results, several runs may be made at various steam qualities.

4) Do several runs with the idea of optimizing the slug size, injection frequency, and nitrogen rate.

3.3 MICROVISUALIZATION OF FOAM FLOW IN A POROUS MEDIUM

(J. Hornbrook)

3.3.1 INTRODUCTION AND OBJECTIVES

Since the late 1950's foam has been recognized as a fluid possessing oil production enhancement capability. Foam may be used to improve the mobility characteristics of an oil reservoir or it may be used as a selective blocking agent to reduce the effects of fingering induced by permeability streaks in the producing formation. Additionally, the surfactants used to produce foams may aid in the production of heavy oils by partially dissolving the oil or by helping to separate oil blobs from the rock in mixed-wet systems.

Study of the flow of foam in porous media may be roughly divided into three broad areas. 1) Foam properties. This area includes studies of the fluid properties of foam, the most important of which is foam viscosity and how it varies with shear rate. 2) Foam flow mechanisms. This area is made up of research into the means of propagation of foam in porous media. Snap-off events and bulk propagation of the gas and liquid fractions of foam are studied in this area. 3) Foam interactions with oil. This area, obviously, concerns itself with the way foams react with oil. The ways in which foam increases the mobility of oil and the mechanisms by which oils destroy foam are of particular interest. Research within the three broad research areas has been undertaken at the field pilot project level, the macroscopic level in laboratory core floods, and at the microscopic level in micromodel studies.

The current research focuses on the third broad area of foam research (foam interactions with oil) and is carried out at the microscopic level. Background work designed to validate experimental procedure was completed in homogeneous micromodels. Presently, the construction of an exact two-dimensional replica of Berea sandstone is being attempted. Upon completion of the replica micromodel, the effects of foam injection procedure upon foam stability in an oil filled micromodel will be studied.

3.3.2 LITERATURE REVIEW

The study of foam with application to petroleum engineering application began with the pioneering work of Bond and Holbrook (1958). Their work concentrated on the mobility effects of injected foam and it pointed out the benefits to foam injection as a method of enhancing oil reservoir performance. Over the next thirty years much research and several field experiments have attempted to understand the flow of foam in porous media on both a qualitative and quantitative level.

Many papers have been written on the fluid properties of foam. The results of these papers are rarely in agreement on the nature of foam and are often contradictory. A chronological review of foam research was carried out by Marsden (1986). In his review, Marsden outlines the major advances in the understanding of foam flow and points out shortcomings and contradictions in existing work. A brief summary of foam fluid properties is: 1) foam is a fluid of high apparent viscosity, 2) foam viscosity is a function of the surfactant concentration, 3) foam viscosity is a function of flow rate (non-Newtonian flow), and 4) the flow history of foam affects its viscosity.

Foam flow mechanisms, the means by which foam propagates through a porous medium, have been studied in numerous papers as well. Most of this work, however, has focused on a qualitative description of foam rather than a quantitative one. Most recently, the research of Owete (1984), and Radke (1988) have attempted to extend the understanding of foam flow mechanisms beyond the description of observed phenomena. Owete studied the flow of foam in the following two areas: 1) the propagation of foam and its components, and 2) the mobility of gas in the presence of foam. Owete carried out his work in micromodels with homogeneous and heterogeneous flow paths and, although most of his conclusions are qualitative, some quantitative results were obtained.

Owete's results for a homogeneous micromodel have been verified as a part of the background work in my research. The quantitative aspects of Owete's work will be extended to include the effects of foam injection procedure on oil displacement. Future research will be carried out in two-dimensional replicas of Berea sandstone.

Research on the effects of oil on foam has been carried out by Manlowe and Radke (1988) and by Sanchez and Hazlett (1989). The work of Manlowe and Radke was most applicable to this project. Manlowe and Radke studied the foam breaking tendency of oil on foam and described the stability of a pseudo-emulsion film as the determinant of foam stability in the presence of oil. This work will involve the study of the pseudo-emulsion film under different foam injection schemes.

Research involving flow of foam through micromodels is relatively new. In addition to the micromodel research mentioned above, several studies on the usefulness of micromodels as a research tool have been carried out. Sarathi (1986) points out the advantages in studying pore level events afforded by micromodels but warns against extrapolating pore level events to a large scale without additional information. He also points out several disadvantages inherent in commonly used micromodels, most of which will be eliminated by the construction process outlined in this report. Sarathi lists the following as important problems with micromodel research: 1) difficulty in obtaining a continuous specific etch depth, 2) introduction of microscopic heterogeneity into the model in the etch procedure, 3) difficulty in replicating reservoir Peclet number due to enlargement of the pores, 4) loss of three-dimensional continuity, and 5) loss of detail - heterogeneity, pore geometry, connectivity, and surface roughness - due to the anealling process used in most micromodel construction processes. Except for the loss of three dimensional continuity, all of the disadvantages listed above are eliminated in the micromodels described in this report.

Huh et al. (1989) point out the importance of differences in heterogeneity on foam generation in porous media, further supporting the need for accurate replication of a porous medium of interest in a micromodel study.

3.3.3 EQUIPMENT

An experimental apparatus has been constructed that will allow the flow of foam through a micromodel to be simultaneously observed, videotaped, and photographed and will allow for monitoring of the pressure drop across the micromodel. The micromodels used are two-dimensional representations of porous media made by etching a flow path into a silicon wafer and then bonding the wafer to a flat piece of glass (Fig. 3.3.1), thus creating a self contained flow path. Two homogeneous micromodels were used in the background portion of the foam flow research. The homogeneous micromodels were used to verify that the experimental apparatus worked as designed and to replicate Owete's results to verify that the experimental procedure was correct. Both homogeneous micromodels were etched to a depth of 30 microns. One micromodel represented cubic packing of spheres of radius 100 microns while the other micromodel represented rhombohedral packing of spheres of radius 30 microns. A heterogeneous model which is an exact two-dimensional replica of Berea sandstone is being constructed. A detailed description of the construction of the Berea replica micromodel follows.

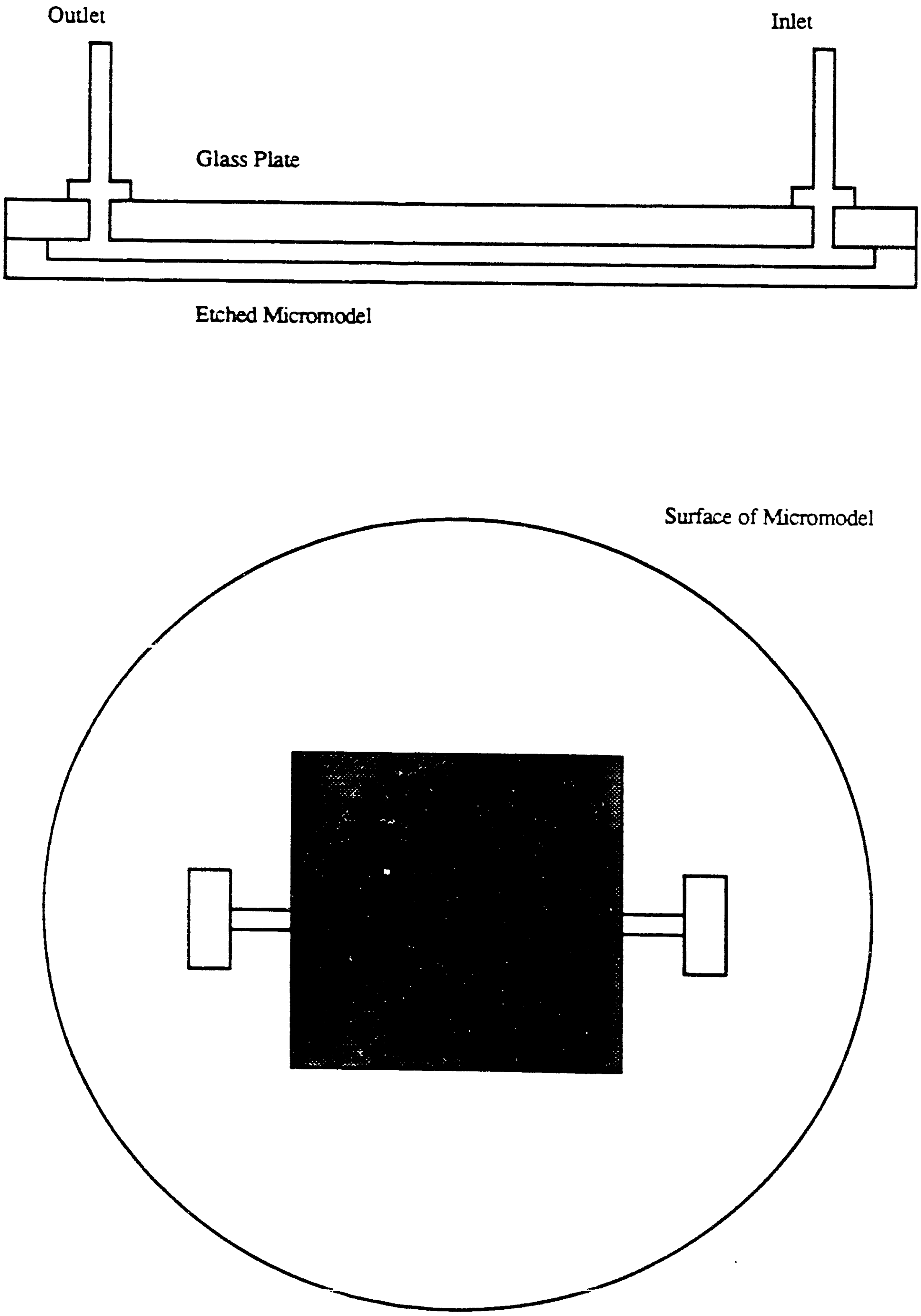

Figure 3.3.1 Micromodel Schematic.

A thin section of clean Berea sandstone was prepared with the pore spaces filled with blue-dyed epoxy. A color photograph of the thin section was taken at 40 times magnification. The result is a photograph in which pore spaces appear blue and the sand grains appear black to grey. Professional slide film was used to get a true color image. The film was then sent to a photography lab where, after the development with the use of color filters, the blue was transformed to white. After this transformation, the pore spaces are white while the sand grains are still black and grey. Finally, a lithograph of the photograph is made. In the lithograph, the pore spaces appear white and the sand grains are strictly black - - there are no grey scales. Now the lithograph image must be transferred to the computer.

The lithograph of the thin section was put into PICT format by using a Macintosh digital scanner. The image was then analyzed by using a digital analysis package called Ultimage (1988). It was noticed that at various points in the image, pore spaces that should have been continuous were blocked off. This is an artifact of the loss of one dimension in transferring the three-dimensional flow path to two-dimensions. By use of the digital analysis package, a small number of pixels were removed to allow for a continuous flow path through the micromodel. When pixels were removed, the nature of the flow path was always maintained, so after manipulation of the digital image, a computer image of a continuous Berea flow path was obtained (Fig. 3.3.2).

The most difficult problem in obtaining a Berea micromodel is in the next step -- moving the computerized image of the sandstone (PICT format) to MEBES (1988) format which is the format used at Stanford's Center for Integrated Systems to transfer complicated images to silicon wafers. First, an ASCII bit map of the image is generated with black pixels given a value of 1 and white pixels given a value of 0. The bit map is then restructured into columnar form with each pixel given an address and size based on its location in the image. Finally, using modified transferring software available at Stanford CIS, the image is transferred to MEBES format. Once the image is put into MEBES format, the final steps are trivial.

A permanent chrome-on-glass mask of the Berea pore space is constructed by the electron beam imaging group at Stanford. Once the mask is complete, the silicon wafer model construction is carried out as in more conventional models (the process will be described in detail). Presently, I am attempting to get an accurate description of the Berea image in MEBES format, a rather complicated problem.

When the image mask has been completed, the following steps are used to generate the etched silicon flow path:

1. Oxidize one side of a silicon wafer (5 cm. diameter).
2. Coat one side of the oxidized wafer with a photoresist material.
3. Position the sample mask on the photoresist side of the wafer.
4. Expose the sample mask to ultra-violet light. The structure of the photoresist is destroyed by contact with ultra-violet light so, since the sample mask is a negative of the sample, the photoresist is destroyed where pores exist.
5. Etch the wafer with hydrofluoric acid to the desired depth.

Only the parts of the wafer not coated with photoresist will be etched, so after etching, the pores and flow channels of the Berea sample will be etched away while the grains will be intact. After etching, the wafer is anodically bonded to a flat glass plate. The process of anodic bonding is uncomplicated and is easy to carry out. The silicon wafer, in contact with the glass plate, is sandwiched between two electrodes (the negative electrode contacting the glass plate) and the entire system is placed on a hot plate (Fig. 3.3.3). The system is heated to

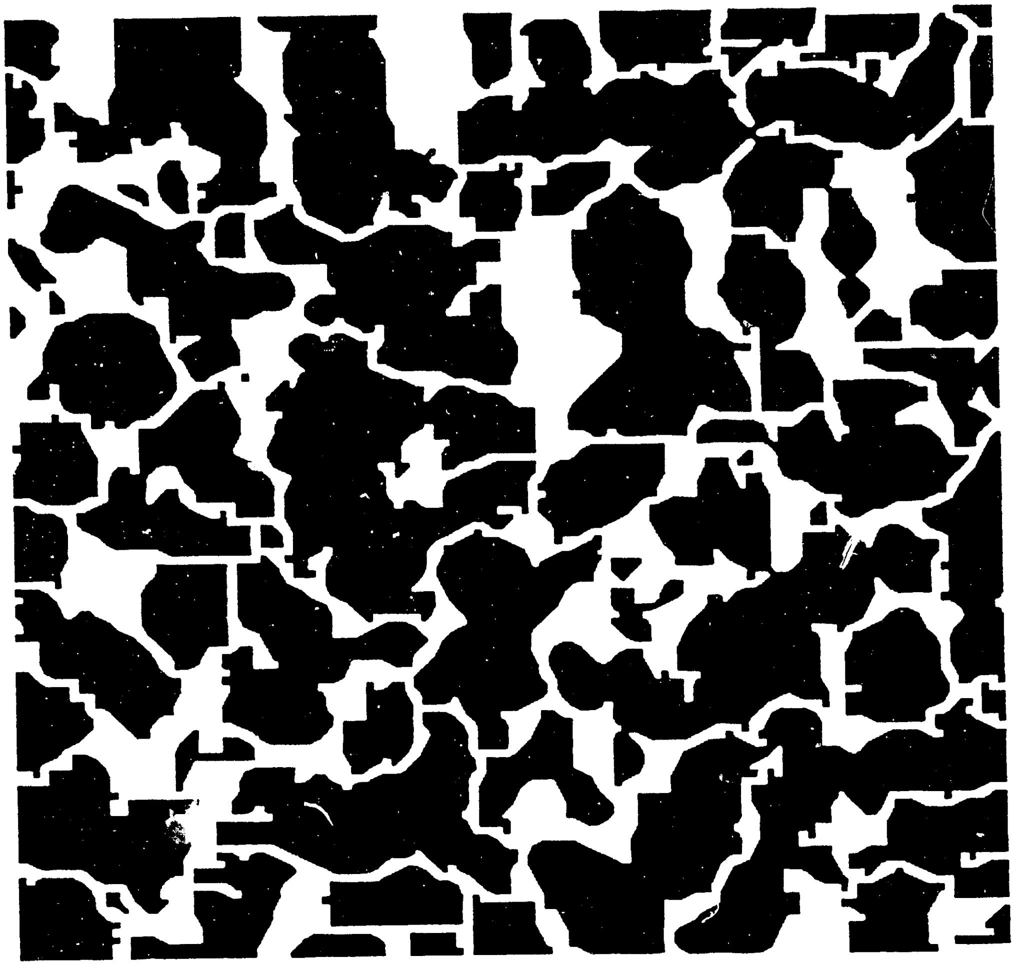

Figure 3.3.2 Digital Image of Flow Path in Brea Sandstone (40 Times Magnification).

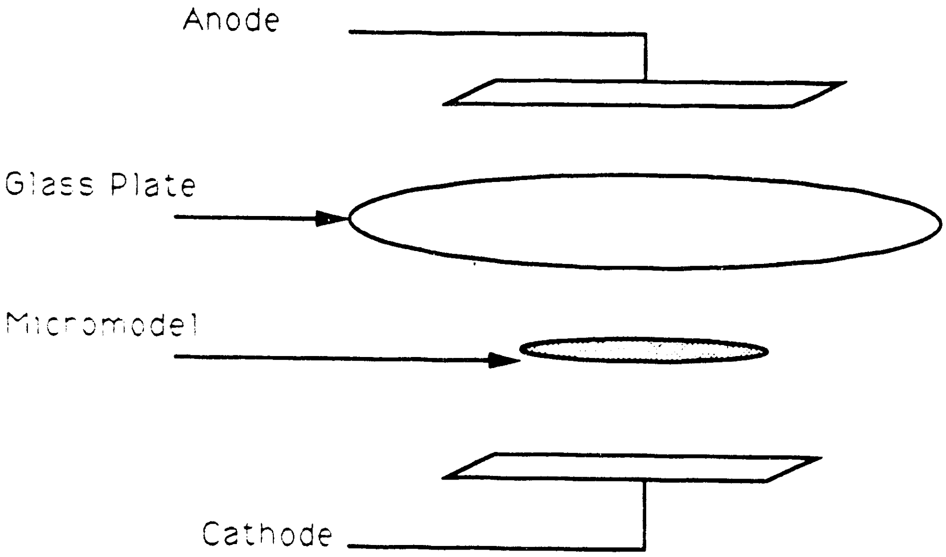

Figure 3.3.3 Anodic Bonding Schematic.

400 C and a potential drop of 600 V is applied across the electrodes. Bonding between the wafer and the glass plate is immediate and is irreversible. The glass plate must be absolutely flat so the small flow channels end up as distinct and separate flow channels.

Figure 3.3.4 is a schematic of the flow visualization apparatus. A syringe pump will be used to either independently or simultaneously inject a surfactant solution and air which may be mixed in a foam generation cell and observed through a view port. While the foam is passing through the view port, it will be photographed and/or described at regular intervals so a record of foam texture may be kept throughout the run. Next, the foam will pass through the micromodel described in detail above. While in the micromodel, video and still cameras will record the movement of the foam (Fig. 3.3.5). After leaving the micromodel the foam will pass through another view port.

Here, the foam will again be observed and compared to the inlet foam to determine if any structural changes have taken place in the foam during the displacement process. The pressure drop across the micromodel will be monitored with the use of a pressure transducer, and the pressure data will be recorded on a chart recorder.

3.3.4 RESULTS AND PLANNED WORK

At this point, only the preliminary work using homogeneous micromodels has been carried out. Air was injected into a surfactant saturated micromodel at a flow rate of 2.5×10-4 cc/s and the general flow characteristics observed were found to be identical to those observed by Owete. The flow rate used was on the order of 100 ft/s which is much higher than normal reservoir rates which are on the order of 1 ft/s. Attempts were made to reduce the flow rate to around 1 ft/s, but no precise procedure was found to do this.

As soon as the Berea replica micromodel is constructed, the following work will be carried out.

1. Foam flowing properties in the micromodel will be compared to results obtained by Owete and others to determine if foam behaves the same in models of the same pore size and configuration of real reservoir rock as it does in the larger pore size micromodels commonly used. Flow rates equivalent to about 100 ft/s will be used in these runs as well.

2. The oil displacement efficiency of foam will be investigated under two different injection schemes. First, the micromodel at residual oil saturation will be injected with 0.5 pore volumes of surfactant solution. The model will then be injected with nitrogen and the foam/oil interactions at the fluid interface will be observed. Then, the same micromodel, again at residual oil saturation will be injected with foam produced in the foam generation cell. The foam/oil interactions will again be observed, and results from the two different injection schemes will be compared. Macroscopic experiments at Stanford have indicated that the former injection scheme is significantly more efficient and a microscopic study of the phenomena may yield useful information.

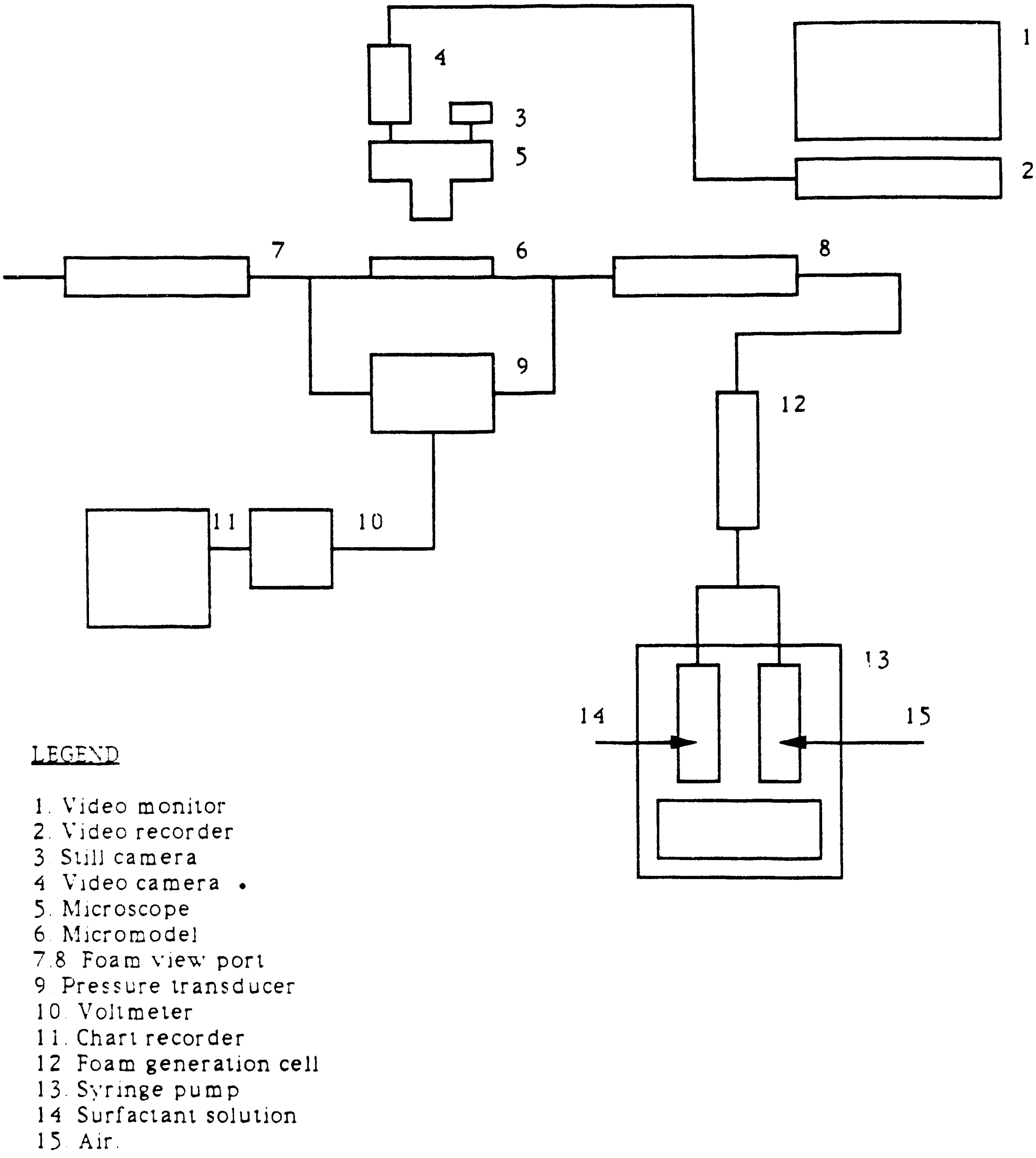

Figure 3.3.4 Schematic of Experimental Equipment.

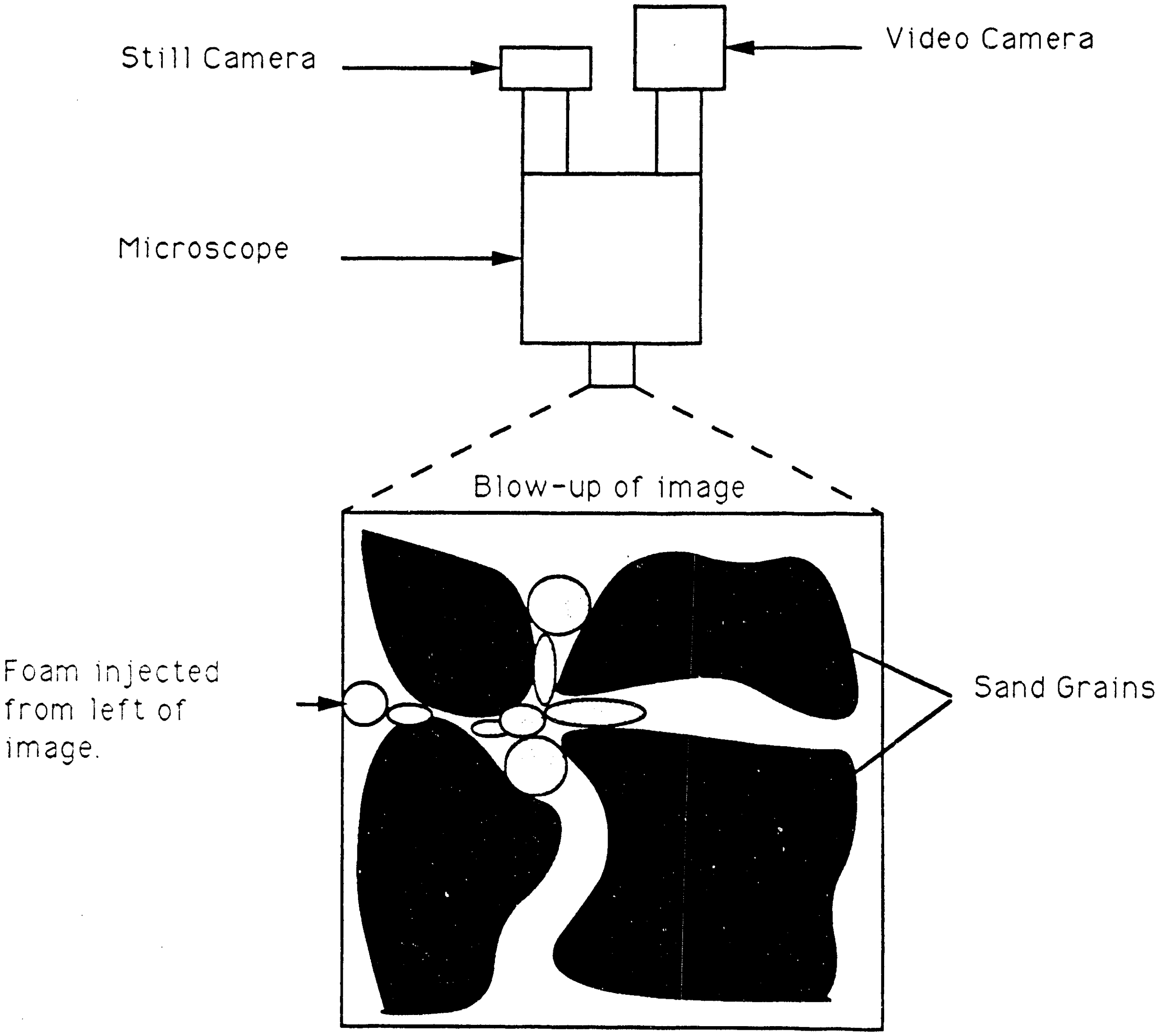

Figure 3.3.5 Foam Observation Process.

3.4 THREE-DIMENSIONAL LABORATORY STEAM INJECTION MODEL
(B. Demiral)

3.4.1 SUMMARY

The objectives of this project are to observe the oil recovery mechanisms of steamflood and steam-foam injection in a 3-D laboratory model by using Computer Aided Tomography (CT Scanning). A stepwise approach has been followed to achieve this goal: 3-D model development, and steam and steam-foam injection experiments using CT Scanning.

3.4.2 3-D MODEL DEVELOPMENT

A three-dimensional laboratory steam injection model which is able to be scanned under CT scanner was developed. During the design period, different geometries that could be the best representative of radial flow and fit the dimensions of the scanning field of SUPRI-A CT scanner were examined in terms of their advantages and disadvantages. As a result of this analysis a 3-D box with dimensions 20 × 20 × 7.5 cm was constructed. This box simulates a 1/4th of a five spot pattern. Aluminum, teflon and fiberfrax were chosen as supporting and insulating materials respectively. As can be seen from the injector producer diagonal cross-section of the model, Figure 3.4.1, the heat insulator (Teflon) is in first contact with the porous medium. Teflon was placed between the porous medium and the aluminum so that one could assume that the rate of heat transfer in the porous medium would be much faster than that in the aluminum during a steam injection run. Aluminum was necessary to back up the Teflon for strength under the proposed pressure and temperature conditions and was chosen as construction material since it absorbs less x-ray energy than other materials. The Teflon box was to be sealed against any gas or liquid leaks by using Chemgrip, a special epoxy which bonds Teflon to Teflon or Teflon to metal. Fiberfrax, a ceramic fiber insulating material which is inexpensive and can be applied as a wet putty which air dries to a semi-permanent cast, was chosen as a secondary insulating material around aluminum construction. As seen from Figure 3.4.1:

a) A top cover was introduced such that the porous medium can be compressed to assure there is no gas cap above it,
b) The injection well system is designed to allow injection of 100% steam through the total depth of the well. This is done by introducing a heater cartridge within an aluminum rod through which the steam flows, as shown in Figure 3.4.2,
c) The thermocouple and pressure tap locations are chosen as seen in Figure 3.4.3. Scanning will be done through the clear area, which has a width of 1.5 cm between these locations, and
d) The positioning tables were modified as seen in Figure 3.4.4. By using these two tables the 3-D model can be precisely positioned at the proper locations within the scan field.

A schematic flow diagram of the experimental apparatus can be seen in Figure 3.4.5. The set up consists of three parts: injection port, 3-D steam injection model, and production port. Each of these parts of the system are discussed next.

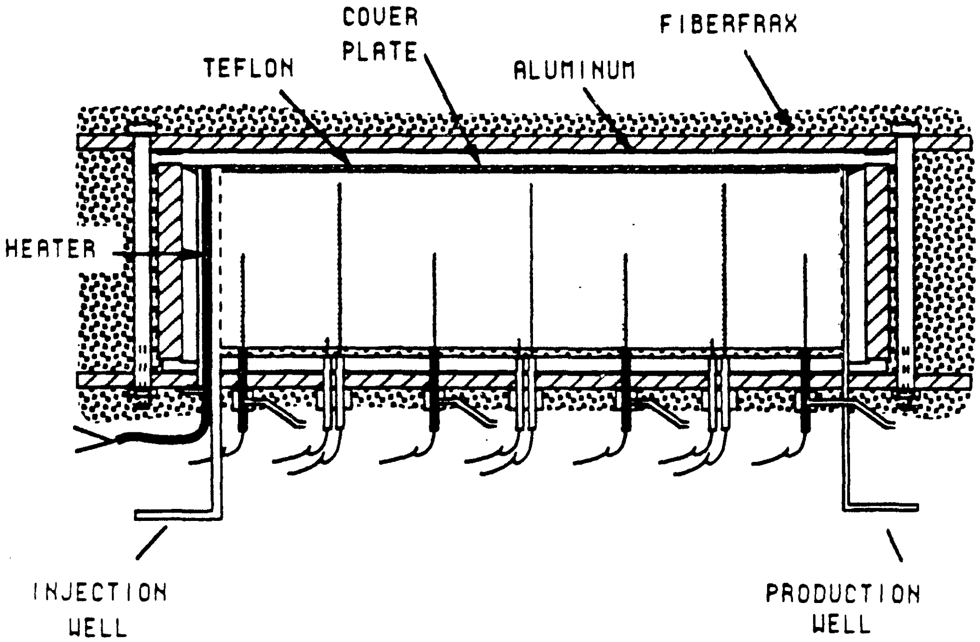

Figure 3.4.1 Injector-Producer Cross-Section of the 3D Model.

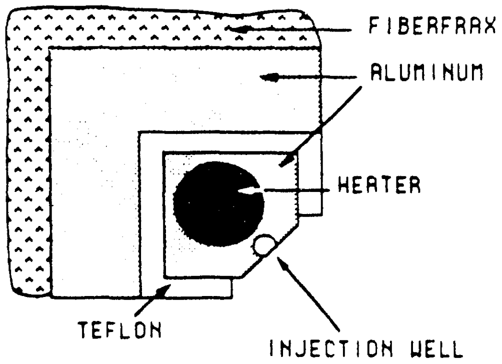

Figure 3.4.2 Cross-Section of the Injection Well.

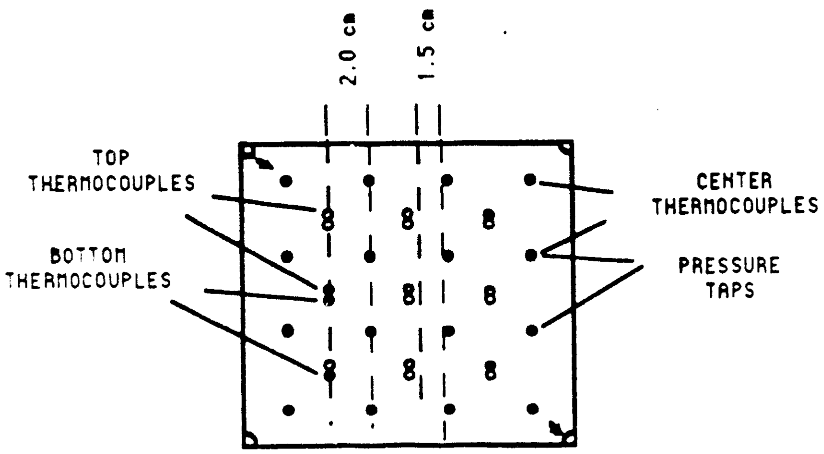

Figure 3.4.3 Thermocouple and Pressure Tap Locations in the 3D Model.

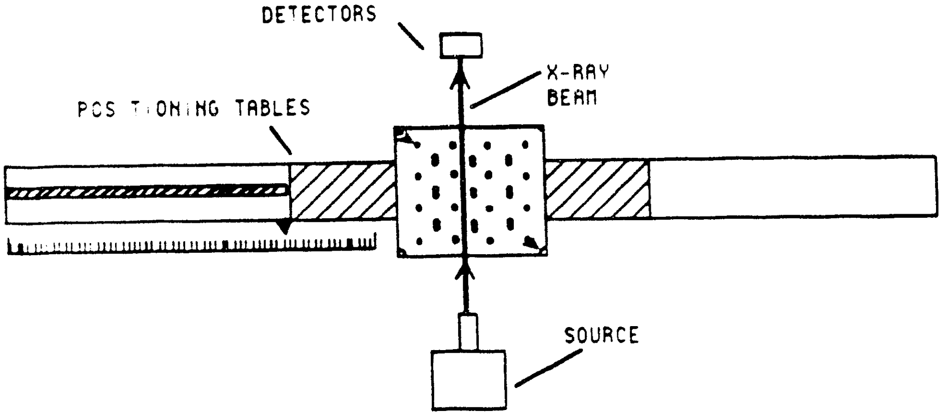

Figure 3.4.4 Positioning Tables.

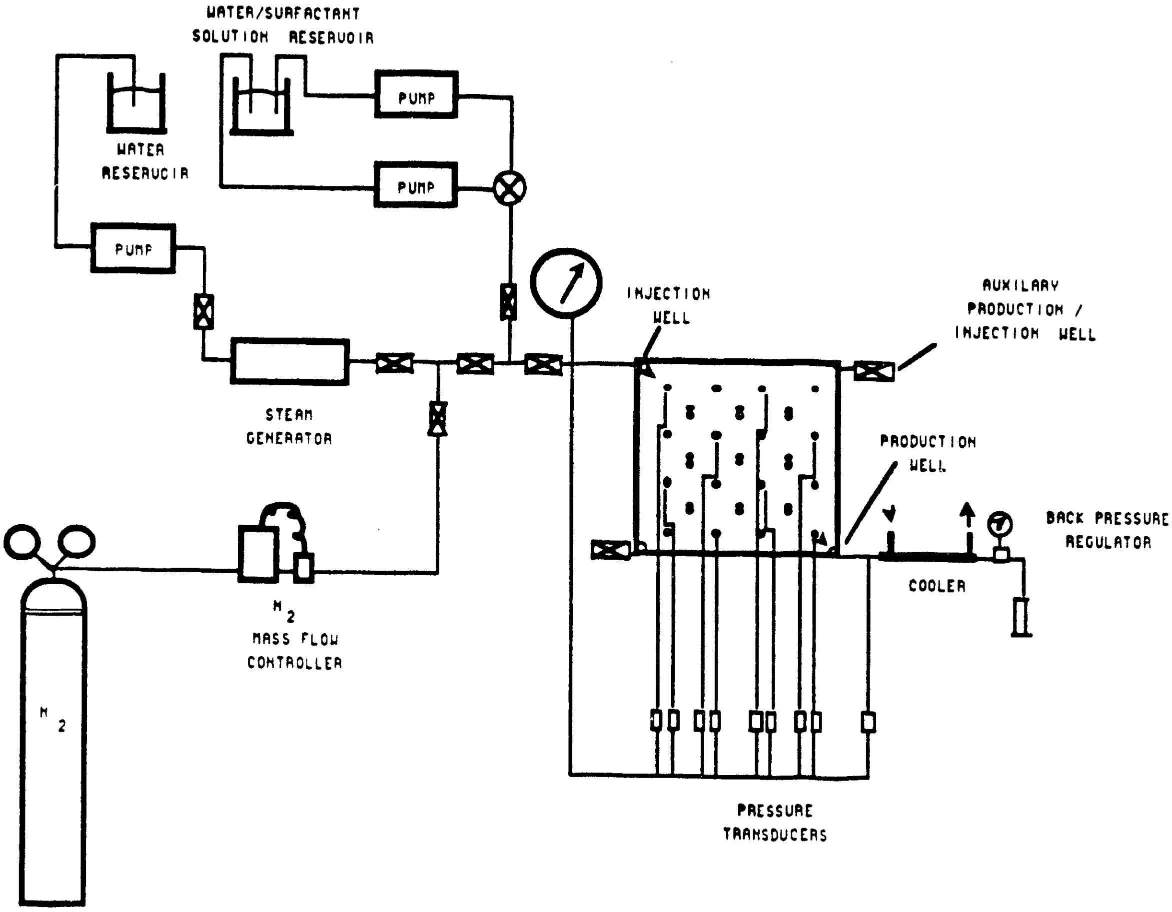

Figure 3.4.5 Schematic Flow Diagram of the 3D Laboratory steam Injection Model.

Injection Port

In the injection port there are two liquid chromatography pumps. One of them is to be used to inject water or surfactant solution and the other one is to feed the steam generator with distilled water. There is also a gas mass flow controller which will be used to inject nitrogen at a constant rate into the model during the experiments.

3-D Steam Injection Model

The 3-D steam injection model has a total of 38 J-type thermocouples which are located at three different levels in the model. Sixteen of them, center thermocouples, are placed at a level of 1.5 in. from the bottom of the model. Eleven top and eleven bottom thermocouples are placed at 2.75 in. and 0.25 in. from the bottom respectively. Sixteen pressure taps (only eight of them are used during the experiments) are located at the same places as the center thermocouples.

Production Port

A back pressure regulator maintains a constant pressure at the producing corner of the model. A cooler is used to condense the produced steam.

3.4.3 PRELIMINARY SCANS

Some preliminary work was done to understand the saturation determination by CT scan. To do this the model was scanned under different combinations of scan speeds, photomultiplier and detector levels, scan modes and energy levels. These preliminary runs showed that CT scanning technology could be applied to petroleum recovery processes in the laboratory and add another analysis tool to the classical temperature-pressure monitoring during steam injection experiments. Figures 3.4.6 and 3.4.7 show sample scan pictures from these runs. In these figures the top one shows the model filled with dry sand and shows settling in the top portion of the model. The bottom one represents the same cross-section after adding more sand to the model and injecting water from the left hand side. According to the theory (Withjack, 1988), there must be a 200 CT unit difference between the dry sand and the wet sand. As can be seen this difference was verified in both attempts at two different energy levels. This showed that it would be possible to differentiate saturating fluids in the model by comparing their CT numbers as well as by comparing them visually.

As an addition to these preliminary scans of 3-D model, some calibration works were also performed. A linear model, 1 in. in diameter and 24 in. in length, was used for that purpose. The model was filled with Berea sand and saturated with water, then NaI solutions at different saturations were injected to displace water. After reaching 100% NaI solution saturation scan pictures at six different locations along the model were taken. These pictures were compared later to see the difference between the average CT numbers as seen on Figure 3.4.8. As it can be seen from this figure there is a linear relationship between the NaI solution concentration and average CT numbers such that by increasing the concentration, one can obtain the optimum contrast between the NaI solution and the distilled water. This property will be used in future experiments.

Figure 3.4.6 Scan Pictures of the 3D Model Before and After Water Injection (140 keV).

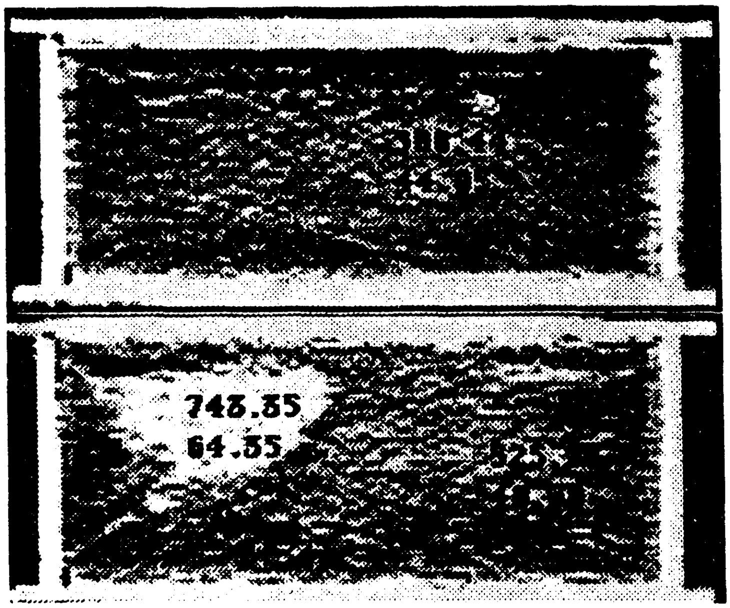

Figure 3.4.7 Scan Pictures of the 3D Model Before and After Water Injection (100 keV).

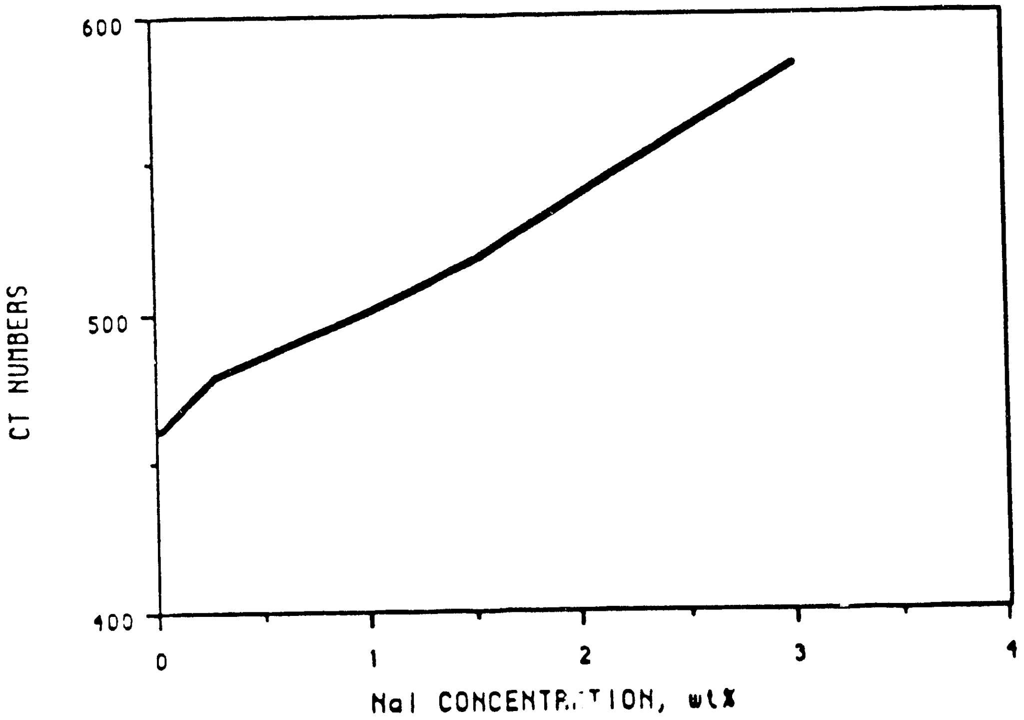

Figure 3.4.8 Change of CT Numbers with NaI Concentration.

3.4.4. DETERMINATION OF SATURATIONS

Saturations in the model will be determined by using the basic principles of Computerized Tomography (CT). Basically CT measures the linear attenuation coefficients across an object within the x-ray scanning field. The linear attenuation coefficient which is dependent upon the nature of the attenuating material is defined by Beer's law:

$$I / I_s = e^{-\mu x} \tag{3.4.1}$$

where:

I_s = the source x-ray intensity
I = the intensity measured by the detectors
μ = the attenuation coefficient, and
x = the thickness of the material

The linear attenuation coefficient depends on electron density (bulk density), atomic number and energy level. The linear attenuation coefficient is expressed as (Evans, 1955):

$$\mu = \rho \left[a + bZ^{3.8} / E^{3.2} \right] \tag{3.4.2}$$

where:

ρ = electron density
a = Klein-Nishina coefficient
b = 9.8×10^{-24}
E = energy level in kV, and
Z = atomic number

If the subject contains a mixture of components, the overall mass attenuation coefficient of the mixture will be (Vinegar and Wellington, 1987):

$$\mu_{mix} = \sum_i \mu_i \, S_i \tag{3.4.3}$$

If the components are not miscible, S_i is the saturation of the phase i, that is, water, oil or gas in our case.

Since in petroleum recovery problems one mostly deals with 2 or 3 phase systems, Equation 3.4.3 is applicable to petroleum engineering research without changing the basic CT technology. The only requirement here is to calibrate it for different phases. For two-phase saturation Equation 3.4.3 can be written as:

$$\mu = \mu_1 \, S_1 + \mu_2 \, S_2 \tag{3.4.4}$$

Here μ_1 and μ_2 are the attenuation coefficients for the medium fully saturated with phase 1 and 2 respectively and since they are known from the calibration scans, using

$$S_1 + S_2 = 1 \tag{3.4.5}$$

one can easily calculate S_1 and S_2.

This analysis can be expanded to three-phase saturation. The additional unknown requires an additional, independent measurement. This is done by scanning at a different energy level. Supposing the phases are water (w), oil (o), and gas (g), the system of equations will then become:

$$S_o + S_w + S_g = 1 \tag{3.4.6}$$

$$\mu_1 = \mu_{o1} S_o + \mu_{w1} S_w + \mu_{g1} S_g \tag{3.4.7}$$

at energy level 1, and

$$\mu_2 = \mu_{o2} S_o + \mu_{w2} S_w + \mu_{g2} + S_g \tag{3.4.8}$$

at energy level 2.

The CT output is not the classic linear attenuation coefficient. Instead, the CT computer converts attenuation coefficients into corresponding numerical values in units of Hounsfields (H or CT numbers). The scale is usually defined by two points: water = 0 and air = - 1000 and behaves as shown in Figure 3.4.9. CT number is defined as:

$$N_{CT} = K\ (\mu - \mu_b)/\mu_b \tag{3.4.9}$$

where:

μ = attenuation coefficient of material occupying volume element (voxel) during scan
μ_b = coefficient for reference material, and
K = constant (typically $K = 1000$)

During the experiments CT computer will compute the CT numbers for each voxel in the scanning area. The voxel has a volume of $0.5 \times 0.5 \times 5$ mm^3. Then the corresponding saturations for every voxel will be calculated by replacing attenuation coefficients in previous equations and using Equations 3.4.4 through 3.4.8.

3.4.5 A TRIAL RUN: CO_2 INJECTION

We decided to make a trial run to see the possible difficulties before making a real steam injection run. In order to do this a immiscible CO_2 injection run was conducted. The experimental procedure is given below.

Experimental Procedure:

1. saturate with distilled water
2. scan each section shown on Figure 3.4.10
3. start CO_2 injection
4. scan each section every 12 minutes
5. process scan pictures for each section at selected times of injection
6. compare scan pictures

The scan pictures at selected times of CO_2 injection at every sections of the model are given in Figures 3.4.11-14. As it can be seen from these figures, injected CO_2 (light color)

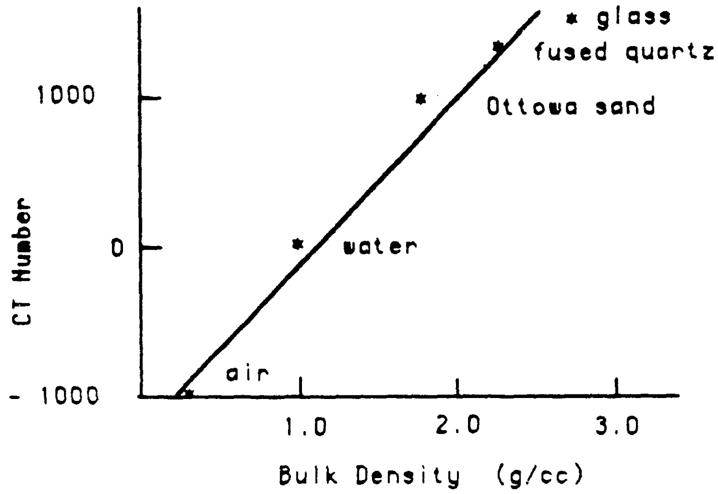

Figure 3.4.9 Effect of Density on CT Number.

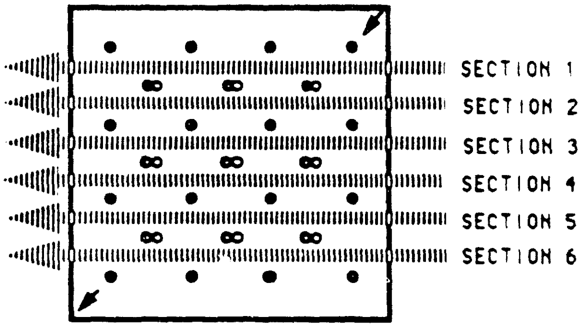

Figure 3.4.10 CT Scanning Sections Through the 3D Model.

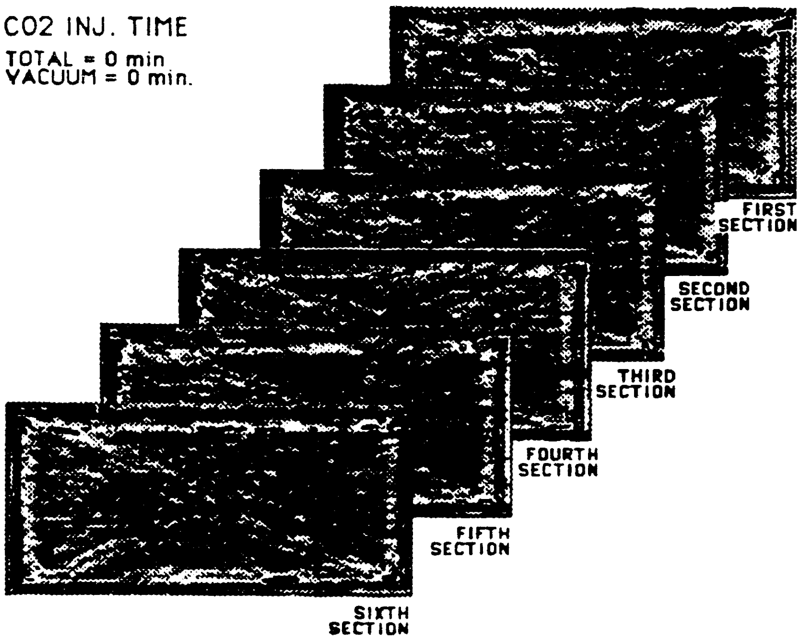

Figure 3.4.11 Saturation Distribution at Each Scanning Section of the 3D Model Before CO_2 Injection.

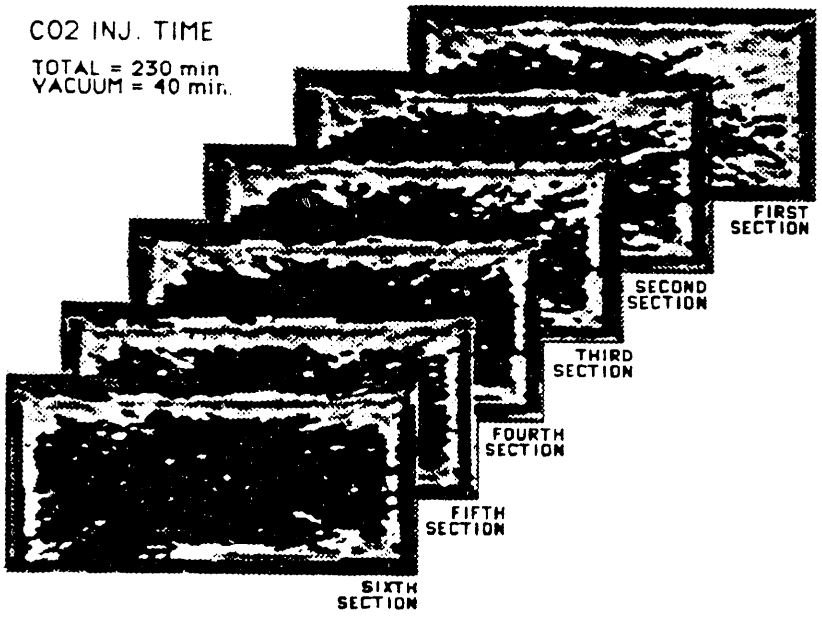

Figure 3.4.12 Saturation Distribution at Each Scanning Section of the 3D Model After 330 min. of CO_2 Injection.

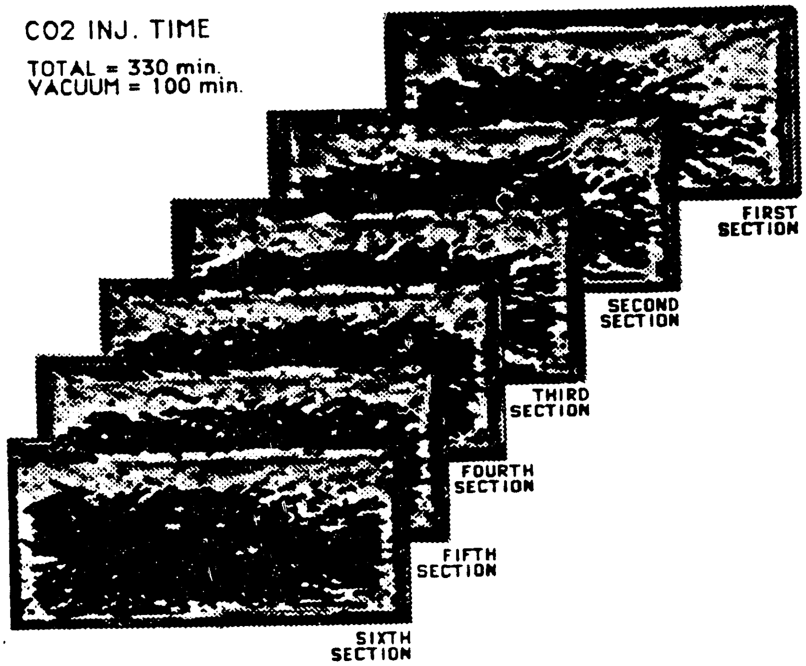

Figure 3.4.13 Saturation Distribution at Each Scanning Section of the 3D Model After 330 min. of CO_2 Injection.

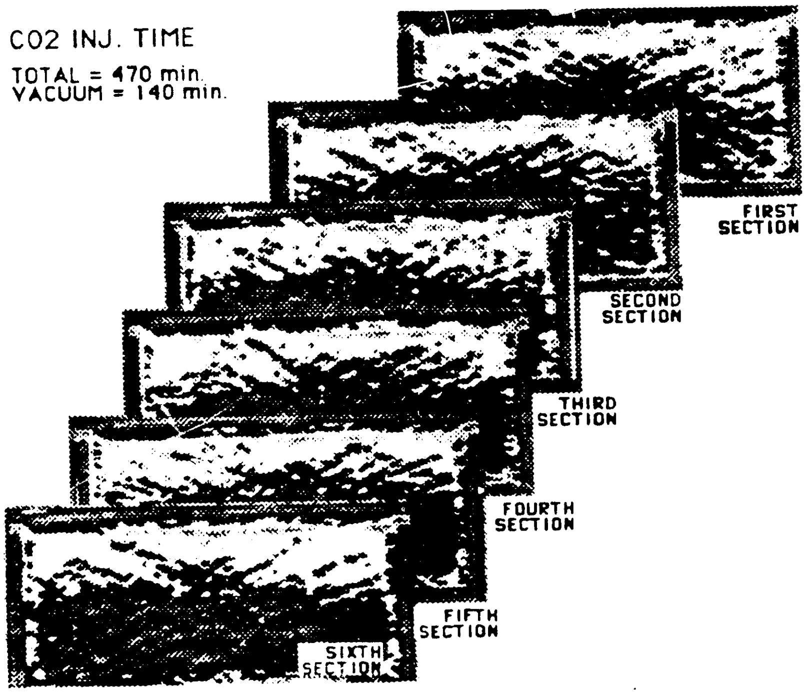

Figure 3.4.14 Saturation Distribution at Each Scanning Section of the 3D Model After 470 min. of CO_2 Injection.

tried to reach the production corner from the top of the model. After breakthrough it started displacing water from the rest of the model behaving as a chest. Although these pictures are raw and unprocessed it is very easy to follow the propagation of CO_2 visually. In future work these pictures will be processed and the noise strikes from corner to corner at each picture will be taken care of by subtraction.

3.4.6 FUTURE WORK

First of all some calibration experiments will be carried out according to the following procedure:

1. The 3-D model will be scanned dry,
2. The 3-D model will be saturated with water,
3. The initial saturation distribution will be scanned. Water injection will be continued until 100% water saturation is achieved.
4. Continuous steam injection will be started, during which:
   a) temperature and pressure data will be taken at one minute intervals,
   b) scan data will be recorded every 12 minutes at each of the 6 sections at two different energy levels,
   c) production will be measured to make overall material balance calculations.
5. The scan data will be analyzed to calibrate CT numbers at two different energy levels, for air, water and steam saturated sand. After measuring these CT numbers, the future scan pictures and CT values can be easily analyzed in terms of saturations within the model at a given time.
6. Steam and steam-foam injection experiments will be run in water saturated model.

4.1 SATURATION EVALUATION FOLLOWING WATER FLOODING

(M. Hashem and H.J. Ramey, Jr.)

A technical report on this topic is in the draft stage. The following is a short abstract of this report.

We consider the case of a multilayer sandstone reservoir that has been under a water flooding program. Injection was balanced in all intervals. Considerable effort is required to evaluate and locate undisplaced oil that was left in the reservoir. It is difficult to find the value of the water saturation by logging because the salinity and temperature of the flood water is different from the original formation conditions. Thus, coring and other expensive operations are required to determine water saturation, and hence estimate oil saturation.

The method found in this study can be used to produce estimates of water saturation using logs from initial wells and from new wells drilled after the flood. This method determines water saturations which agree well with water saturations obtained by other methods such as the Electromagnetic Propagation Log, and core analysis. The results agree within a tolerance of 7% of water saturation values obtained from the other methods.

4.2 NUMERICAL SIMULATION OF WELL-TO-WELL TRACER FLOW TEST AT NONUNITY MOBILITY RATIO

(D. A. Alvarado)

A numerical simulation of tracer flow was carried out for a nonunity mobility ratio flood in a five-spot pattern. The UTCHEM simulator from the University of Texas at Austin was used to model physical dispersion phenomena and, also, to study numerical dispersion phenomena associated with the finite difference solution of the convection-dispersion equation. New correlations were found which relate some properties of the dimensionless tracer concentration after breakthrough for a tracer slug test in a nonunit mobility ratio displacement, to the same properties defined for the unit mobility case. Also for the zero dispersion case, a new correlation was developed for the continuous tracer injection at favorable mobility ratios. We have found that the numerical solution obtained by using UTCHEM is sensitive to the values of cell Peclet number, i.e., the ratio of the grid size to the dispersity constant. From our results we can conclude that, for cell Peclet number greater than 8.33, the numerical solution based on Leonard's third order convective difference scheme as used in UTCHEM does not give an acceptable answer to the test problem. Hence, we decided to perform our computations for cell Peclet number lower than or equal to 8.33. More research has to be done with UTCHEM to investigate the behavior of this model under mesh refining and time step considerations, to study other mobility ratio injection conditions, and to consider other patterns of wells.

4.2.1 OBJECTIVES OF THE STUDY

In any enhanced oil recovery (EOR) project, it is important to detect reservoir heterogeneities, for the overall efficiency of the project depends on the nature of the flow from well to well. So, there is a need for a detailed description of the reservoir to be exploited. Traditional studies include geology, geophysics, coring, well logging and single well testing to help define reservoirs and their heterogeneities. Two additional types of test which have become popular in recent years are well-to-well transient pressure tests and well-to-well tracer tests. These two tests complement each other, for they measure different characteristics. The pressure transient test tends to measure average properties between wells. The tracer tests have the ability to indicate the extent of heterogeneity that exists in the region tested.

When well-to-well tracer tests are used, usually a small slug of tracer is injected and this in turn is followed by tracer free fluid. Several methods have been presented in the literature (Yuen et al. 1979; Brigham and Abbaszadeh-Dehghani, 1987; and Mishra, 1987) to analyze the tracer concentration data recorded at the production well, in order to obtain qualitative and quantitative information about the characteristics of the reservoir region tested. Indeed, the main objective of these studies was to examine the sensitivity of test responses to the presence of heterogeneity and to extract layer parameters from an overall tracer breakthrough profiles.

In most cases, quantitative analysis of well-to-well tracer tests has been performed for a multilayer five-spot pattern. However, Abbaszadeh-Dehghani and Brigham (1982) developed equations for computing tracer breakthrough curves in several flooding patterns (five-spot, direct drive line, staggered line drive and seven-spot) by analytically formulating tracer slug concentration in a general streamtube. Since the exact equations for streamlines of repeated patterns are known (Abbaszadeh-Dehghani and Brigham, 1982; Aronosky and Heller, 1957; and Brigham and Abbaszadeh-Dehghani 1987) the velocity of the fluid at any point in the system can be calculated by differentiating the streamline functions and by using the Cauchy-Riemann relationships. At any injected pore volume of displacing fluid, the production well concentration is the sum of concentrations from the streamtubes, which are computed at the production well. To simplify the analysis, tracer breakthrough curves for different patterns were correlated into a single set of curves. The five-spot system was chosen as a reference for correlation. Finally, a computer program was developed, based on a method presented by

Yuen, et al. (1979) to decompose a tracer profile form a multilayered reservoir into several responses from individual layers.

In the study of Abbaszadeh-Dehghani and Brigham (1982), the theory and analysis of tracer flow behavior was formulated on the assumption of unit mobility ratio, and exact analytical equations were obtained in the form of elliptic integrals which provided breakthrough curves for the different patterns. An attempt was made to define pattern breakthrough curves analytically for nonunit mobility ratio in a developed five-spot, but the results obtained contradicted experimental observations. This was because of the unrealistic assumption that streamlines are independent of the mobility ratio.

Because the streamtube procedure can not generate correct breakthrough curves at nonunity mobility ratio and because there is a need to describe tracer flow in such systems, we have pursued a numerical study of interwell tracer tests when mobility ratio contrast exists. Along the lines of the work of Abbaszadeh-Dehghani and Brigham (1982), a correlation will be sought between the curves from several patterns and mobility ratios. Proper numerical modeling is necessary for an accurate representation of these processes. Of importance are some features in the formulation of the problem, such as numerical dispersion and grid orientation effect associated with finite difference solutions of the convection-dispersion equation.

To reach these objectives, we decided to test the University of Texas UTCHEM simulator (User's Guide for UTCHEM-V.22, 1989). UTCHEM is a three-dimensional compositional chemical flooding simulator, adapted to describe tracer flow in different patterns, and also to control numerical dispersion and grid orientation effects. Several differencing schemes are available in the simulator. Of particular interest is a third-order scheme based on Leonard's method.

In the simulation of tracer studies conducted before and during many of the EOR projects for reservoir characterization, one of the main objectives is to determine the level of physical dispersion and heterogeneity. In numerical reservoir simulation, however, artificial numerical dispersion can further smear concentration fronts by increasing the level of dispersion. This numerical dispersion results in inaccurate predictions of both concentrations and breakthrough times. Therefore, accurate simulation of physical processes involved in EOR requires that numerical dispersion be essentially eliminated.

We will not describe the UTCHEM simulator in detail. The main features of this program have been the subject of several papers and theses (Datta Gupta, 1985; Datta Gupta et al., 1986; Descant III, 1989; and Saad, 1989). We will give some information about the principal characteristics of this simulator. Because of the need to simulate mixing phenomena, and, therefore, to minimize numerical dispersion, the four convective differencing schemes available in UTCHEM will be reviewed briefly.

Since it is possible to consider many recovery phenomena in the program, UTCHEM has many input options to specify which phenomena will be included. Therefore, one of the main difficulties for a user of UTCHEM is to define the input data choice correctly. Four input data files are needed. The first file is used to describe the run. The second file concerns the grid characteristics, initial conditions, and the output options. Injection/production data are specified in the third file, while the fourth one is related to physical properties.

The main assumptions made in UTCHEM are: isothermal reservoir, slightly compressible fluid and solid, Darcy's law applies, thermodynamic equilibrium, dispersion follows Fick's law for multiphase flow, and surfactants and polymer are treated as monospecies without a molecular weight distribution.

The derivation of the conservation equations and the slightly compressible formulation of the pressure equation are given in detail by Saad (1989) but some of the more important concepts on the mixing equations are reviewed here.

Most current reservoir simulators use single point upstream weighting to approximate the first order derivative of the convection term in the equations. This method has a first order local truncation error, and the global truncation error of an algorithm using this differencing operator is also first order. This method suffers from artificial numerical dispersion and the results are implemented by grid orientation. This method is stable; furthermore, it can be cause dispersion that is considerably larger than the physical dispersion, leading to inaccurate results. For convection dominated flow, at high Peclet number, the hyperbolic nature of the equations produces oscillatory solutions.

A second order explicit method, proposed by Chaudhari and implemented in UTCHEM produces accurate results for chemical flooding applications when the cell Peclet number is kept below two (Saad, 1989); this is, unfortunately, a limiting factor in large scale or convection dominated applications. At low cell Peclet numbers, the two point upstream weighting method produces more accurate results than single point upstream weighting; however, at higher cell Peclet numbers (convection dominated flows), it too produces inaccurate results (Saad, 1989).

A third order convective differencing scheme based on Leonard's method is especially suited for convection-dominated flow problems. This method results in a minimal increase in storage or computation time per time step per grid block compared to the lower order methods. This method is referred to as the higher order method in this work.

The details on the finite difference operators and its implementation in UTCHEM are discussed thoroughly by Saad (1989).

4.2.2 RESULTS AND DISCUSSION

We have been using UTCHEM-V-4.22 released on September 1989. The first step of our research consisted of a learning period to run the simulators. A good description of how to deal with the input data is given in the User's Guide for UTCHEM-V-4.22 (1989). Although, the input information is well documented, the output information is poorly commented. The author is in the process of writing a summary about the characteristics of the output files.

Next, UTCHEM-V-4.22 was validated for one dimensional miscible displacements (tracer in aqueous phase). Figure 4.2.1 shows a one-dimensional problem. In this case we considered a linear reservoir initially saturated with water, and tracer injection is at unit mobility ratio. We used constant viscosity polymer as a tracer and the Leonard's third order scheme was used. Since we assumed zero physical dispersion, the Peclet number is infinite, and we have a purely convective displacement. The analytical solution to this problem is the unit step function. As can be seen from Figure 4.2.1, the solution oscillates after breakthrough.

Figure 4.2.2 shows dimensionless tracer concentrations for Leonard's third order scheme together with those of single-point upstream weighting, two-point upstream weighting and Chaudhari's method for a Peclet number of 1,000 (cell Peclet number, $P_\Delta = 10$). The agreement between the analytical solution and the higher order method for this convection dominated test problem is remarkable, especially when compared with the diffused solution of single-point upstream weighting and the oscillatory nature of the solution using Chaudhari's dispersion control.

At lower cell Peclet numbers, Chaudhari's method and two-point upstream weighting will also give an accurate solution to the model problem (Chaudhari, 1971; Saad, 1989). This illustrates that, for the model problem and the same degree of accuracy using the higher order method requires a much lower level of grid refinement than the two-point upstream weighting or Chaudhari's method. On the other hand, at a large cell Peclet number, the higher order method will also oscillate and the inaccuracies reappear. This is seen in Figure 4.2.4 which compares the higher order method and the exact solution at Peclet number of 10,000 ($P_\Delta = 100$).

Figure 4.2.3 presents a graph of normalized concentration as a function of normalized distance, for the analytical and numerical solutions for a linear reservoir. Initially, we have only water in the reservoir and we are injecting a tracer solution of the same mobility as the

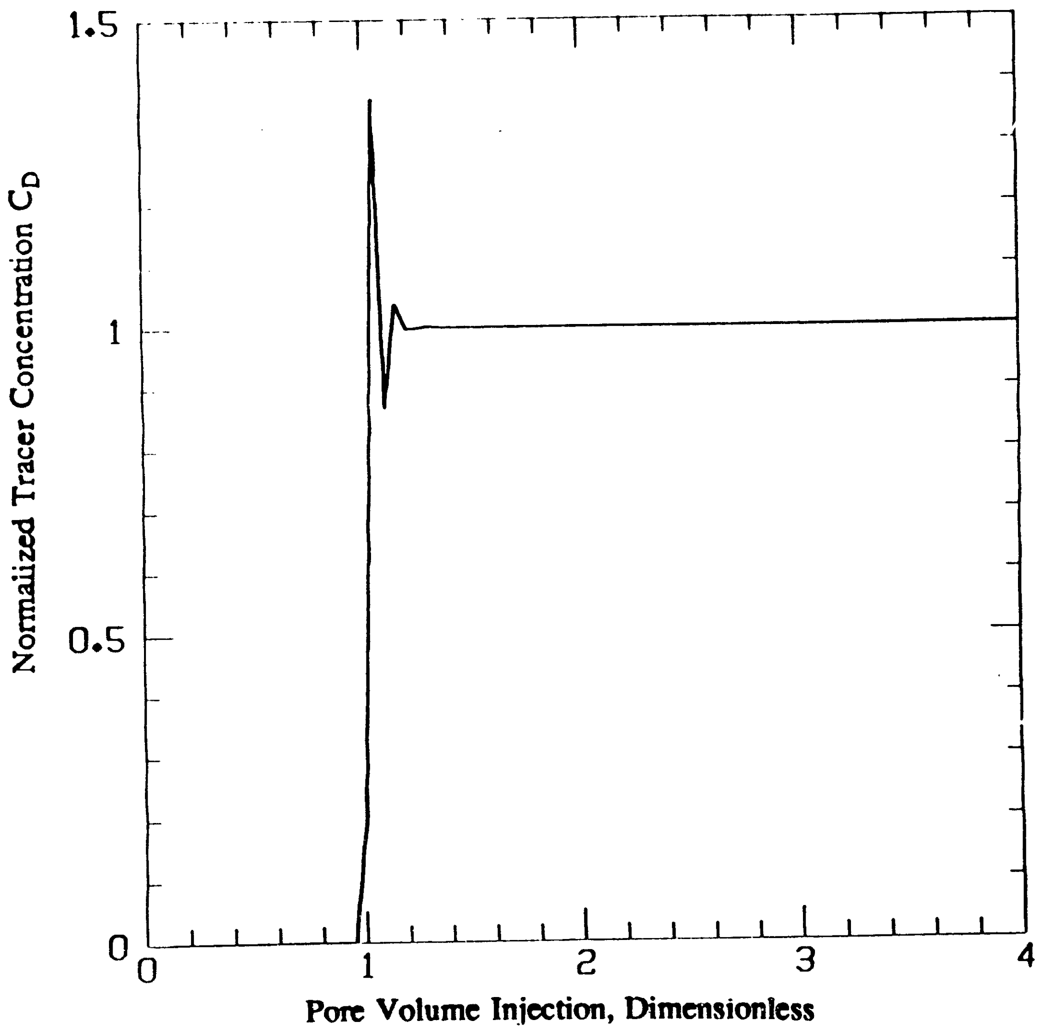

Figure 4.2.1 Tracer Concentration as a Function of Pore Volume Injected. 1 Dimension Case, Zero Physical Dispersion. Leonard's Method.

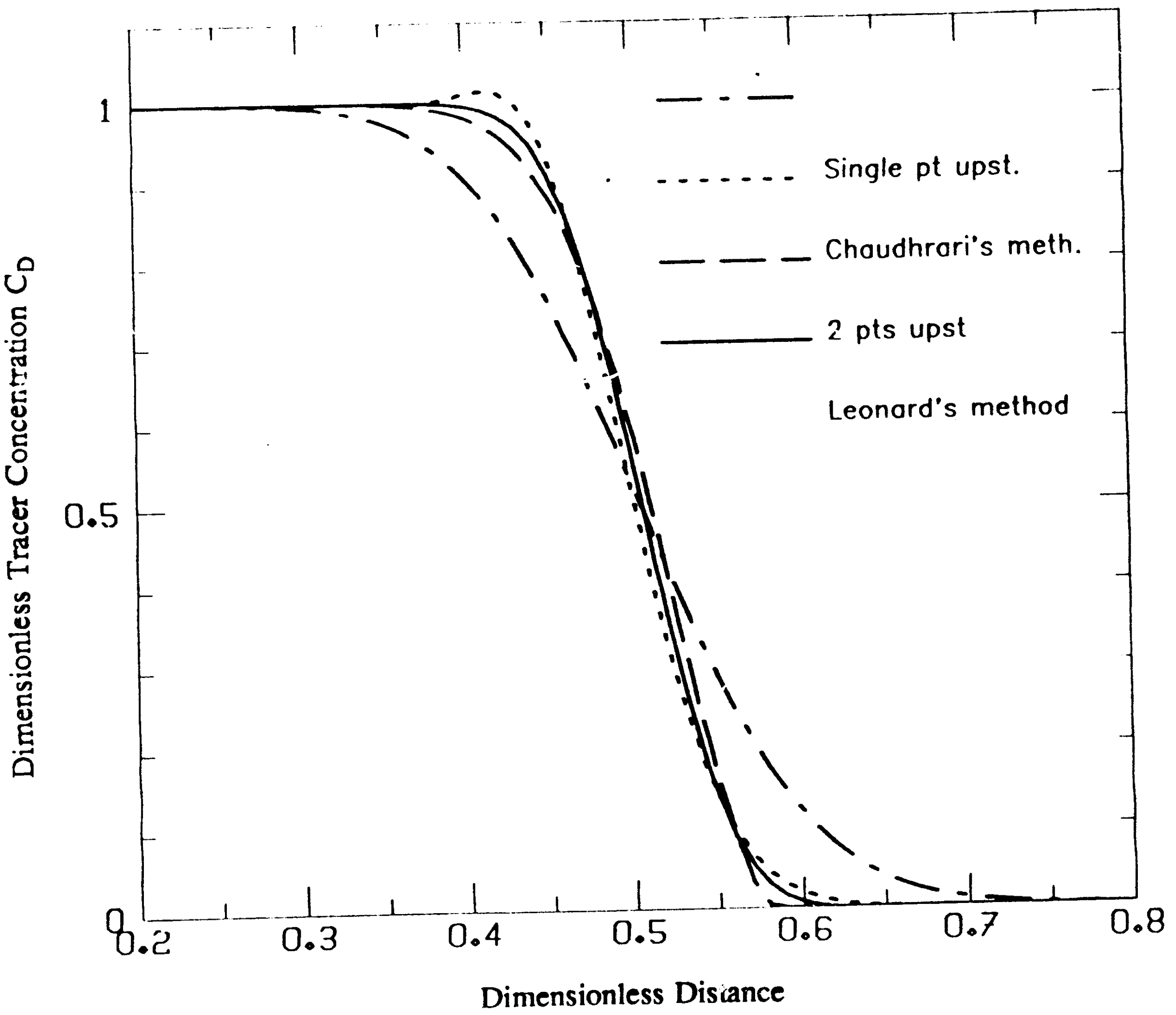

Figure 4.2.2 Tracer Concentration vs Dimensionless Distance Showing Numerical Dispersion. 0.5 Pore Volume Injected. Cell Peclet Number, $P_\Delta = 10$ $\alpha_L = 0.01$ ft.

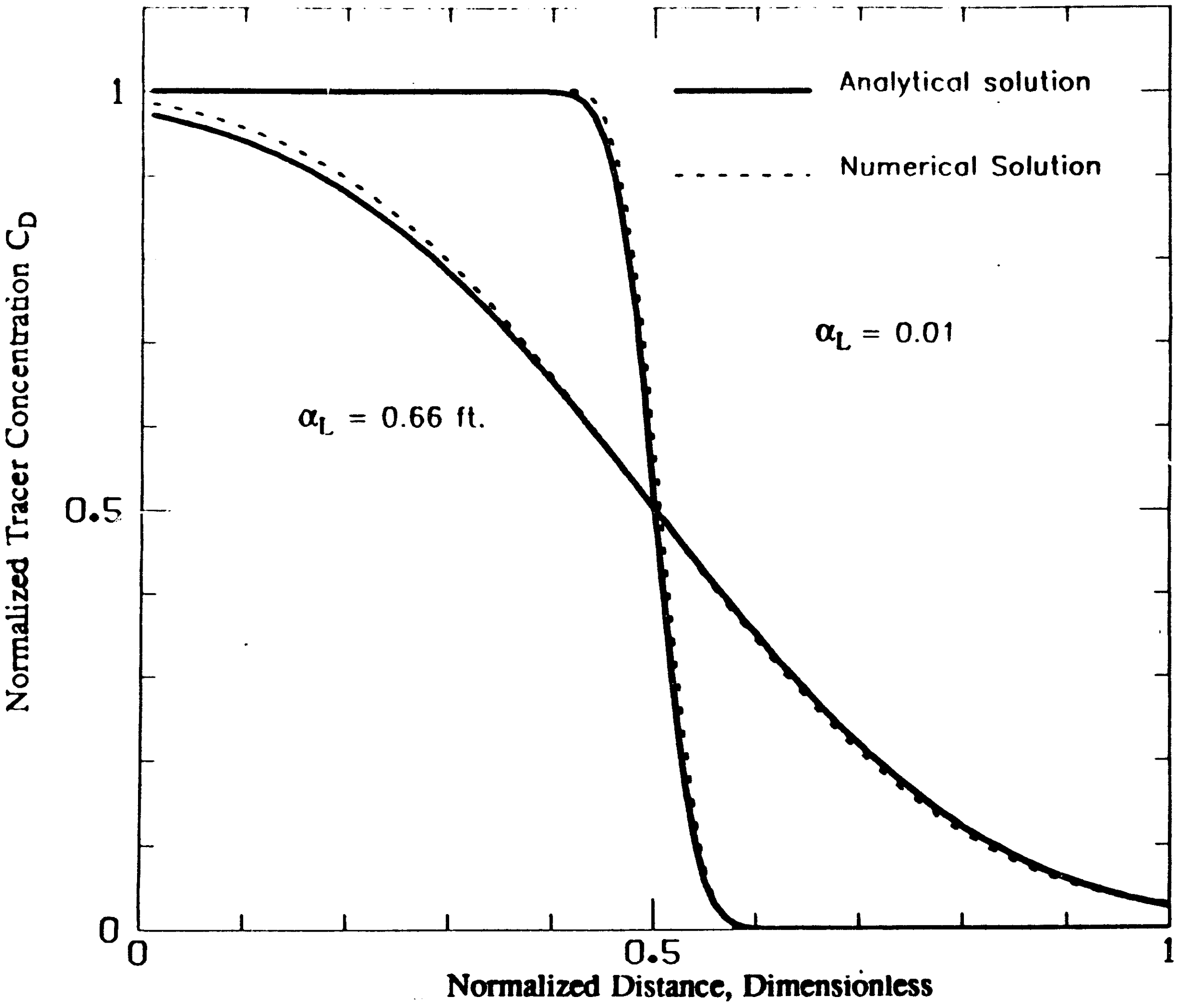

Figure 4.2.3 Comparison of the Numerical Solution with the Analytical Solution for Cell Peclet Number of 0.15 ($\alpha_L = 0.66$) and for Cell Peclet Number of 10($\alpha_L = 0.01$). Leonard's Method.

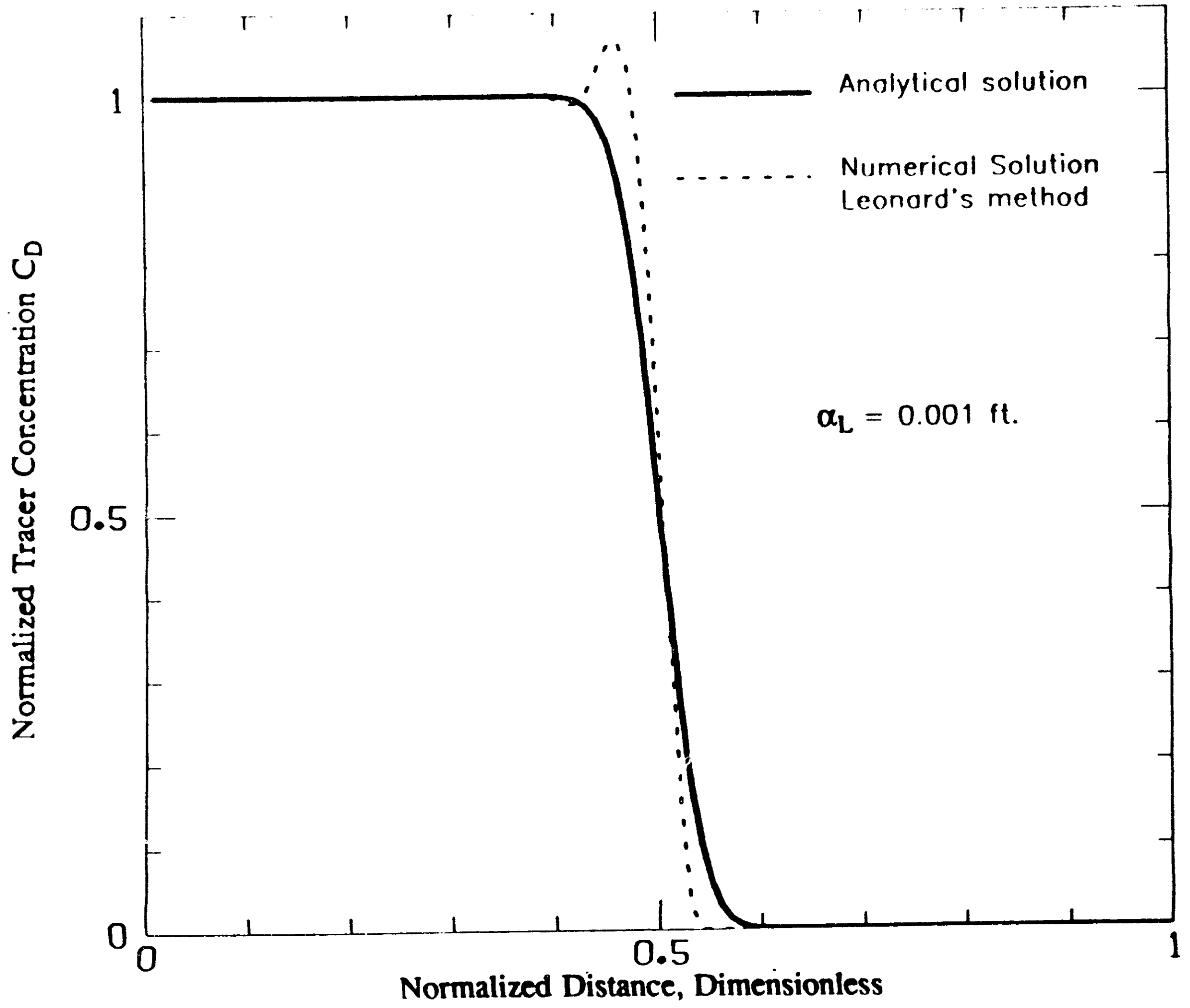

Figure 4.2.4 Comparison of the Numerical Solution Using the Higher Order Method (Leonard's Method) with the Analytical Solution. Cell Peclet Number of 100. One-Dimension. PV Injected = 0.5.

initial fluids in the reservoir at constant flow rate. Two different values of the dispersion constant were considered $\alpha_L = 0.66$ ft and $\alpha_L = 0.01$ ft. As can be seen in Figure 4.2.3, the agreement between both solutions is adequate.

Next, we attempted to use UTCHEM to describe the tracer flow in a developed five-spot pattern. A unit symmetry area was chosen as a physical domain, the distance between like wells is 330 ft, so the unit symmetric area is a 165 ft square. Other data used are shown in Table 4.2.1.

Figure 4.2.5 shows a comparison of the numerical solutions for different methods of dispersion control in the five-spot pattern. We have plotted the normalized concentration as a function of the pore volume injection for zero dispersion. The injection rate is constant and the fluid injected is composed of water plus tracer. The mobility ratio of the displacing fluids to the displaced fluids is equal to one. Note that Chaudharis' method oscillates around the analytical solution. The single point upstream method and the two point upstream method both show appreciable differences from the analytical solution and from experimental results at, and shortly after breakthrough. The calculated pore volumes injected at breakthrough. are lower than the true value. Later, the numerical solutions converge to the analytical solution. The differences shortly after the breakthrough are due to numerical dispersion. Remember that this is a pure convection problem; there is no physical dispersion. The method which appears to have the least numerical dispersion is the Leonard's third order method, so we used the Leonard's method as a method henceforth.

Figure 4.2.6 is a graph of dimensionless tracer concentration as a function of pore volume injected, for continuous injection of tracer solutions of different viscosities. We considered mobility ratios of 0.2, 0.5, 0.8 and 1, i.e., favorable mobility ratios.

Figure 4.2.7 shows the basic information at $m = 0.2$ presented on Figure 4.2.6, plus the extrapolation of the maximum slope straight line to the x axis (pore volume injected axis). Experimental values presented by Caudle and Witte (1959), were taken from Figure 4.12, page 87 of "Mechanics of Secondary Oil Recovery," by C.R. Smith (1975). Table 4.2.2 shows the comparison between those values. A maximum difference of 2% was found for the breakthrough obtained numerically. Based on this fact, we take the value of the extrapolated maximum slope curve, as the pore volume injected at breakthrough. A FORTRAN program was written which computes the maximum slope straight line tangent to the given concentration curve; and then from the tangent point; the intersection of this line at concentration on the x axis is taken to be the pore volume injected at breakthrough. Next, we use this point to correct the curve of concentration vs pore volume injected, by setting the breakthrough point as the first point, the second being the tangent point, and the other points after these points remained unchanged.

Figure 4.2.8 presents the correlation which was obtained when we plotted the displacing water cut, dimensionless continuous tracer injection concentration, as a function of the dimensionless pore volume function, $(V_{pD} - V_{PDbt})/(1 - V_{pDbt})$, previously used by other investigators (Morales, 1975; Morgan, 1977; and Abbaszadeh-Dehghani and Brigham, 1982). As we can see from this figure, it appears that all the curves for different mobilities of the displacing phase, collapse into a single curve. The values used of pore volume injected at breakthrough are shown on Table 4.2.2, as compared with those obtained from experimental tests.

Figure 4.2.9 shows a comparison of the results of analytical solution and numerical solution for different values of Peclet number (a/α_L ratio) for tracer flow in a homogeneous developed five-spot pattern at unit mobility ratio. In Figure 4.2.9, for Peclet number greater than 500, the numerical solution does not match the analytical solution. On the other hand, for a/α_L ratio values 500 or lower, the analytical and numerical solutions are much closer, with only slight differences. Based on this test, we decided to investigate further the tracer flow behavior for different mobility ratios at the leading slug interface, but only by using values of a/α_L ratios equal to or lower than 500.

Table 4.2.1 Reservoir Simulation Data for the Two-Dimensional Developed Five-Spot Pattern Tracer Flow Problem.

Tracer slug size, % PV	2.00
Longitudinal dispersion, ft.	0.066-3.30
Transverse dispersivity, ft.	0.00
Cell peclet number, dimensionless	1.66-83.3
a/α_L, dimensionless	100-5000
Simulated area, ft.	165x165
Number of grid blocks	30x30x1
Grid sizes, ft.	
$\Delta x = \Delta y$	5.50
Δz	5.00

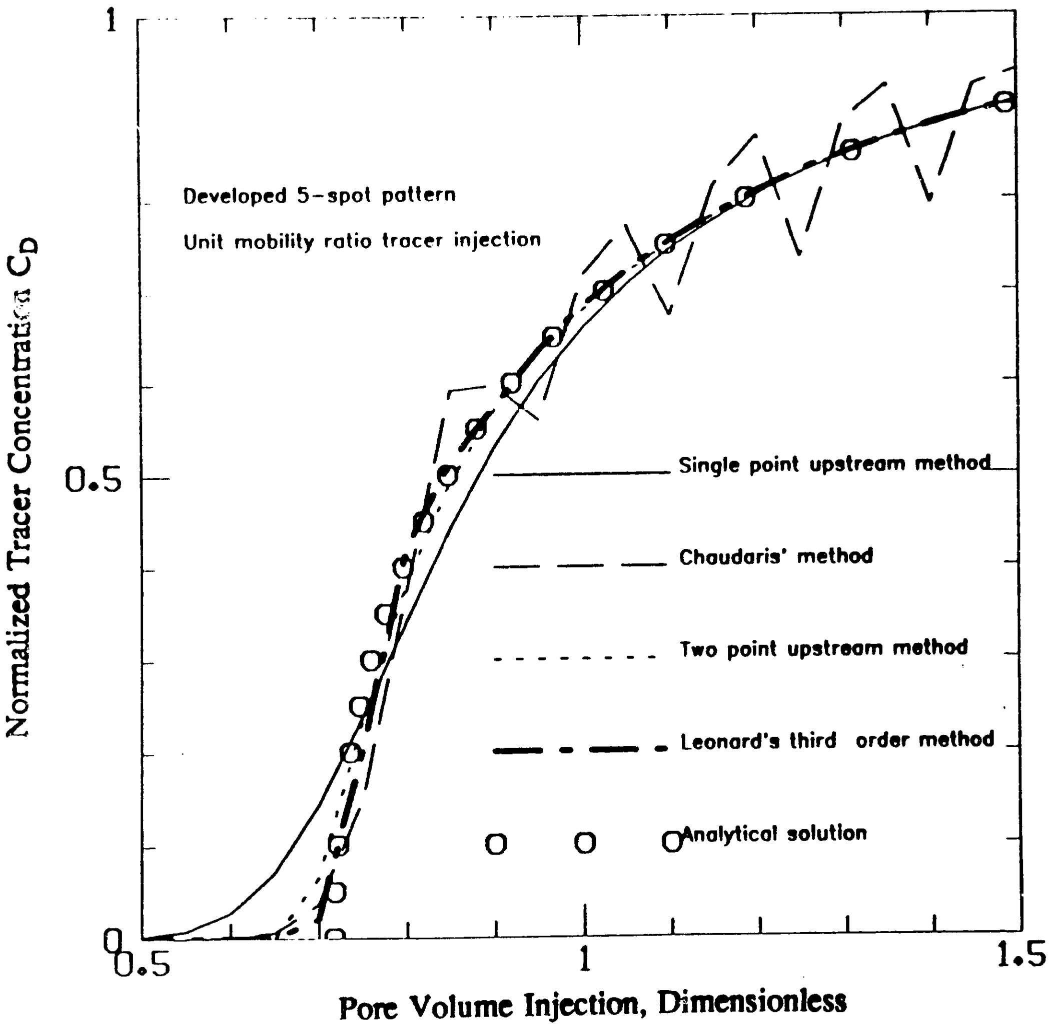

Figure 4.2.5 Comparison of Numerical Solutions by Using Different Methods of Numerical Dispersion Control for the Continuous Constant Rate Tracer Injection in a Developed Five-Spot Pattern.

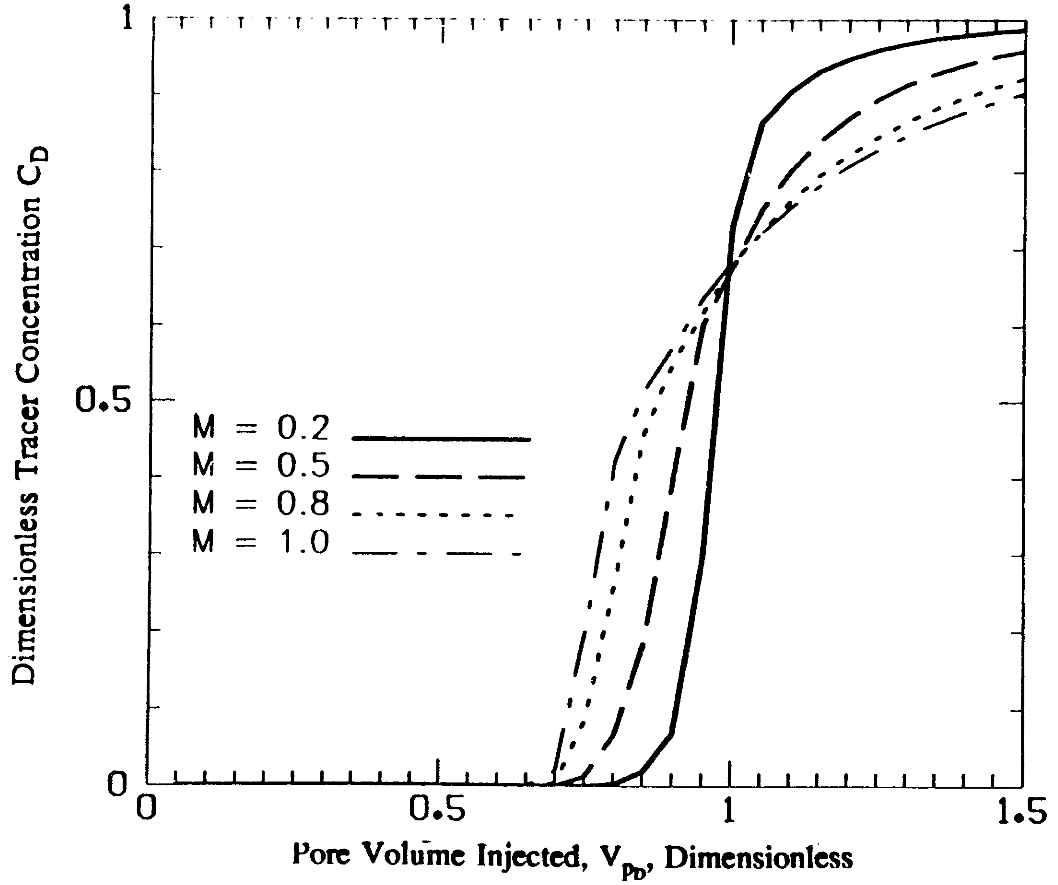

Figure 4.2.6 Tracer Concentration as a Function of Pore Volume Injected for Continuous Injection of a Tracer Slug. Mobility Ratios: 0.2 to 1.0. Leonard Method.

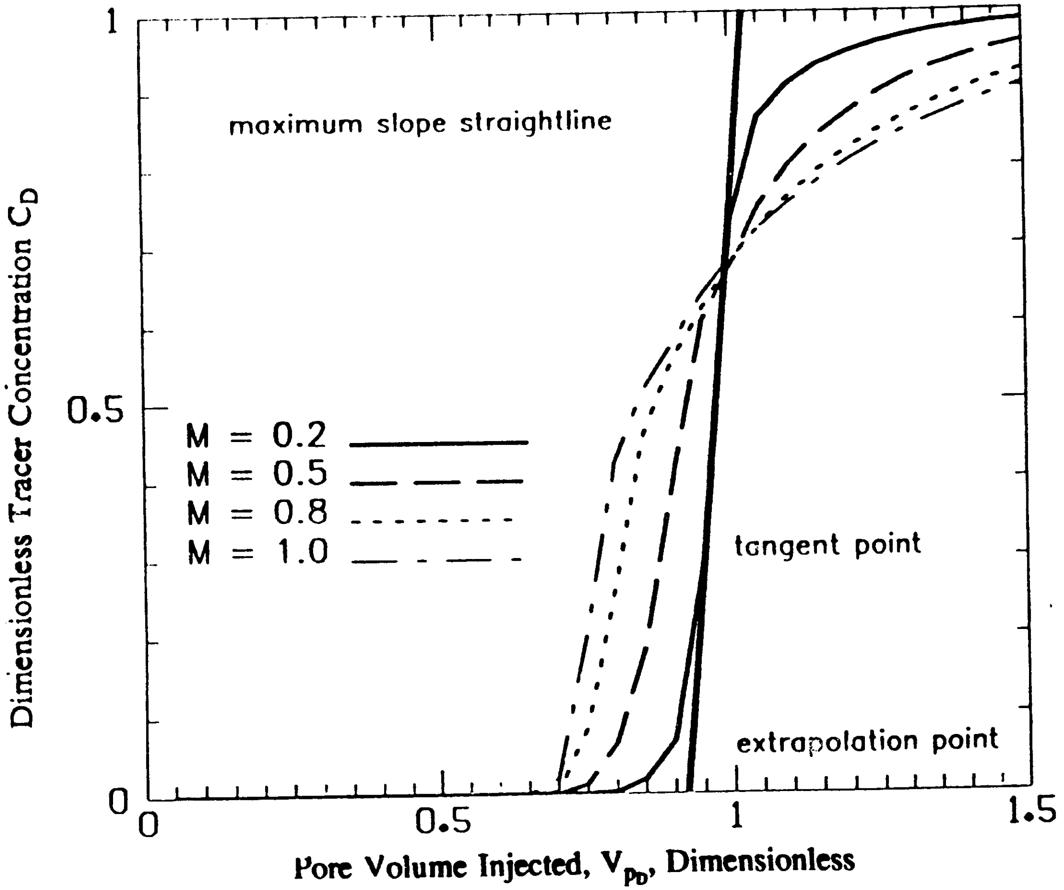

Figure 4.2.7 This is the Same Figure 4.2.6 Showing the Maximum Slope Straightline Tangent to the Breakthrough Concentration Curve Corresponding to Mobility Ratio Equal to 0.2. Zero Physical Dispersion.

Table 4.2.2 Comparison of Experimental Values of Pore Volume Injected at Breakthrough and Those Obtained by Extrapolating the Maximum Slope Straightline, for Different Values of Mobility Ratio.

Mobility Ratio	Experimental (*) Value	Extrapolated Value
0.2	0.930	0.912
0.5	0.800	0.816
0.8	0.725	0.732
1.0	0.700	0.707

(*) After Caudle, B.H., and Witte, M.D., AIME Tech. Note 2047, J. Pet. Tech. (Dec. 1959) 63

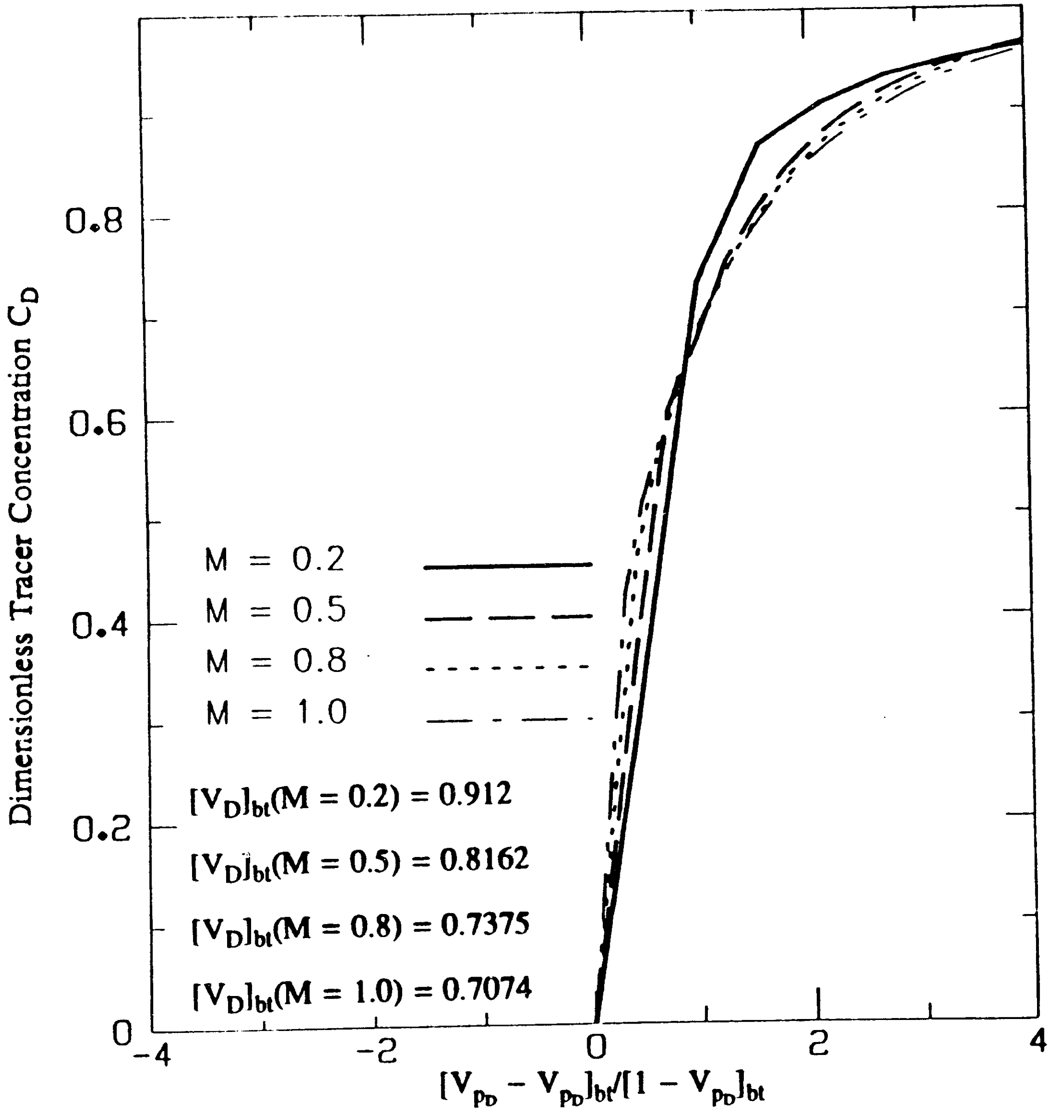

Figure 4.2.8 Dimensionless Tracer Concentration as a Function of the Dimensionless Pore Volume Function. $(V_pD - V_pDbt)/(L - V_pDbt)$.

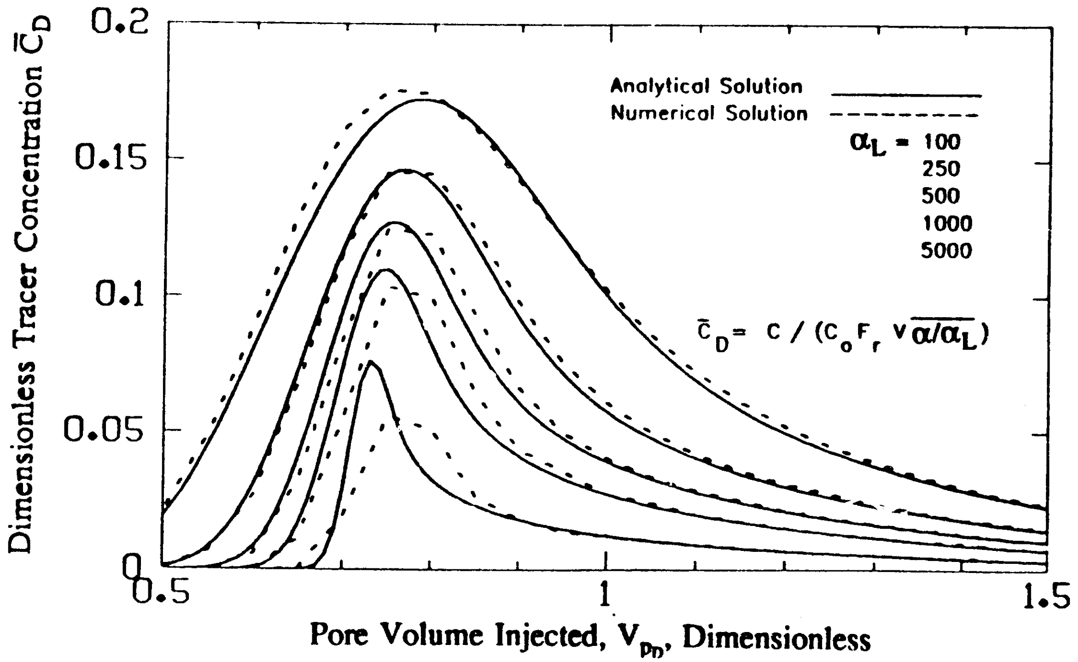

Figure 4.2.9 Comparison of the Results of Analytical Solution and Numerical Solution for Different Values of Peclet Number (a/α_L) for Tracer Flow in Homogeneous Five-Spot Pattern. Unit Mobility Ratio.

We try now to study the case of injecting tracer slug of different mobility ratios with respect to the initial fluid mobility. We consider only favorable mobility ratios, from 0.2 to 1. The tracer slug viscosity was varied by using polymer as a component in order to increase the viscosity of the slug. The mobility ratio of the interphase slug-injected fluid was kept equal to one.

Figures 4.2.10, 4.2.11 and 4.2.12 depict the dimensionless concentration, $\bar{C}_D$ (as defined by Abbaszadeh-Dehghani and Brigham, 1982), as a function of the pore volume injected, Vp_D for different values of the parameter a/α_L (100, 250 and 500). The three figures present some common features. First, for values of the mobility ratio greater than 0.50 (0.50 to 1.00) the peak concentration is approximately constant independent of the mobility ratio. For values of mobility ratios lower than 0.50 the peak height increased at higher mobility ratios. This means that if we are injecting a tracer slug with a mobility ratio lower than one, (favorable mobility ratio), but higher than 0.50 the peak concentration is approximately equal to the one for unit mobility ratio.

Figure 4.2.13 summarizes the peak height data of Figs. 4.2.10-4.2.12. This figure shows that the peak concentration, $\bar{C}_{D_{\max}}$, is approximately constant for values of mobility between 0.5 and 1, and for mobility ratios lower than 0.5 the peak concentration increases slightly. Further research is required on this topic, because a mathematical analysis of the nature of this problem, indicates that the peak concentration height should increase as the mobility ratio is reduced. So, Figure 4.2.13 can be used to translate the results of a tracer test for favorable mobility ratios other than one to an equivalent developed five-spot pattern of unit mobility.

From Figures 4.2.10-4.2.12, we can see that the value of the pore volume injected V_{pD}, at the peak concentration is displaced to the right for the different mobility ratio considered with respect to the position of the peak concentration $\bar{C}_{D\max}$ for the unit mobility ratio case. This effect was found for all of the a/α_L values studied. Figure 4.2.14 presents the pore volume injected at peak concentration, $V_{pD\max}$ as a function of mobility ratio. By inspecting Figure 4.2.14, it appears that there is an approximately linear relationship between these variables. This means that the peak position of a given tracer slug test, could be translated into an equivalent developed five-spot pattern slug concentration, by applying Figure 4.2.14.

In summary, it appears that the variables we need in a slug tracer injection test for further calculations, i.e., the peak concentration, $\bar{C}_{D\max}$, and the volumetric position at the peak, can be, in principle, translated into equivalent values to the unit mobility ratio injection condition. Thus, now, we can apply the procedure developed by Abbaszadeh-Dehghani and Brigham (1982) for analyzing a tracer injection test at a favorable mobility ratio.

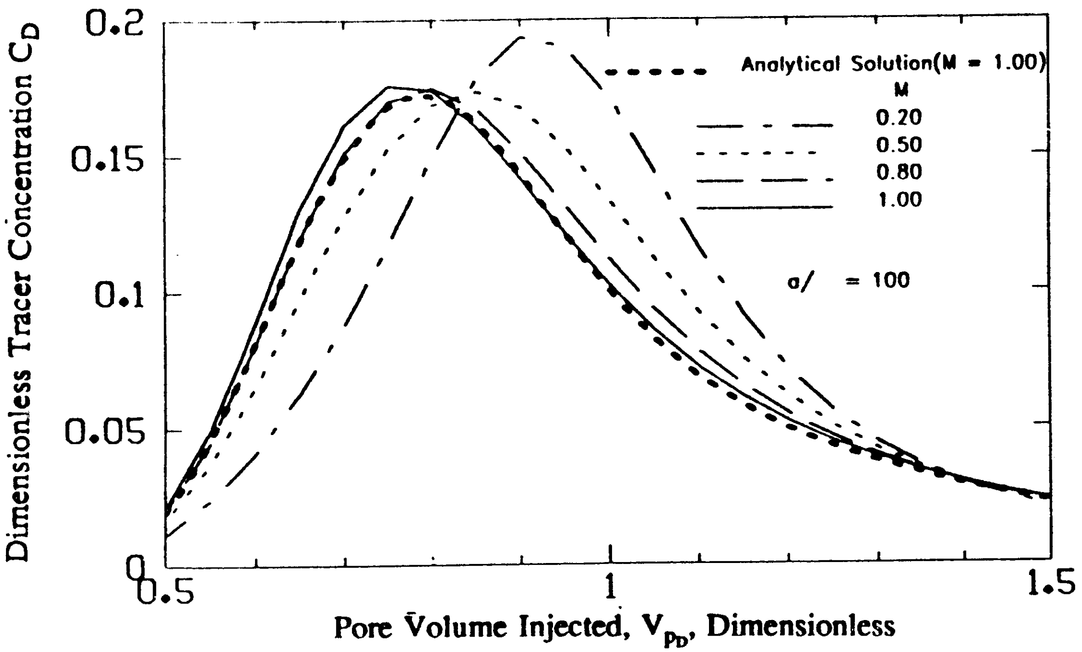

Figure 4.2.10 Dimensionless Slug Tracer Concentration. $\overline{C}_D$, as a Function of Pore Volume Injected. V_pD, for Different Values of Mobility Ratio as the Front Interphase. $a/\alpha_L = 100$.

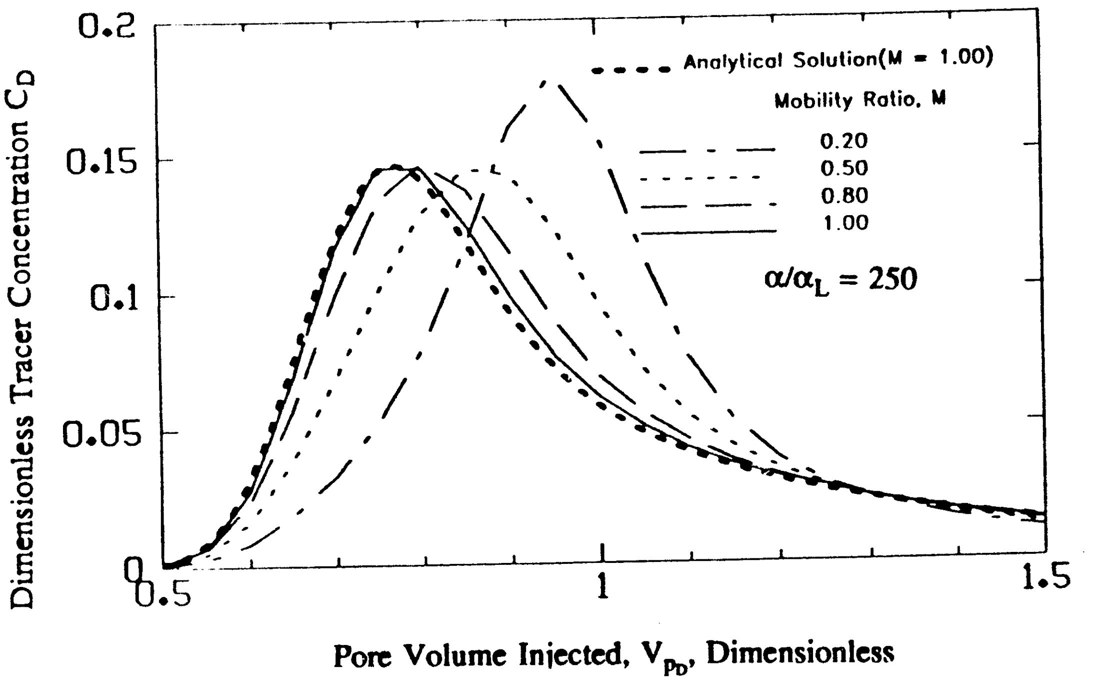

Figure 4.2.11 Dimensionless Slug Tracer Concentration, $\overline{C}_D$, as a Function of Pore Volume Injected. V_pD, for Different Values of Mobility Ratio at the Front Interphase. $a/\alpha_L = 250$.

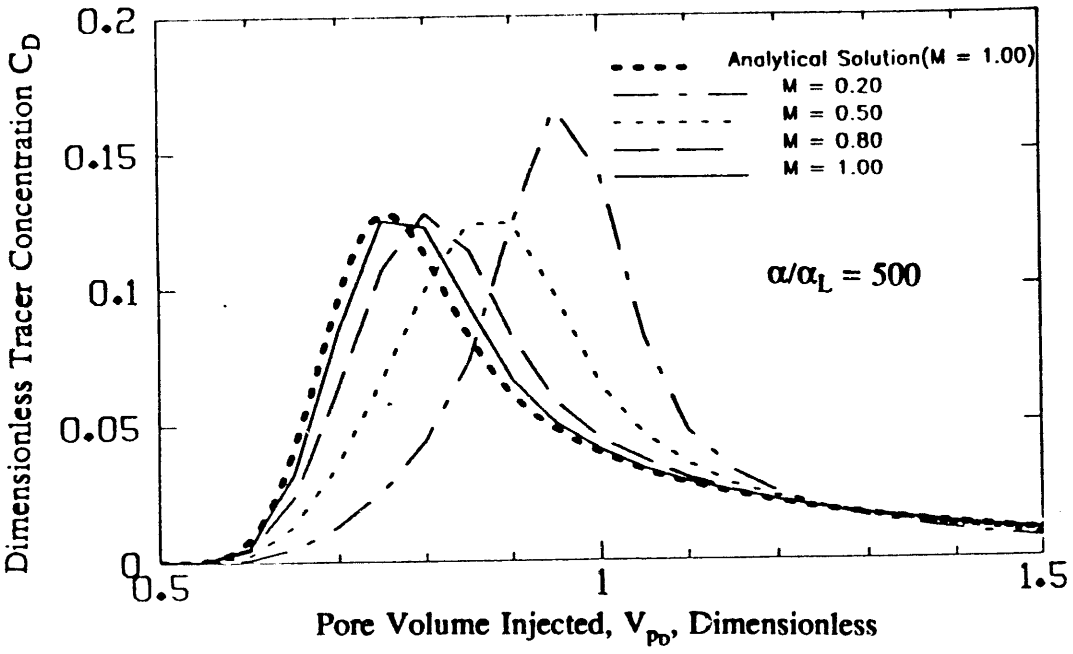

Figure 4.2.12 Dimensionless Slug Tracer Concentration, $\overline{C}_D$, as a Function of Pore Volume Injected, V_pD, for Different Values of Mobility Ratio at the Front Interphase. $a/\alpha_L = 500$.

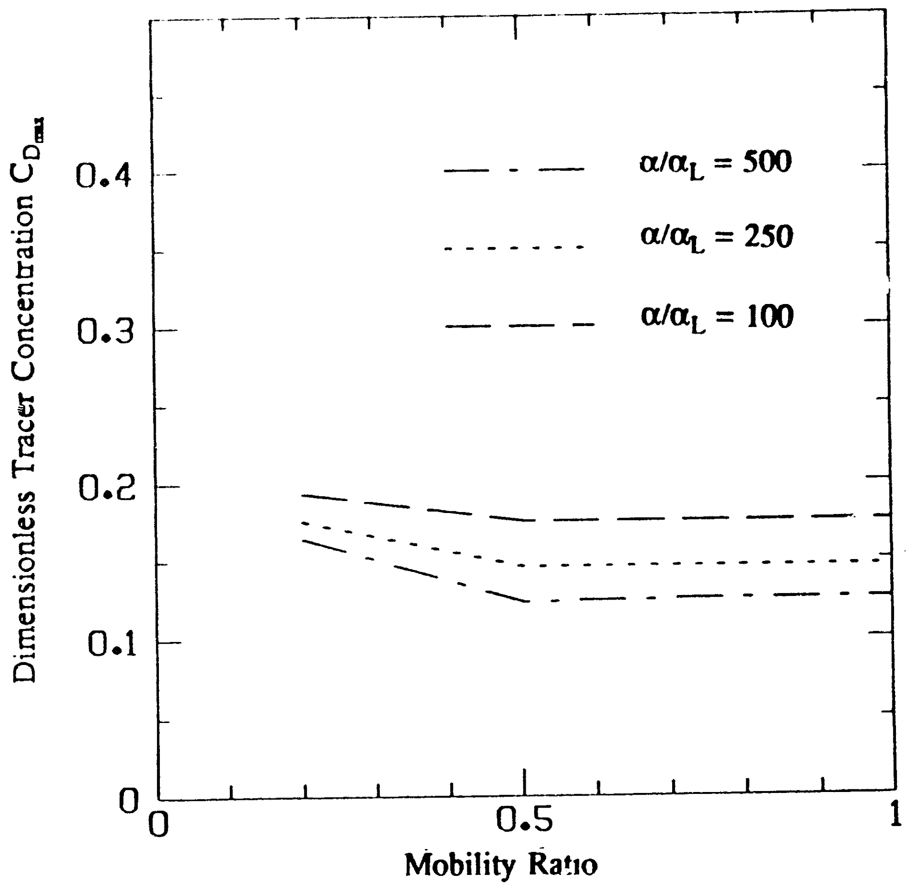

Figure 4.2.13 Peak Concentration $C_{D\,\max}$, as a Function of Mobility Ratio for Different Values of Peclet Number, a/α_L.

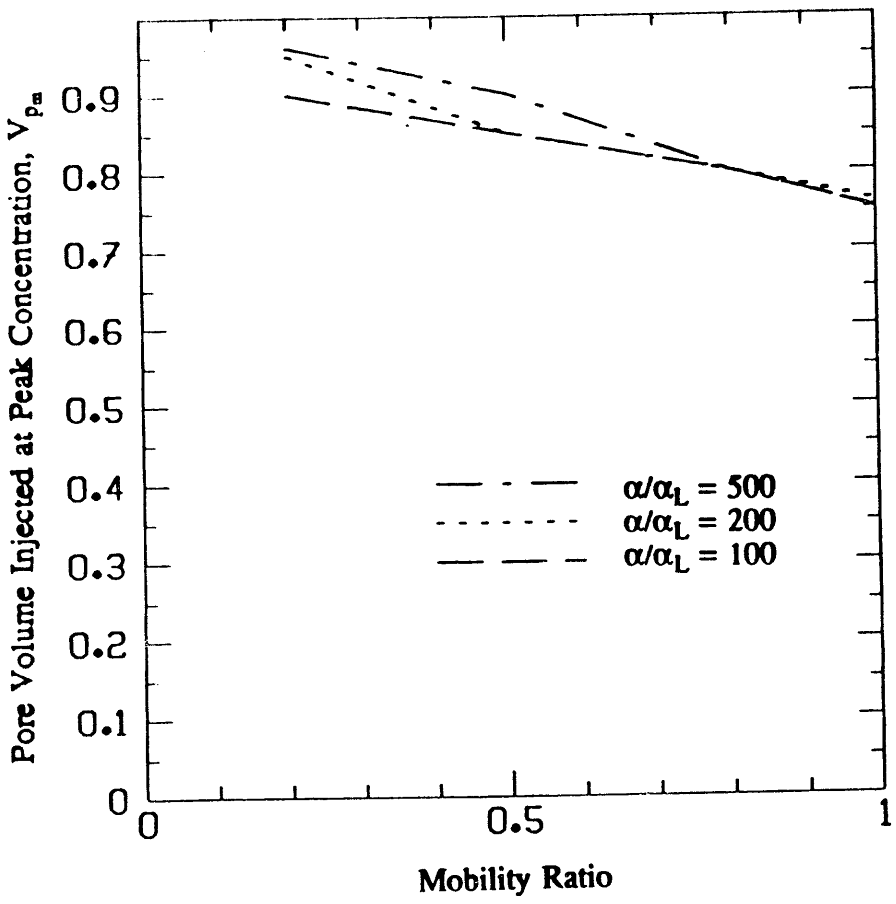

Figure 4.2.14 Pore Volume Injected at Peak Concentration, $V_{p\,D\max}$, as a Function of Mobility Ratio for Different Values at Peclet Number, a/α_L.

REFERENCES

1. Abbaszadeh-Dehghani, M. and Brigham, W.E.: "Analysis of Unit-Mobility Ratio Well-to-Well Tracer Flow to Determine Reservoir Heterogeneity", Stanford University, Petroleum Research Institute Report SUPRI-TR-36, 1982, Stanford, California.
2. Alexander, J.D., Martin, W.L., and Dew, J.N.: "Factors affecting Fuel Availability and Composition During In-Situ Combustion," J. Pet. Tech. (Oct. 1962) 1154-1164; Trans., AIME, 225.
3. Aronosky, J.S. and Heller, N.R.: "A Diffusion Model to Explain Mixing of Flowing Miscible Fluids in Porous Media", Trans. AIME, 1957, 210, 345-349.
4. Baena, C.J.: "Effect of Metallic Additives on In-Situ Combustion of Huntington Beach Crude" TR78 U.S. Dept. of Energy DE-FG19-87BC14126 (1990).
5. Belvins, T.R., Duerksen, J.H. and Ault, J.W., "Light-Oil Steamflooding -- An Emerging Technology", J. Pet. Tech., (July 1984), 1115-1122.
6. Bond, D.C. and Holbrook, O.C.: "Gas Drive Oil Recovery Process", U.S. Patent 2,866,507 (1958).
7. Bousaid, I.S. and Ramey, H.J., Jr.: "Oxidation of Crude Oil in Porous Media" SPEJ <u>8</u> 137-148 (1968).
8. Brigham, W.E. and Abbaszadeh-Dehghani, M.: "Tracer Testing for Reservoir Description", J. Pet. Tech., 1987, 519-527.
9. Brigham, W.E., Ramey, H.J., Jr., and Castanier, L.M.: "SUPRI Heavy Oil Research Program Thirteenth Annual Program, SUPRI-TR-76, Stanford University Petroleum Research Institute, Stanford, CA, (Aug. 1990).
10. Burger, J.G. and Sahuquet, B.C.: "Chemical Aspects of In-Situ Combustion" SPEJ <u>12</u> 410-422 (1972).
11. Castanier, L. M., and Brigham, W. E.: "Selecting Foaming Agents for Steam Injection Improvement," Chemical Engineering Progress, Vol. 6, (1985) 37-40.
12. Caudle, B.H., and Witte, M.D.: "Production Potential Changes During Sweep-Out in a Five-Spot System," <u>Trans.</u> AIME (1959), <u>216,</u> 446.
13. Chaudhari, N.M.: "An Improved Numerical Technique for Solving Multidimensional Miscible Displacement Equations", Soc. Pet. Eng. J., Sept. 1971, 277-284.
14. Coleman, H.J., Shelton, E.M., Nichols, D.T. and Thompsom, C.J., "Analysis of 800 Crude Oils From United States oil Fields", DOE BETC/RI-78/14, (November 1978).
15. Datta Gupta, A.: "Three Dimensional Simulation of Chemical Flooding", Master's dissertation, 1985, Univ. of Texas, Austin, Texas.
16. Datta Gupta, A., Pope, G.A., Sepehrnoori, K., Tharsher, R.L.: "Asymmetric, Positive Definite Formulation of a Three-Dimensional Micellar/Polymer Simulator". SPE Reservoir Engineering, Nov., 1986, 622-632.
17. De Los Rios, C.F., Brigham, W.E. and Castanier, L.M.: "The Effect of Metallic Additives on the Kinetics of Oil Oxidation Reactions in In-Situ Combustion" U.S. Dept. of Energy Technical Report DOE/BC/14126-4 (DE88001248) (1988).
18. Demiral, M. R. B., and Okandan, E.: "Experimental Analysis of Steam Foam Injection to Heavy Oil Limestone Reservoirs," SPE 15734. Presented at the Fifth SPE Middle East Oil Show, Manama, Bahrain, March 1987.
19. Descant III, F.J.: "Simulation of Single-Well Tracer Flow", Master's dissertation, 1989, Univ. of Texas, Austin, Texas.
20. Dew, J.N. and Martin, W.L.: "Air Requirement for Forward Combustion" Pet. Eng. J. (December 1964) 82 and (January 1965) 82-85.

21. Dilgren, R. E., Hirasaki, G. J., Hill, H. J., and Whitten, D. G.: "Steam-Channel-Expanding Steam Foam Drive," U. S. Patent 4,393,937, issued May 2, 1978.

22. Duerksen J.H. and Hsueh, L., "Steam Distillation of Crude Oils", Soc. Pet. Eng. J., (April 1983), 265-271.

23. Duerksen, Rr. E., Wall, R. G., and Knight, J. D.: "Steam Injection Including Alpha-Olefin Sulfonate Dimer Surfactant Additives and a Process of Stimulating Hydrocarbon Recovery from a Subterranean Formation," U. S. Patent 4,556,107, issued December 3, 1985.

24, Ettinger, R.A. and Radke, C.J.: "The Influence of Texture on Steady Foam Flow in Berea Sandstone", Presented at the 64th Annual Conference of SPE, San Antonio, Texas, Oct. 8-11, 1989.

25. Evans, R. D.: The Atomic Nucleau, McGraw-Hill Book Co., New York City, (1955).

26. Fassihi, M.R., Brigham, W.E., and Ramey, H.J., Jr.: "Reaction Kinetics of In-Situ Combustion" SPEJ 24 399-416 (1984).

27. Gates, C.F. and Ramey, H.J., Jr., "Field Results of South Belridge Thermal Recovery Experiment", Trans. AIME, Vol. 213, (1958), 236-244.

28. Hirasaki, J. G.: "The Steam Foam Process," JPT (May 1989) 449-456.

29. Hougen, O.A., Watson, K.M. and Ragatz, R.A., "Chemical Process Principles -- Part I", 2nd Ed., John Wiley & Sons., N.Y., (1954), 403-408.

30. Huh, D.G., Cochrane, T.D., and Kovarik, F.S.: "The Effect of Microscopic Heterogeneity on CO-Foam Mobility: Part 1 - Mechanistic Study", JPT, Aug. 1989, pp. 872-879.

31. Konopnicki, D. T., Traverse, E. F., Brown, A. and Diebert, A. D., "Design and Evaluation of the Shiells Canyon Field Steam- Distillation Drive Pilot Project", J. Pet. Tech., (May 1979), 546-552.

32. Lake, L. W.: "Enhanced Oil Recovery", Englewood Cliffs, N. J. Prentice Hall, 1989.

33. Langmuis, I.: "Theory of Adsorption", Phys. Rev. (January 1915) 6.

34. Law, H. C., and Borchardt, J. K.: "Improved Steam Foam Formulations: Concepts and Laboratory Results," SPE 18783. Presented at the 1989 SPE California Regional Meeting, Bakersfield, California, April 1989.

35. Law, H. C., and O'Brien, S. M.: "Effects of Spreading and Nonspreading Oils on Foam Propagation Through Porous Media," SPE RE (August 1988) 893-896.

36. Lee, B.I. and Kesler, M.G., "Improve Vapor Pressures Prediction", Hydrocarbon Processing, (July 1980), 163-167.

37. Leonard, B.P.: "A Survey of Finite Difference of Opinion on Numerical Muddling of the Incomprehensible Defective Confusion Equation", Finite Element Methods for Convection Dominated Flows, ASME, New York, NY, Dec. 2-7, 1979, 1-17.

38. Manlowe, D.J., and Radke, C.J.: "A Pore-Level Investigation of Foam/Oil Interactions in Porous Media", SPE 18069, Presented at 1988 SPE Annual Technical Conference and Exhibition, Houston, Texas, Oct. 2-5, 1988.

39. Marsden, S.S.: "Foams In Porous Media", SUPRI TR-49, DOE Contract No. DE-AC03-81SF11564, May, 1986.

40. McPhee, C. A., Tehrani, A. D. H., and Jolly, R. P. S.: "Foam Flooding of Cores Under North Sea Reservoir Conditions," SPE/DOE 17360, Presented at the Sixth SPE/DOE Symposium of Enhanced Oil Recovery, Tulsa, Oklahoma, April 1988.

41. Mishra, S.: "On the Use of Pressure and Tracer Test Data for Reservoir Description", Ph.D. dissertation, 1987, Stanford University, Stanford, California.

42. Morales, E.C.: "A First Step to Obtain a Single Correlation Characterizing the Different Patterns in Waterflooding," M.S. Report, Stanford University, Stanford, California (June 1975).
43. Morgan, H.T.: "A Single Correlation Characterizing Areal Sweep for the Different Patterns in Waterflooding after Breakthrough," M.S. Report, Stanford, (June 1977).
44. Muijs, H. M. and Keijer, P. P. M.: "Steam Foam Process," U. S. Patent 4,693,311, issued September 15, 1987.
45. Muijs, H. M., Keijer, P. P. M., and Wiersma, R. J.: "Surfactants for Mobility Control in High Temperature Steam-Foam Applications," SPE/DOE 17361, presented at the Sixth SPE/DOE Symposium of Enhanced Oil Recovery, Tulsa, Oklahoma, April 1988.
46. Owete, O.S. and Brigham, W.E.: "Flow of Foam Through Porous Media", SUPRI TR-37, DOE Document No. DOE/SF/115646, July, 1984.
47. Patzek, T. W., Koinis, M. T.: "Kern River Steam Foam Pilots," Proceedings of the 1988 SPE/DOE Sixth Symposium on Enhanced Oil Recovery, Tulsa, Oklahoma, (April 1988) pp. 663-676.
48. Racz: "Development and Application of a Thermocatalytic In-Situ Combustion Process in Hungary", Proceedings, 1985 European Meeting on Improved Oil Recovery, Rome, April 1985.
49. Robin, M.: "Utilisation D'agents Moussants Pour Ameliorer L'efficacite De L'injection De Vapeur," Proceedings, 3rd European Meeting on Improved Oil Recovery, Roma, Italy, April 1985, 349-361.
50. Saad, N.: "Field Simulation of Chemical Flooding", Ph.D. dissertation, 1989, Univ. of Texas, Austin, Texas.
51. Sanchez, J.M. and Hazlett, R.D.: "Foam Flow Through on Oil-Wet Porous Medium: A Laboratory Study", SPE 19687, Presented at 64th Annual Conference of SPE, San Antonio, Texas, Oct. 8-11, 1989.
52. Sarathi, P.: "Using Micromodels to Study Steam Displacement Processes in Porous Media", NIPER 180 (DE87001201), Oct., 1986.
53. Satman, A. "In-Situ Combustion Models for the Steam Plateau and for Fieldwide Oil Recovery", Ph.D. Thesis, Stanford University (1982).
54. Shallcross, D. C., and Wood, D. G.: "The Accurate Measurement of Heat Flux Using a Film Heat Sensor with Application to Axisymmetric Bodies," Proceedings, Eighth International Heat Transfer Conference, 1986, 3.
55. Shallcross, D. C., Castanier, L. M., and Brigham, W. E.: "Characterization of Surfactants as Steamflood Additives," Proceedings, III International Symposium on Enhanced Oil Recovery, Maracaibo, Venezuela, February 1989, 561-581.
56. Shallcross, D.C., De Los Rios, C.F., Castanier, L.M., and Brigham, W.E.: "Modifying In-Situ Combustion Performance by the Use of Water-Soluble Additives", Paper SPE 19485, Proceedings Asia Meeting of SPE (September 1989).
57. Showalter, W.E.: "Combustion Drive Tests," Soc. Pet. Eng. J. (March 1953) 53-58; Trans., AIME, 228.
58. Smith, R.C.: "Mechanics of Secondary Oil Recovery, Reprint 1975, Robert E. Krieger Publishing Co., Inc., Malabar, Florida (1975).
59. Tadema, H.J.: "Oil Production by Underground Combustion," Proc., Fifth World Pet. Cong., New York (1959) Sec. II.
60. Tavares, C.: "Effect of Metallic Additives on Hamaca Crude Oil Combustion", Stanford University Petroleum Research Report to be published 1990.
61. ULTIMAGE © 1988 Graftek France. 9, Route de Verriere, 92360 Meudon-La-Foret, France.

62. User's Guide for UTCHEM-V.22, Center for Enhanced Oil and Gas Recovery Rese University of Texas, Austin, September, 1989.

63. Valleroy, V. V., Willman, B. T., Cambell, J. B. and Powers, L. W., "Deerfield Pilot Test of Recovery by Steam Drive", J. Pet. Tech, (July 1967), 956-964.

64. Vinegar, H. G. and Wellington, S. L.: "Tomographic Imaging of Three-Phase Flow Experiments", Rev. Scientific Instruments, (January 1987), 96-107.

65. VLSI Technology, Second Ed., S. M. Sze. McGraw Hill, 1988.

66. Volek, C .W. and Pryor, J. A., "Steam Distillation Drive - Brea Field, California", J. Pet. Tech., (August 1972), 899-906.

67. Wang, F. P., and Brigham, W. E.: "A Study of Heat Transfer During Steam Injection and Effect of Surfactants on Steam Mobility Reduction," DOE Report DE-AC03-81SF-11564, SUPRI Report TR 55, August 1986.

68. Willman, B. T., Valleroy, V. V., Runberg, G. W., Cornelius, A. J. and Powers, L. W., "Laboratory Study of Oil Recovery by Steam Injection", J. Pet. Tech., (July 1961), 681-690.

69. Withjack, E. M.: "Computed Tomography for Rock Property Determination and Fluid-Flow Visualization", SPE Formation Evaluation, (December 1988), 696-704.

70. Wu, C. H. and Fulton, P. F., "Experimental Simulation of the Zones Preceeding the Combustion Front of An In-situ Combustion Process", Soc. Pet. Eng. J., (March 1971), 38-46.

71. Wu, C.H. and Brown, A., "A Laboratory Study on Steam Distillation in Porous Media", SPE 5569, (1975).

72. Wu, C.H. and Elder, R.B., "Correlation of Crude Oil Steam Distillation Yields With Basic Crude Oil Properties", Soc. Pet. Eng. J., (December 1983), 937-945.

73. Yuen, D.L. Brigham, W.E. and Cinco-L., H.: "Analysis of Five-Spot Tracer Tests to Determine Reservoir Layering", U.S. DOE Report SAN 1265-8, Washington D.C., 1979.

END

DATE FILMED

2 / 24 / 92